2016-04-22

Synthesis and Optical Properties of Novel Turn-On, Fluorescent Nuclear Stains with Live Cell Compatability

Demar R. G. Pitter
University Of Miami, demarpitter@hotmail.com

UNIVERSITY OF MIAMI

SYNTHESIS AND OPTICAL PROPERTIES OF NOVEL TURN-ON, FLUORESCENT NUCLEAR STAINS WITH LIVE CELL COMPATIBILITY

By

Demar R.G. Pitter

A DISSERTATION

Submitted to the Faculty
of the University of Miami
in partial fulfillment of the requirements for
the degree of Doctor of Philosophy

Coral Gables, Florida

May 2016

UNIVERSITY OF MIAMI

A dissertation submitted in partial fulfillment of
the requirements for the degree of
Doctor of Philosophy

SYNTHESIS AND OPTICAL PROPERTIES OF NOVEL TURN-ON, FLUORESCENT NUCLEAR STAINS WITH LIVE CELL COMPATIBILITY

Demar R.G. Pitter

Approved:

_____
James Wilson, Ph.D.
Associate Professor of Chemistry

_____
Francisco Raymo, Ph.D.
Professor of Chemistry

_____
Marc Knecht, Ph.D.
Associate Professor of Chemistry

_____
Guillermo Prado, Ph.D.
Dean of the Graduate School

_____
James D. Baker, Ph.D.
Professor of Biology

PITTER, DEMAR R. G. (Ph.D., Chemistry)

Synthesis and Optical Properties of Novel Turn-On, Fluorescent Nuclear Stains with Live Cell Compatibility. (May 2016)

Abstract of a dissertation at the University of Miami.

Dissertation supervised by Professor James Wilson.
No. of pages in text. (126)

Flurorphores are an important class of compounds that are used as tools to better understand the processes that occur in cells. A subset of biologically useful fluorophores are nucleic acid binding probes. The inherent problems of many of the nucleic acid binding probes used on the market today is three-fold; (1) that the probes used produce some amount of autofluoresence from the biological sample due to the excitation wavelength needed for them to emit, (2) that most of the common probes lack cell membrane permeability, thus requiring fixation and pemeablization which limits the ability to observe dynamic processes of the biological sample and (3) that probes tend to have excitation maxima that poorly match commonly used visible laser lines. This research focuses on synthesizing probes that overcome these limitations by: exploiting the twisted intramolecular charge transfer (TICT) phenomena of probes to produce high on/off ratios when bound to nucleic acids, are membrane permeable, are live cell compatible, and match the major laser lines available for microscopy. Furthermore, with help fom the development of these probes a new method for detecting DNA binding modes has been established through the use of two-photon spectroscopy.

In Loving Memory of Helen Maxine Pitter

ACKNOWLEDGEMENT

Throughout my journey in life I have been privileged to be apart of things that I once wasn't able to believe were possible for me, and along the way I have had the help of so many.

I would like to sincerely thank Dr. James Wilson for giving me the opportunity to partake research in his lab, and for his guidance throughout my time here at the University of Miami.

I would also like to thank Dr. Clare Muhoro, who awakened my love for chemistry during my undergraduate studies at Towson University which led me to pursue a career in Chemistry.

Additionally I would like to thank the members of my committee; Dr. Franciso Raymo, Dr. Marc Knecht and Dr. James Baker for their willingness to share their knowledge and willingness to answer any questions that I had. I express my gratitude to Dr. Adrienne Brown, Dr. Frederick Westerlund, Dr. Jens Wigenius and Dr. Theodore Goodson for their contributions to my research.

Thanks to Mr. Edward Torress who was always willing to run my countless mass spec samples. Thanks to Dr. Hudson for sharing his invaluable guidance and knowledge. I also want to take this opportunity to thank Dr. Edward Mensah, Dr. Jyothi Dhuguru, Heagin Lee, and Anthony Cauley for being awesome labmates.

Finally, I would like to thank my family, my aunts and uncles for their unwavering support, my sister for being the best big sister anyone could ask for, and to the most important person in my life--my mother, I miss you, love you and will continue to live my life to honor you. Thank you.

TABLE OF CONTENTS

LIST OF FIGURES

LIST OF TABLES

SUMMARY

The main goal of my research is to design and synthesize probes that are able to bind to nucleic acids with live cell compatibility in a manner that enhances their fluorescent capabilities (i.e. turn-on probes). Fluorophores have long been used as a tool in obtaining images of cells, and also to study the processes that occur in cells. Through structural modification, fluorophores can be tuned to either have specific fluorescent characteristics in solvent, or can be further modified to interact with specific biological structures. Proteins and nucleic acids are two of the most widely studied macromolecules in biotechnology, where fluorophores are often used to aide in the elucidation of their functionality.

Binding to macroscale biological molecules with small chemical compounds can occur through two main means, through covalent and non-covalent interactions. For fluorescence studies non-covalent bonding is the preferred method of interaction due to its reversibility. The mechanisms by which non-covalent interactions occur with nucleic acids are through groove binding and intercalation between bases and each is dependent on the structural identity of the interacting molecule. For small molecules to bind efficiently to nucleic acids they have to have the following characteristics; the molecule should be planar and should have an aromatic moiety, the molecule should also have an extended conjugated system to allow excitation and emission wavelengths in the visible spectrum.[1] The shape of the interacting molecule is also important, it has been found that crescent shaped molecules have been most successful as intercalators, while modification to the extended conjugated system may allow for efficient groove binding.[2]

There are several nuclear stains currently present on the market that are capable of targeting nucleic acids, but they have intrinsic disadvantages like that their excitation wavelengths are harmful to cells, or their requirement of the cell to be fixed due to lack of membrane permeability, and their mode of binding that may cause adverse effects on the cell biology resulting in the fluorophore being toxic to cells.[3-7] **Chapter 1** discusses the synthesis and the optical properties of two novel fluorophores when bound to DNA. These probes exhibit high turn-on ratios when bound to DNA due to the their high sensitivity achieved by TICT phenomena. Restriction of the rotation of the N-methylpiperazine substituted aryl arms allowed for a 80-fold and 30-fold increase in emission for **1** and **2** respectively in octanol when compared to PBS. These two probes also showed high turn-on ratios when bound to calf thymus DNA, where the **1** and **2** had a 75-fold and 27-fold respectively. Linear flow dichroism showed that **1** is a intercalator and **2** is a groove binder. Confocal microscopy also proved the live cell compatibility of these probes and the bathochromic shifts of the excitation spectra of these probes, allowed for the excitation at longer wavelengths reducing the autofluroesence from the sample and the use of commonly available laser lines.

Chapter 2 describes the sensitivity of **1** and **2** to GC and AT base pairs. Through photophysical and electrochemical studies it was found that binding of the probes to AT rich base pair regions resulted in an enhanced emission, compared to the binding of the probes to GC rich regions. Electrochemical studies indicate that a photoinduced electron transfer mechanism unique to GC base pairs has the ability to quench the emission of these probes through a donation of electrons to the vacant lowest unoccupied molecular orbital (LUMO) of the probes.

In **Chapter 3** modeled and synthesized probes that would have a "redder" excitation wavelength and still maintain all the advantages gained from the synthesis of the probes in **Chapter 1**. Modeling studies revealed that through the extension of the conjugated π-system this redder excitation wavelength might be achieved. Introduction of one or two vinylic groups to the core established core moiety, allowed synthesis of four new probes. Probes with one vinylic group produced a red and an orange emissive dye, which also exhibit high turn-on ratios when bound to DNA (92-fold and 64-fold). Confocal microscopy shows that both single vinyl probes are vital, having the capability to stain the nuclei and cytosol, and are environmentally sensitive enough to be resolved into separate channels. Allowing for a single dye to two-color image both the cytosol and nucleus.

Chapter 4 describes a new highly sensitive optical methodology for determining the binding modes of dyes using two-photon absorption (TPA). The TPA cross-sections of intercalating and groove binding dyes are influenced by the electric field of the DNA backbone upon binding. By using known grove binding and intercalative probes as standards (**12** and **13**), TPA groove binding probes were identified by exhibiting an enhanced TPA cross-section due to the electric field enhancement of the transition dipole moment. While intercalative binding molecules exhibited a decrease in the TPA cross-section. It is believed that TPA is a more sensitive technique especially when using low DNA concentrations.

Finally, **Chapter 5** reports the experimental approaches and the synthetic procedures undertaken throughout this research. The appendix shows the characterization of compounds that were also synthesized as potential nucleic binding probes.

Chapter 1

TURN-ON, FLUORESCENT NUCLEAR STAINS WITH LIVE CELL COMPATIBILITY

1.1 Introduction

Fluorescent nuclear stains are widely employed in cell life cycle analysis and flow cytometry and as counterstains in fluorescence microscopy.[3,8] Probes possessing well-defined binding modes also find applications in quantification of nucleic acids[3,9] as well as investigations into statistical-mechanical properties,[10] solution orientation, and dynamics of DNA.[11] Despite the availability of several classes of fluorescent nuclear stains, there remain limitations to their universal application due to available excitation wavelengths,[3,4] membrane permeability,[5] and toxicity.[6,7] Indole and benzimide vital dyes, such as DAPI and Hoechst 33342, possess excitation maxima in the UV that are poorly matched to visible laser lines.[3,4] On the other hand, DNA-intercalating carbocyanine dyes,[12] such as TOTO or YOYO,[13] offer long wavelength excitation and emission but require cell fixation and permeabilization.[14]

Two novel fluorescent nuclear stains are reported, which have interesting properties: 4,6-bis(4-(4-methylpiperazin-1-yl)phenyl) pyrimidin-2-ol, **1**, and [1,3-bis[4-(4-methylpiperazin-1-yl)phenyl]-1,3-propandioato-κO, κO'] difluoroboron, **2** (Figure 1.1B). Optical spectroscopy reveals that they are optimally matched to available 405 nm (**1**) and 514nm (**2**) lasers lines and are also compatible with standard filter sets. DNA binding was investigated by fluorescence and flow-aligned linear dichroism (flow-LD) spectroscopy. Both dyes exhibit high on/off ratios with improved brightness over DAPI

and Hoechst dyes. This enables lower dye loadings and/or illumination intensities, which, coupled to their low cytotoxicity, makes **1** and **2** attractive alternatives to existing stains.

1.2 Results and Discussion

1.2.1 Design and Synthesis

Probes were designed as DNA-targeting 'turn-on' fluorescent probes and incorporate three key design elements (Figure 1.1A). First, their optical properties are addressed through the incorporation of a donor-acceptor-donor π-system that enables excitation and emission wavelengths in the visible spectrum as well as high sensitivity toward their microenvironment.[15,16] Second, the pendant aryl arms control optical switching with emission enhancements expected when rotation is limited. Finally, recognition units may be incorporated via the 4 positions of the arms; for **1** and **2**, N-methylpiperazine was chosen, as, at physiological pH, protonation will result in a dicationic species suitable for electrostatic interactions with the phosphate backbone of DNA. With an aromatic core capable of interacting with nucleobases and charge spacing well matched to the interbackbone phosphate distance of 18.3 A , we anticipated that **1** and **2** were ideally suited as intercalators, though a groove binding mode is possible as well, due to their concave shape (Figure 1.1C, D).

1 is the product of the Begnelli reaction of 4-(4-methyl-1-piperazinyl) benzaldehyde, 4-(4-methyl-1-piperazinyl)acetophenone, and urea, isolated in 22% yield as a bright yellow solid. Reaction of 1,3-bis(4-fluorophenyl)-1,3-propanedione with boron trifluoride followed by nucleophilic aromatic substitution with N-methylpiperazine

afforded **2** as a bright orange solid in an overall yield of 11%. ^{1}H NMR ^{13}C NMR, HRMS, and IR characterized 1 and 2.

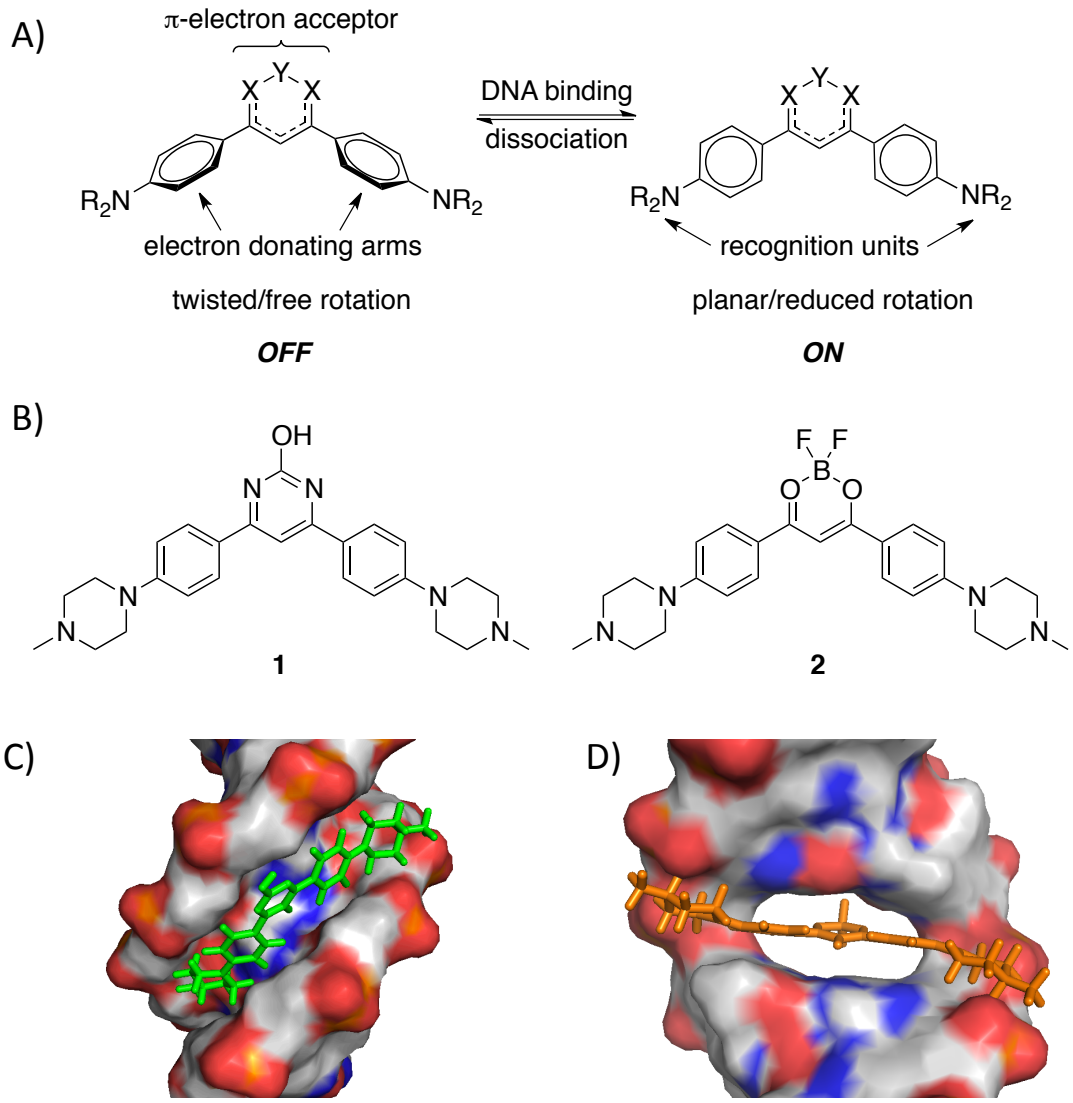

Figure 1.1 (A) Design strategy for DNA- binding, turn-on probes include a donor-π-acceptor core, rotatable arms that control emission, and R-group represents recognition units to interact with the phosphate backbone. (B) Chemical structures of probes. Possible modes of interaction of N-methylpiperazine substituted probe with DNA include (C) groove binding or (D) intercalation.

1.2.2 Spectroscopy and Computational Studies

Absorption and emission spectroscopy demonstrate that **1** and **2** are responsive to their chemical environment (Table 1.1). Both probes show moderate absorption enhancements in methanol and octanol compared to phosphate buffered saline (PBS). The absorption maximum of **2** is bathochromically shifted by 70 nm relative to **1** in all the solvents examined. As both dyes possess the same electron donating arms, the red shift observed for **2** is the result of a lower energy LUMO due to the increased electron-withdrawing ability of the propandionato-difluoroboron cores.

The emission of **1** is enhanced 80-fold in octanol compared to PBS, while, for **2**, a 30-fold enhancement was observed. The emission maxima of **1** range from 475 nm in octanol to 511 nm in ethylene glycol, and the emission maxima of **2** vary from 523 nm in methanol to 533 nm in ethylene glycol. The solvent-dependent emission enhancement is likely the result of the donor-acceptor π-system that yields an excited state with charge transfer (CT) character, while the rotational freedom of the pendant aryl arms may contribute to a twisted intramolecular CT (TICT) excited state. Φ_{em} appears to correlate with solvent polarity and higher in less polar solvents (octanol > methanol > ethylene glycol > PBS).

TD-DFT calculations (B3LYP 6-31G(d)) provide insight into the electronic structure responsible for the observed optical properties. **1** and **2** are largely isoelectronic with respect to their frontier molecular orbitals and related electronic transitions, which is not surprising given their similar architecture (Figure 1.2). The relevant excited states

Table 1.1 Optical Data 1 and 2

	$\lambda_{max, abs}$ nm	ε M^{-1}, cm^{-1}	$\lambda_{max, em}$ nm	$\Delta\upsilon$ cm^{-1}	Φ_{em}
PBS					
1	388	35,000	502	5850	0.003
2	469	40,000	535	2600	0.006
ethylene glycol					
1	410	33,000	511	4800	0.03
2	492	44,000	553	2200	0.05
MeOH					
1	392	39,000	493	5230	0.04
2	455	50,000	523	2860	0.07
octanol					
1	399	42,000	475	4010	0.24
2	464	51,000	527	2600	0.18
ctDNA[a]					
1	392	28,000	504	4200	0.11
2	472	38,000	556	3200	0.06
DAPI	350	22,000	451	6400	0.57
Hoechst[b]	350	47,000	452	6400	0.82

[a] [ctDNA] = 50uMin PBS, [dye] = 1.0uM in PBS. [b]Hoechst 33342

with significant oscillator strength ($f > 0.10$) are shown in Figure 1.2A. The calculated transition $S_0 \rightarrow S_1$ energies of 394 nm for **1** and 467 nm for **2** are in very good agreement with the experimentally observed values (Table 1.1). Both the HOMO and $HOMO^{-1}$ exhibit greater orbital contributions from the pendant aryl arms, while the LUMO shows

a greater contribution from the electron-withdrawing core. The polarization of the HOMO and LUMO confirms the notion of an excited state with CT character[17] which has been previously described for structurally related 4,6-diaryl-pyrimidones.[15,16] This CT state should be stabilized in polar solvents leading to the observed fluorescence quenching.

We next examined the optical response **1** and **2** upon exposure to calf thymus DNA (ctDNA). It was anticipated that probes interacting with DNA, either in groove-binding mode or as intercalators, would experience a less polar and/or more restrictive environment in which quenching processes would be limited.[12,15,18] In the presence of ctDNA, emission of the probes increases substantially: 40-fold increase was found for **1** and a 10-fold increase for **2** (Table 1.1) based on quantum yields. Interestingly, the excitation spectra of the bound probes were bathochromically shifted relative to the absorption maxima; in the case of **1**, $\lambda_{max,\ abs}$ = 392 nm and $\lambda_{max,\ ex}$ = 415 nm, while, for **2**, $\lambda_{max,\ abs}$ = 472 nm and $\lambda_{max,\ ex}$ = 501 nm. The bathochromic shift effectively increases the on/off ratios of the probes when exciting at the longer wavelengths; for **1** an on/off ratio of 75 is obtained with 405 nm excitation, and for **2** a ratio of 27 is obtained with 514 nm excitation.

In order to investigate the binding mode of **1** and **2** in more detail, we used flow-aligned dichroism (flow-LD)[19] in which DNA is aligned in a shear flow and the absorption is measured parallel and perpendicular to the flow direction. The DNA bases will be oriented perpendicular to the flow and thus have a strong negative LD signal centered around 260 nm. Any molecule that is bound to DNA will also be aligned and give rise to an LD signal, and the sign and amplitude of the LD signal is related to the

angle between its transition dipole moments and the DNA long-axis. The LD spectra for **1** and **2** are quite different with respect to each other in shape and magnitude (Figure 1.3A), and they also differ from their corresponding isotropic absorption spectra (Figure 1.3B-C). For **2** the magnitude of the peak at 475 nm, corresponding to the $S_0 \rightarrow S_1$ transition, indicates that the transition dipole is aligned roughly parallel with the DNA base pairs, an orientation that is consistent with an intercalated binding, as the $S_0 \rightarrow S_1$ transition dipole of **2** lies within the plane of the molecule. To assign the peak to a binding mode in a quantitative manner, we calculated the reduced linear dichroism (LD^r). The LD^r is directly related to the angle between the transition moment and the orientation axis through the following equation:

$$LD^r = LD / A_{iso} = 3 / 2 * S * (3 \cos^2\alpha - 1) \qquad (1)$$

where α is the angle between the orientation axis and the transition dipole moment and S is an orientation factor that is identical for DNA and ligands bound to DNA in the same sample. The LD^r for the 475 nm peak of **2** has a value that is very similar to the DNA band, confirming a binding angle close to 90^0 (Figure 1.3A).

The LD spectrum of **1** is most readily explained by a dominant groove-binding mode since the main transition at 410 nm gives rise to a very weak LD signal and an LD^r value close to 0. Interestingly we observe a distinct negative peak at 360 nm that is barely visible in the isotropic peak and corresponds to the weak $S_0 \rightarrow S_2$ transition ($f = 0.11$).

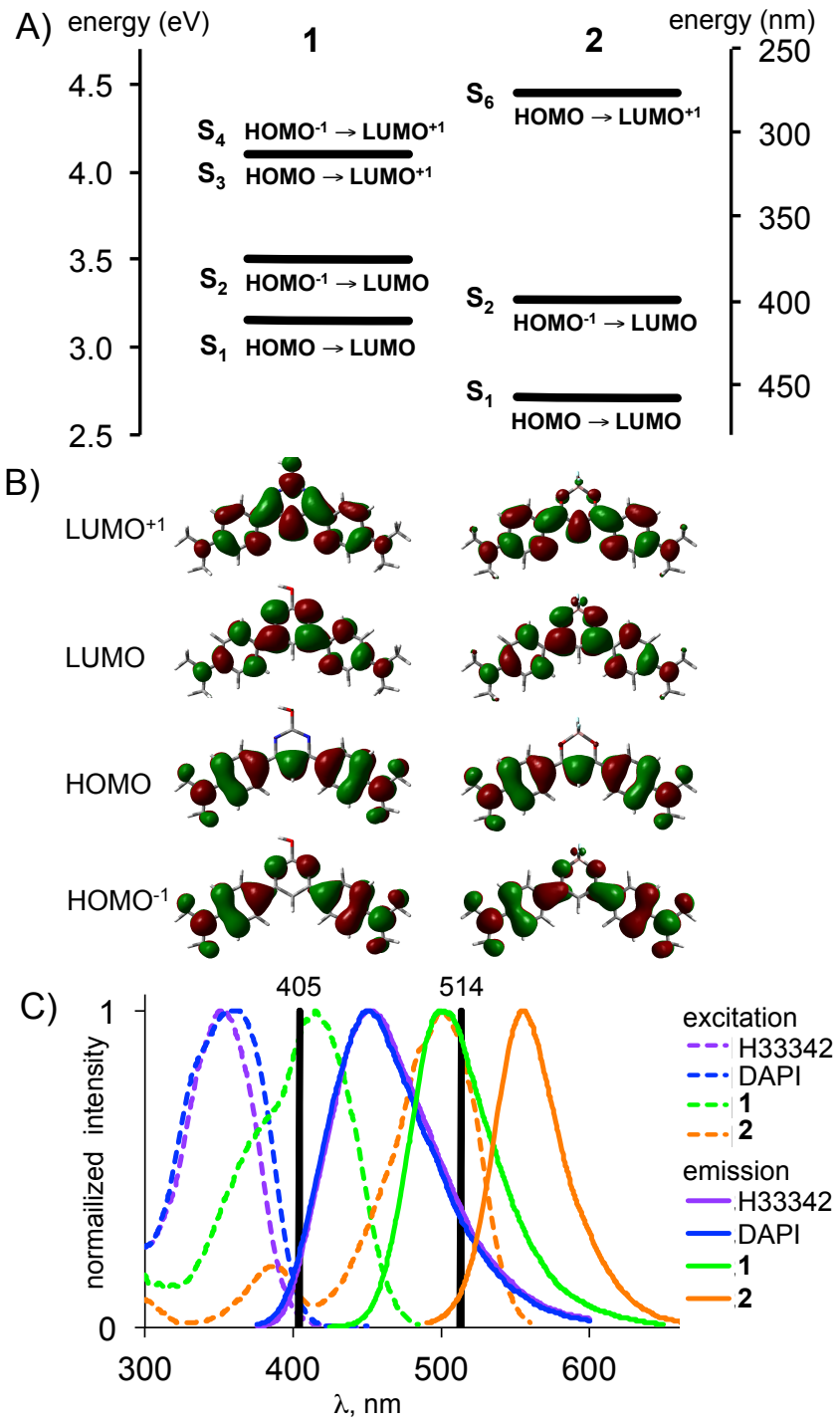

Figure 1.2. (A) Excited state manifold with relevant contributing molecular orbitals indicated TD-DFT B3LYP/6-31G(d) in MeOH using the SMD solvent model. (B) Frontier (±) molecular orbitals; 4-methylpiperazine is truncated to dimethyl amino groups. (C) Excitation and emission of **1** and **2** compared to Hoechst 33342 and DAPI bound to ctDNA; the 405 nm and 514 nm laser lines are indicated.

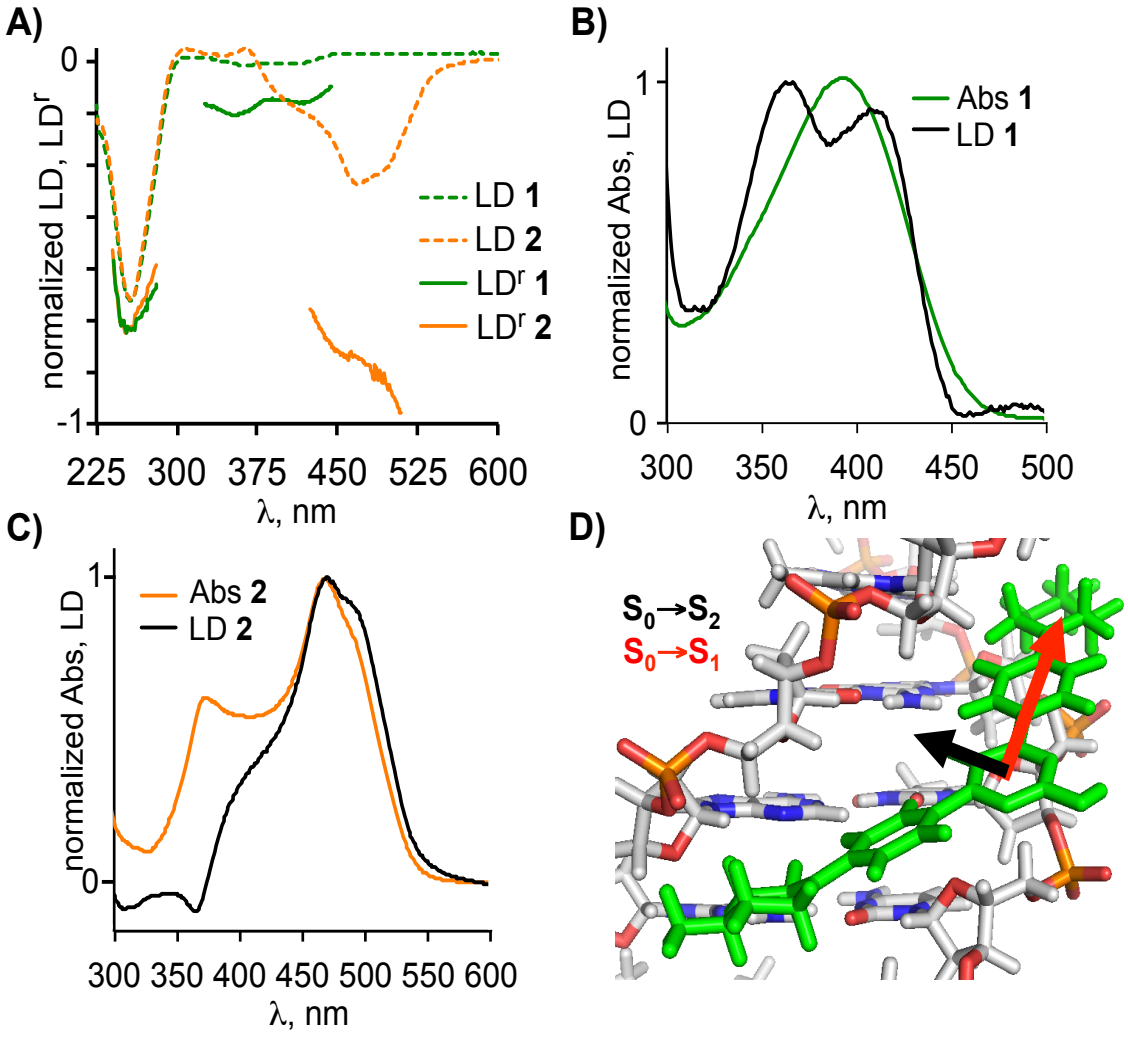

Figure 1.3. (A) LD and LD^r spectra for **1** and **2** bound to ct-DNA, normalized at 260 nm. Comparison of the normalized LD and isotropic absorption spectra of (B) **1** and (C) **2**. (D) Possible orientation of the $S_0 \rightarrow S_1$ (red) and $S_0 \rightarrow S_2$ (black) transition dipoles of groove-bound **1** based on the LD^r spectra.

This transition dipole is oriented perpendicular to the $S_0 \rightarrow S_1$ transition dipole (Figure 1.3D), and its stronger negative LD suggests that it is nearly perpendicular to DNA helix axis. This is in good agreement with groove binding, since such a binding geometry would position the $S_0 \rightarrow S_2$ transition parallel to the DNA bases (Figure 1.3D). The LD^r for the $S_0 \rightarrow S_1$ transition corresponds to an angle of 57^0, and while this is slightly larger than that for typical groove binders such as DAPI,[20] it may be the result of major groove binding where a slightly larger binding angle is possible.

1.2.3 Confocal Imaging

The performance of **1** and **2** as nuclear stains was evaluated using two common cell lines, HEK 293 and MCF-7. Representative images of **1** (λ_{ex} = 405 nm) with HEK 293 cells and **2** (λ_{ex} = 514 nm) with MCF-7 cells are shown in Figure 1.4. Both **1** and **2** were found to illuminate cell nuclei in a manner consistent with DAPI and Hoechst 33342 staining. For all imaging experiments cells were not fixed, no antifade reagent was used, and no rinsing was necessary to remove nonfluorescent unbound probe; optimum probe concentration was found to be in the range of 1 to 10 μM. The higher molar absorptivity of **1** at 405 nm makes it 6 to 10 times brighter than either DAPI or Hoechst 33342 at identical dye loadings and optical settings. The improved brightness of the probes allows for lower illumination intensities and/or dye loading, which is useful for prolonged imaging experiments using live cells or tissue. Both **1** and **2** exhibit low cytotoxicity: cells cultured in media with probe concentrations of 1.0 μM or less do not differ from untreated cells in time confluence, while higher probe concentrations, between 2.5 and 10 uM, are tolerated for up to 24 h. Longer exposure to **2** does lead to vesicular

accumulation in cells that otherwise appear healthy and continue to grow normally; no such accumulation was found for **1**.

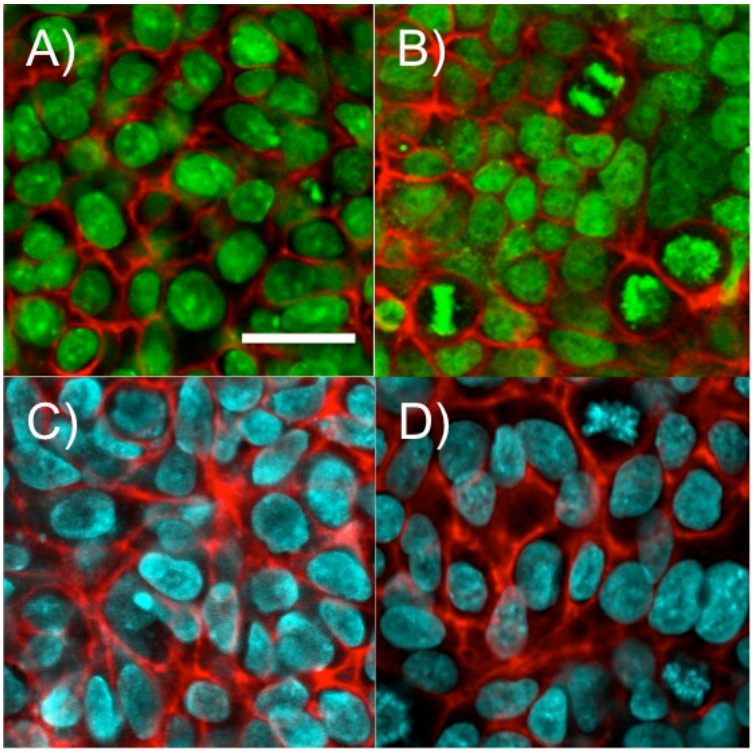

Figure 1.4. Comparison of nuclei stained with **1** and **2** (top) versus Hoescht 33342 and DAPI (bottom): (A) **1** with HEK293 cells, (B) **2** with MCF7 cells, (C) Hoechst 33342 with HEK293 cells, and (D) DAPI with HEK293 cells; Cellmask Deep Red (Life Technologies) is the membrane stain; scale = 20 μM.

1.3 Conclusion

We have designed and synthesized two DNA-binding, turn-on fluorescent probes that function as live cell compatible nuclear stains. Optical spectroscopy shows **1** and **2** exhibit emission enhancements upon exposure to nonpolar solvents and ctDNA. Linear dichroism studies reveal that, despite their isoelectronic structures, **1** is predominantly a groove binder while **2** is an intercalator. We have demonstrated their use in live cells, and both probes were found to be membrane permeable, exhibit low toxicity, and selectively stain cell nuclei. Overall the dyes compare favorably to widely employed vital nuclear stains DAPI and Hoechst 33342 in terms of brightness, photostability, and compatibility with common laser lines.

Chapter 2

BASE PAIR SENSITIVITY AND ENHANCED ON/OFF RATIOS OF DNA BINDING: DONOR-ACCEPTOR-DONOR FLUOROPHORES

2.1 Overview

We were interested in exploring previously synthesized probes **1** and **2** (Figure 2.1) interaction with specific DNA sequences (Table 2.1) in order to see what effect binding to these sequences may have on their turn-on capabilities. The optical properties of DNA-interacting dyes are strongly influenced by the unique chemical environment in which they reside.[21-25] Pronounced spectroscopic differences can be observed between probes interacting with DNA and unbound probes in solution while the identity of the neighboring bases serves to further modulate absorption and emission.[26-27] **1** and **2** stain the nucleus of living cells and exhibit low toxicity compared to traditionally employed dyes, such as DAPI and Hoechst 33242, [28,29,30] they possess longer wavelength excitation and emit in the green and yellow region of the spectrum, respectively. Access to longer wavelength excitation is important, as it lowers exposure of the cells to harmful UV excitation, avoids autofluorescence of endogenous fluorophores, i.e. “blue haze”, and allows use of standard laser lines in fluorescence microscopy.

The ON/OFF emission switching of **1** and **2** is dictated by the solvent and environmentally sensitive donor-acceptor-donor motif.[15,16] Unbound dyes are very weakly fluorescent, i.e. OFF, while DNA-bound probes fluoresce, i.e. emission is turned ON. Given the high sensitivity of these novel fluorophore scaffolds, and the reported base pair dependence of DAPI[31] and other fluorophores that interact with DNA,[25,32] we

undertook a photophysical investigation of the induced optical properties of **1** and **2** when bound to DNA with different sequences.

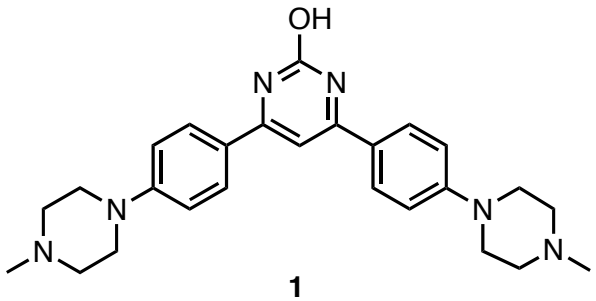

1

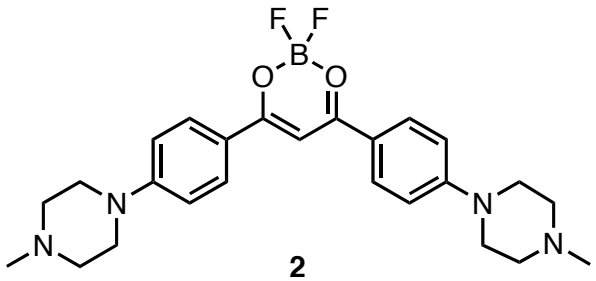

2

Figure 2.1. Chemical structures of DNA-binding donor-acceptor-donor fluorophores **1**, 4,6-bis(4-(4-methylpiper-azin-1-yl)phenyl)-pyrimidin-2-ol, and **2**, [1,3-bis[4-(4-methylpiprazin-1-yl)phenyl]-1,3-propandioato-κO, κO']difluoroboron.

We demonstrate that the emission from **1** and **2** is sequence dependent: while both dyes are brightly fluorescent when bound to DNA consisting of AT base pairs, the emission is almost fully quenched when bound to DNA containing only GC base pairs. Through steady state and time-resolved fluorescence spectroscopy, we study the spectral response of the dyes when bound to oligonucleotides with a central AT tract of increasing length and conclude that the emitting species is identical in all cases and originates from dyes bound to AT-rich regions. Electrochemical studies implicate electron transfer with GC base pair as a plausible quenching mechanism. Finally, we observe that the brightly

emissive, AT-bound probes exhibit significantly red-shifted absorption profiles. This bathochromic shift can be utilized to improve the signal-background ratio of the dyes both in solution-based measurements as well as in live cell imaging.

2.2 Materials

The synthesis of **1** and **2** was described;[28] the low solubility of **1** in acetonitrile necessitated the synthesis of **3** (Figure 2.2) in order to carry out electrochemical measurements. Self-complimentary oligomers with the sequences shown in Table 2.1 and ctDNA were obtained from Sigma-Aldrich. Phosphate buffered saline (PBS, pH 7.2) with 1.0 M NaCl was used for optical spectroscopy.

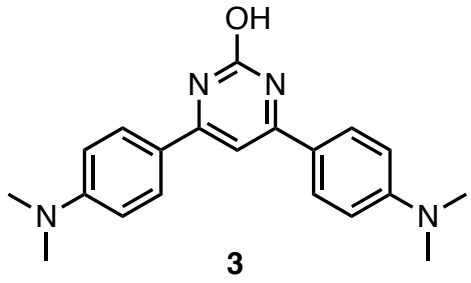

3

Figure 2.2. Structure of **3**, 4,6-bis-(4-(-dimethylamino)phenyl)-pyrimidin-2-ol.

Table 2.1 DNA Oligomer Sequences

Cmpd	sequence
0AT	5′-GGC GCG CGC C-3′
2AT	5′-GGC GCA TGC GCC-3′
4AT	5′-GGC GCA TAT GCG CC-3′
6AT	5′-GGC GCT TAT AAG CGC C-3′
8AT	5′-GGC GCT TAT ATA AGC GCC-3′
10AT	5′-GGC GCT TAT TAA TAA GCG CC-3′
12AT	5′-GGC GCT TAT TAT AAT AAG CGC C-3′
14AT	5′-GGC GCT AAT TAT ATA ATT AGC GCC-3′
24AT	5′-ATT ATT AAT TAT ATA ATT AAT AAT-3′
24GC	5′-GCC GGC GGC CGC GCG GCC GCC GGC-3′

2.3 Results

2.3.1 Absorption and Steady State Emission

1 and **2** is quenched in aqueous solutions, however, binding to calf thymus DNA (ctDNA) results in a significant emission enhancements for both **1**, which exhibits a groove binding mode, and **2**, an intercalator.[28] Given their alternate binding modes, we were interested in the influence of specific base pair interactions on the binding and photophysical properties of these dyes. Using UV-vis absorption and fluorescence spectroscopy, we investigated their optical response to the presence of an all AT oligomer (**24AT**, sequence in Table 2.1) and of an all GC oligomer (**24GC**) for comparison with ctDNA, which contains a mix of base pairs. Self-complimentary sequences can form

duplexes as well as hairpins depending on the concentration and ionic strength of the solution; to ensure preferential formation of the duplex, PBS (pH 7.2) with 1.0 M NaCl

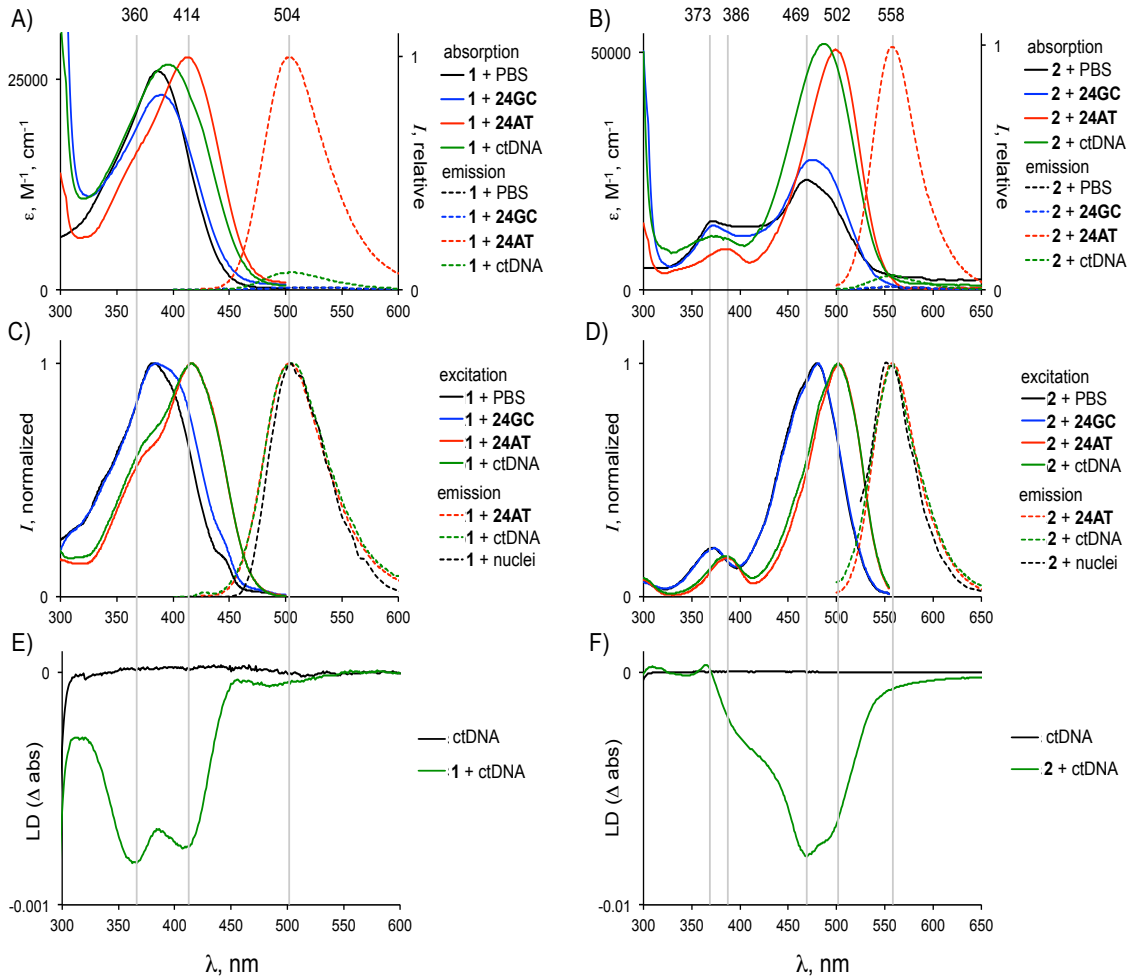

Figure 2.3. Molar absorptivity and relative emission intensity of **1** (A) and **2** (B); normalized excitation and emission spectra of **1** (C) and **2** (D); LD spectra of ctDNA and ctDNA with **1** (E) or **2** (F). The light gray lines show correlations of the optical transitions between graphs.

was utilized.[33,34] The absorption maxima of **1** and **2** in PBS alone and in the presence of ctDNA were previously reported,[28] but they are presented here again in 1.0 M NaCl for comparison (Figure 2.3A, B and Table 2.2); at high ionic strength, ε is somewhat attenuated. The absorption spectra of **1** and **2** in the presence of **24AT** differ markedly from those observed in PBS alone. For both dyes, the absorption maxima are red-shifted: 26 nm in the case of **1** and 30 nm for **2**. For **2**, the unbound probe shows pronounced hypochromicity, with ε approximately half of the value previously observed in methanol (ε = 50,000 $cm^{-1}M^{-1}$).[28] In the presence of **24AT**, ε is similar to the value in methanol (Table 2.2).

Table 2.2. Photophysical Parameters of **1** and **2**

	$\lambda_{max,abs}$ (nm)	ε ($cm^{-1}M^{-1}$)	$\lambda_{max,ex}$ (nm)	$\lambda_{max,em}$(nm)	Φ_{em}	$\Delta\upsilon$ (cm^{-1})
1						
PBS	387	26,000	382	523	<0.001	6700
+24GC	390	23,000	386	521	<0.001	6400
+24AT	414	28,000	416	503	0.12	4300
+ctDNA	396	27,000	416	507	0.02	5500
2						
PBS	469	23,000	479	557	0.002	3400
+24GC	475	27,000	481	558	0.002	3100
+24AT	499	51,000	502	558	0.14	2100
+ctDNA	487	52,000	502	558	0.02	2600

Exposure to **24GC** produces only moderate bathochromic shifts in the absorption maxima: 3 nm for 1 and 6 nm in the case of **2**. A slight hypochromic effect is seen for **1** when exposed to **24GC**, while for **2** with **24GC** a moderate hyperchromic effect can be observed. Not surprisingly, exposure to ctDNA results in bathochromic shifts of intermediate values, reflecting interactions with both AT and GC base pairs; for **1**, the shift is 9 nm, and for 2 the bathochromic shift is 18 nm.

The emission of **1** and **2** is also dependent on the DNA sequence. The emission profiles of either probe in the presence of **24GC** vary little from those observed in PBS alone (Figure, 2.3A, B). However, upon introduction of either **24AT** or ctDNA, the emission is enhanced significantly. A much larger emission enhancement is observed for **1** and **2** exposed to **24AT** compared to ctDNA. The emission maxima of probes bound to **24AT**, ctDNA, and cell nuclei are identical, indicating that emitting species is the same in all three cases.

The excitation spectra exhibit similar behavior to that observed for the absorption spectra, with bathochromic shifts observed for **1** and **2** when exposed to **24AT** or ctDNA. The lowest energy transition for **1** in the presence of **24AT** is observed at 416 nm while, for **24GC**, the transition is at 386 nm. In the case of **2**, the excitation maximum is at 502 nm in the presence of **24AT** and 481 nm in the presence of **24GC**. While the absorption maxima for the dyes were at intermediate values when exposed to ctDNA, the excitation maxima in the presence of ctDNA are identical to those observed for **24AT** (Figure 2.3C, D).

The linear dichroism (LD) spectra of **1** and **2** bound to ctDNA are presented here again in order to compare and assign the optical transition of **1** and **2**. For **1**, the overall magnitude

of the LD signal is low, consistent with groove binding (Figure 2.3E). Two peaks are observed: one at 414 nm and the other at 360 nm. The 414 nm peak corresponds well to the maximum in isotropic absorption and was assigned to a transition along the long axis of the molecule. The 360 nm transition is barely visible in the isotropic absorption and was assigned to a transition along the short axis of the molecule and is oriented perpendicular to the DNA long axis, as expected if the molecule is bound in one of the grooves. In the case of **2**, a much larger negative signal is observed in the LD spectrum, consistent with an intercalated binding mode (Figure 2.3F; note the difference in y-axis scale). Three overlapping peaks are visible: the most prominent peak is centered at 470 nm and aligns closely with the absorption maximum of **2** with **24GC**, and a strong red shoulder at 500 nm aligns very well with the absorption maximum with **24AT**; a smaller shoulder appears at approximately 400 nm, roughly aligning with the 386 nm transition apparent in the excitation spectrum of **2** in the presence of ctDNA or **24AT**.

2.3.2 Variation of AT Base Pairs

Given the marked difference in emission intensities upon exposure to GC or AT sequences, we decided to investigate the effect of increasing the AT content in oligonucleotides in defined steps from **0AT** to **14AT** (see Table 2.1 for sequences) on the absorption and emission of **1** and **2**. The absorption maxima of both dyes showed a gradual progression toward redder wavelengths with increasing AT base pair content (Figure 2.4), consistent with the difference observed **24GC** and **24AT**. The emission intensity also increased with a greater number of AT base pairs for both **1** and **2**. The red

shift in the absorption maxima correlates very well with increase in emission intensity, indicating that the ground state and excited state phenomena are linked.

Lifetimes of **1** and **2** across the series of **0AT** to **14AT** (Table 2.3, Figure 2.5) were examined. A pulse-limited lifetime component was observed in all samples, including those without DNA present, and was assigned to unbound dyes. The trace for **0AT** is dominated by a pulse-limited component (2.1 and 2.0 ns for **1** and **2**, respectively) is present for both dyes. While a stepwise progression was observed for the emission intensity and absorption maxima, the emission lifetimes were essentially constant at 2.7-2.8 ns for **1** and 2.4-2.5 ns for **2** going from **4AT** through **14AT**. Beginning with **4AT**, the longer lifetime component gains more amplitude, consistent with the increase in emission intensity when the AT tract is extended.

Table 2.3 Fluorescence lifetimes (in nanoseconds) of **1** and **2** bound to **0AT** through **14AT**

	0AT	**2AT**	**4AT**	**6AT**	**8AT**	**10AT**	**12AT**	**14AT**
1	1.0	2.1	2.8	2.7	2.8	2.8	2.8	2.8
2	1.3	2.0	2.4	2.4	2.5	2.4	2.5	2.5

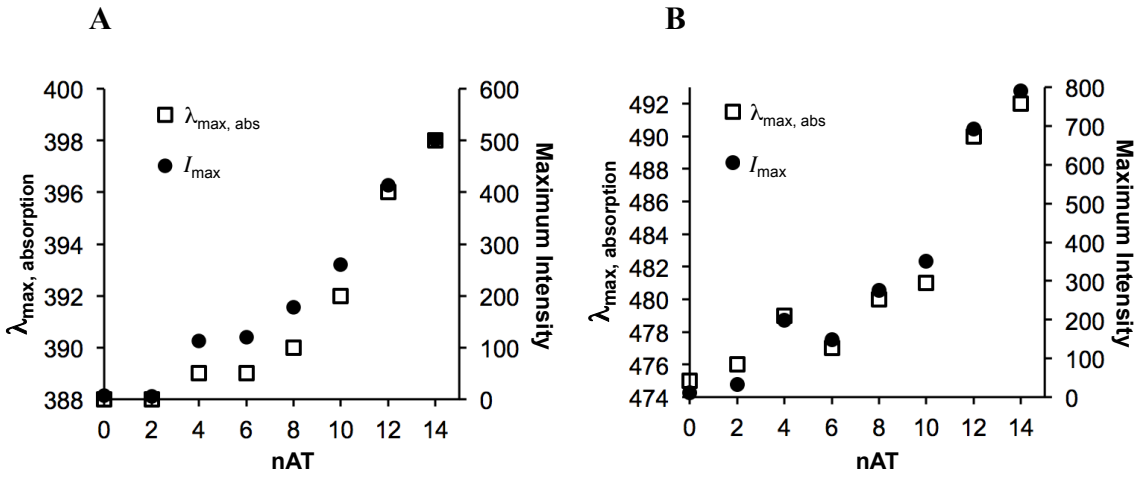

Figure 2.4. Absorption maxima and emission intensities of **1** (A) and **2** (B) as a function of AT tract length. For sequences, see Table 2. Absorption wavelengths and emission intensity increase with increasing length of the AT tract.

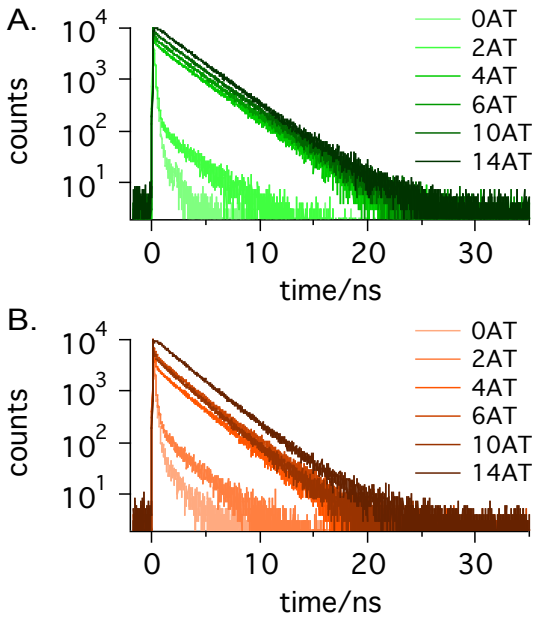

Figure 2.5. Emission lifetimes of **1** (top) and **2** (bottom) bound to the nAT series. For **4AT** through **14AT**, the emission lifetime does not change significantly, although the emission intensity increases.

2.3.3 Electrochemistry

The sequence dependent fluorescence demonstrates that increasing the length of AT tracts increases the emission intensity of the dyes. In the case of **2AT**, the emission is still very weak, suggesting that the proximity of the GC pairs may result in quenching. A Försters quenching mechanism can be ruled out based on the optical transition energies, implicating electron transfer as the most likely quenching mechanism. Guanine possesses a lower excitation oxidation potential than cytosine and, therefore, could serve as an electron donor, quenching photoexcited **1** or **2** via a photoinduced electron transfer (PET) mechanism.[35] However, cytosine has a lower reduction potential than guanine and therefore could serve as an electron acceptor should the dyes donate a high energy, photoexcited electron.[35-39] To distinguish between these two possibilities, we determined the one-electron oxidation and reduction potentials of the two dyes. Due to the low solubility of **1** in acetonitrile, a dimethylamino derivative, **3**, was utilized. As **1** and **3** possess identical π systems and electronic transitions, the small change in peripheral solubilizing groups should not produce a significant change in redox potentials. The electrochemical data **2** and **3** is presented in Table 2.4 along with redox potentials of guanine and cytosine in acetonitrile (oxidation) and DMF (reduction) as reported by Seidel et al.[35] While the redox potentials may vary with solvent, hydrogen bonding, stacking, and hybridization,[36-39] the redox potentials obtained implicate guanine as an electron donor to the photoexcited dyes. Neither guanine nor cytosine can serve as an

Table 2.4. Redox Potentials of **2**, **3**, **G**, and **C**

	Anodic process (V vs Ag/AgCl)	Cathodic process (V vs Ag/AgCl)	Fc potential (V vs Ag/AgCl)
2	+1.184	-1.240	+0.480
3	+1.360	-1.108	+0.484
G	+1.27[a]	-2.98[a]	
C	+2.36[a]	-2.57[a]	

[a]Originally reported vs NHE.[35]

electron acceptor, as the S_1 state of **2** and **3** places the photoexcited electron 1.3 to 1.8 eV below the LUMO of the nucleobases. Conversely, the oxidation potential of cytosine is 1.0 and 0.8 V greater than the observed for **2** and **3,** respectively. This excludes cytosine as an electron donor to the photoexcited dyes, even when accounting for the additional free energy shift (-0.55 eV) that has been observed in water,[35] leaving electron transfer from guanine to the dyes as the most likely mechanism of quenching.

2.3.4 Resolution of Bound and Unbound Dyes

The significant bathochromic shift in absorption and excitation maxima of the bound probes compared to free in solution suggests that it is possible to preferentially excite the bound dyes and thereby increase the signal-to-noise ratio.[40] This has practical implications for both improving the sensitivity of the nucleic acid detection in solution and improving the resolution in live cell imaging. Figure 2.6 shows the ratio of the emission intensities of DNA-bound dyes and dyes in PBS at increasing excitation wavelengths. While excitation near the absorption maxima will result in greater

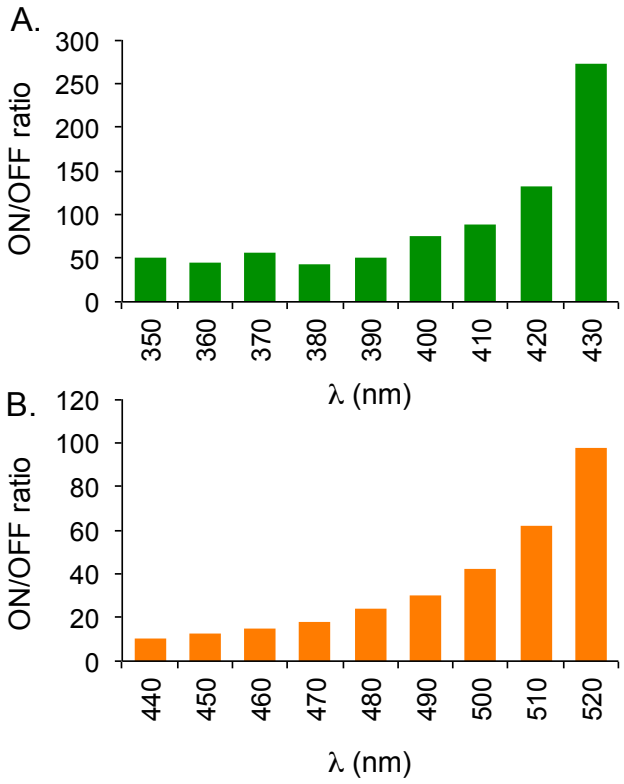

Figure 2.6. Contrast, i.e. ON/OFF, ratio of bound and unbound **1** (A) and **2** (B) as a function of excitation wavelength.

brightness ($\varepsilon \bullet \Phi_{em}$), shifting to longer wavelengths significantly increases the ON/OFF ratio of **1** and **2**. Figure 2.7 depicts live cell images resulting from excitation of **2** using the 476, 496, and 514 nm lines of an argon laser. A cross section of a single cell's nuclei is shown below each image. The shift in excitation to longer wavelength significantly affects the contrast between nuclei and the surrounding cellular matrix. With 514 nm excitation, the nuclei are clearly distinguishable, with very few puncta visible outside the nuclei. At short wavelengths, the contrast ratio between the nuclei and adjacent

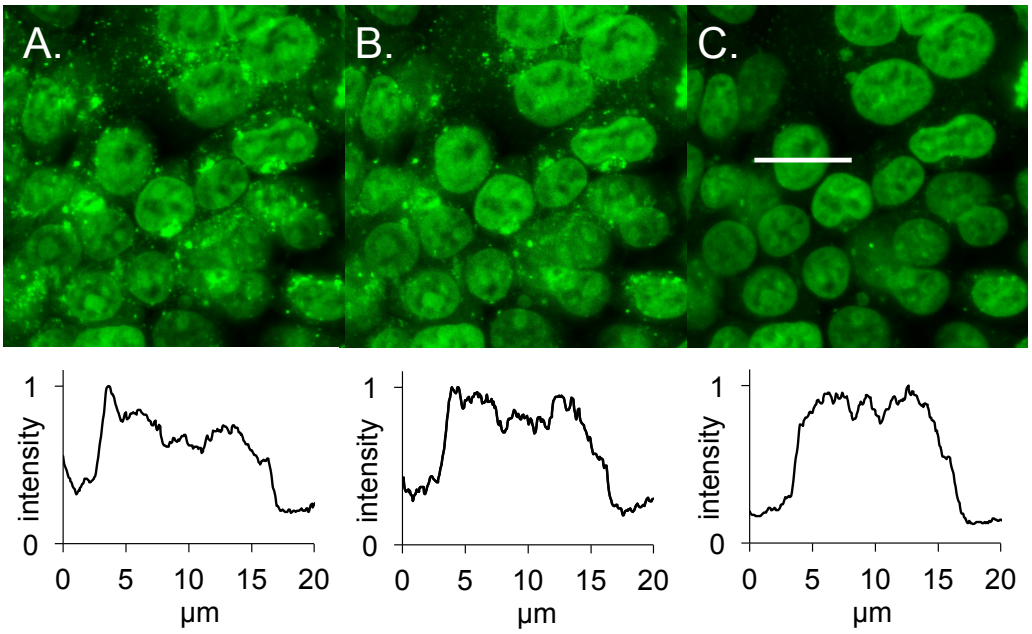

Figure 2.7. Longer wavelength of **2** (2.0 μM, 30 min incubation) leads to improved resolution of cell nuclei via selective excitation of the bound probe. Panels A, B, and C show identical regions of HEK293 cells excited using the 476, 496, and 514 nm lines of an argon laser, respectively. The plots below each image depict the cross section of a single cell (20 μM line shown in panel C), demonstrating quantitatively the improved resolution obtained with 514 nm illumination.

cellular material is diminished and numerous puncta are visible. It is not clear if these correspond to specific cellular substructures or if they are the result of vesicular accumulation of **2**. In either case, the population of probes localized to the cell nuclei is spectroscopically distinct and can be resolved from the off-target probes through longer wavelength excitation. (Figure 2.8).

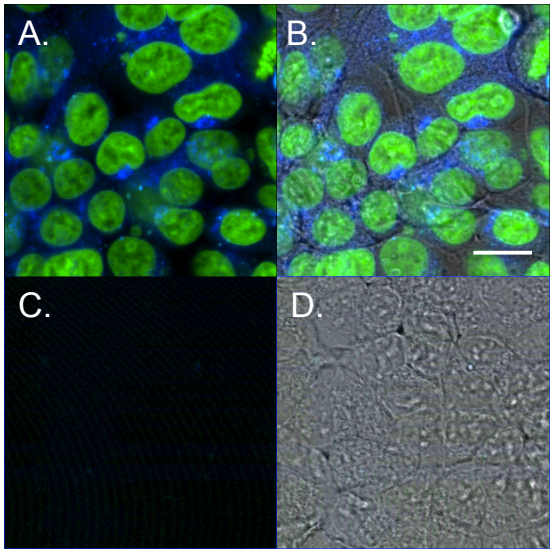

Figure 2.8. A) Dual excitation at 514 nm and 458 nm reveals the pool of nuclei bound (green channel, emission = 525 to 575 nm) and unbound 2 (blue channel, emission = 470 to 500 nm); B) overlay with phase contrast image of treated cells ([2] = 2.5 μM, exposure time = 45 min). C) Untreated HEK293 cells imaged under identical conditions show no emission in either the blue or green channels; D) overlay with phase contrast image of untreated cells. [2] = 2.5 μM, exposure time = 45 min

2.4 Discussion

The results of the sequence dependent absorption and emission studies reveal that both **1** and **2** exhibit turn-on emission when bound to sequences containing only AT base pairs while exposure to sequences containing only GC base pair does not produce a response significantly different from that observed in PBS alone. Binding to ctDNA also produces a turn-on emission response; however, the fluorescence appears to result only from dyes bound adjacent to AT base pairs, as the excitation and emission profiles are nearly identical to those observed for the dyes bound to **24AT**, indicating that in all three cases the emitting species are the same. Overall, the emission intensity of the dyes is lower

when bound to ctDNA than for **24AT**, demonstrating that the presence of GC base pairs contributes to quenching. Increasing the length of the AT tract, as in **0AT** to **14AT**, increases the emission intensity in a predictable manner. Thus, the distance from GC pairs appears to be the key parameter that controls the emission response.

The emission lifetime studies of dye binding to the **nAT** series reveal that the interaction with GC base pairs results in static or "sphere of action" quenching.[41] While the emission intensity increases across the series, with increasing AT content, no change in the emission lifetime is observed between **4AT** and **14AT** for either **1** and **2**. The emitting species for each of the respective dyes thus appear to experience the same electronic environment, as they have the same emission and excitation spectra as well as the same emission lifetimes. Quenching does not appear to be linked to the orientation of the dyes, as **1** is a groove binder while **2** exhibits and intercalating binding mode. This data, combined with the electronic transition energies excludes resonance energy transfer as a quenching mechanism. GC base pairs are frequently implicated in quenching via electron transfer mechanism.[31,35,42-43] In particular, guanine, with its relatively low oxidation potential, can serve as an electron donor to photoexcited dyes.[35,43]Our electrochemical characterization of **2** and the dimethyamino analog of **1** support the notion that electron transfer, or proton-coupled electron transfer, from guanine leads to quenching of these probes.

DNA-binding dyes find widespread use in solution-based assays, such as the quantification of DNA and in whole cell assays such as flow cytometry as well as imaging agents for fluorescence microscopy. In all of these applications, it is desirable to have a probe that exhibits turn-on emission upon binding with a high ON/OFF ratio. As

brightness of the bound dyes is the product $\Phi_{em}\varepsilon$, increasing either of these parameters will produce a higher ON/OFF ratio. Φ_{em} is enhanced by eliminating nonradioactive excited state processes such as the electron transfer discussed above. Increasing ε, i.e. hyperchromicity, is one means to enhance the overall brightness of the bound dyes; however, a bathochromic (or hyperchromic) shift also provides a means of increasing the relative brightness of the bound dyes. The absorption and relative excitation spectra of **1** and **2** (Figure 2.3A-D) show that both a hyperchromic effect and bathrochromic shift can contribute to produce a higher ON/OFF ratio for these DNA-binding dyes at longer wavelengths (Figure 2.6A, B). For both **2**, this effect is clearly demonstrated via confocal microscopy by comparing images obtained with closely spaced lines of an argon laser. The contrast between the pool of intranuclear and extranuclear dyes improves at longer excitation wavelengths and is optimally matched to 514 nm line. In the case of **1**, the 405 nm diode laser is the most viable option as an excitation source for confocal microscopy, though slightly longer wavelengths, ca. 420-430 nm would provide the greatest contrast ratio (Figure 2.6). For epifluorescence microscopy, where excitation is achieved via filter sets **1** is well matched to a CFP filter set, while **2** is compatible with YFP filter sets.

2.5 Conclusion

In summary, we have demonstrated that **1** and **2** are emissive when binding adjacent AT base pairs but are sensitive to the presence of GC pairs, likely due to quenching via a PET mechanism. The binding induced optical properties of the dyes were also explored. In contrast to DAPI and Hoechst 33342, the molar absorptivities of **1** and **2** are not attenuated upon binding. Both dyes also possess excitation maxima at visible

wavelengths and exhibit bathochromic shifts in their absorption maxima upon binding. This effect can be exploited to selectively excite the bound dyes, improving their contrast ratio in solution assays and in fluorescence microscopy of nuclei of live cells.

Chapter 3

ONE PROBE, TWO-CHANNEL IMAGING OF NUCLEAR AND CYTOSOLIC COMPARTMENTS WITH ORANGE AND RED EMISSIVE DYES.

3.1 Overview

As stated in Chapter 1 and 2 we had previously synthesized probes that incorporate a tunable donor-acceptor-donor scaffold and exhibit large emission enhancements, i.e. turn-on emission, upon binding to DNA.[28,51] These probes also have the ability to offset some of the limitations of common DNA probes on the market. An example of such probes are STYO® series, cyanine dyes, which offers longer wavelengths excitation and emission spectra, but their cationic structures make interactions with RNA, mitochondria or acidic vesicles unavoidable.[48-50] Unlike theses cyanine dyes such as the STYO® series, **1** and **2** can exist in a neutral form, allowing facile diffusion across membranes, yielding staining times and patterns similar to 4',6-diamindo-2-phenylindole (DAPI) or Hoechst 33342. Compared to the latter dyes, **1** and **2** are excited at longer wavelengths, 405 and 514 nm, respectively, eliminating the need for harmful UV excitation. A hypothesis that an expansion of the aromatic core of **1** or **2** could further shift their excitation (and emission) wavelengths providing additional imaging options compatible with yellow to red excitation sources while minimizing spectral overlap with common biomolecular tags such as blue, cyan or green fluorescent proteins was developed. Four expanded analogues (**4**-**7**) of **1** and **2** produced via introduction of one (**4**, **5**) or two (**6**, **7**) vinyl bridges between the electron-withdrawing core and the electron-donating aniline arms were explored. Optical spectroscopy reveals that **4** and **5** retain the or two (**6**, **7**) vinyl bridges

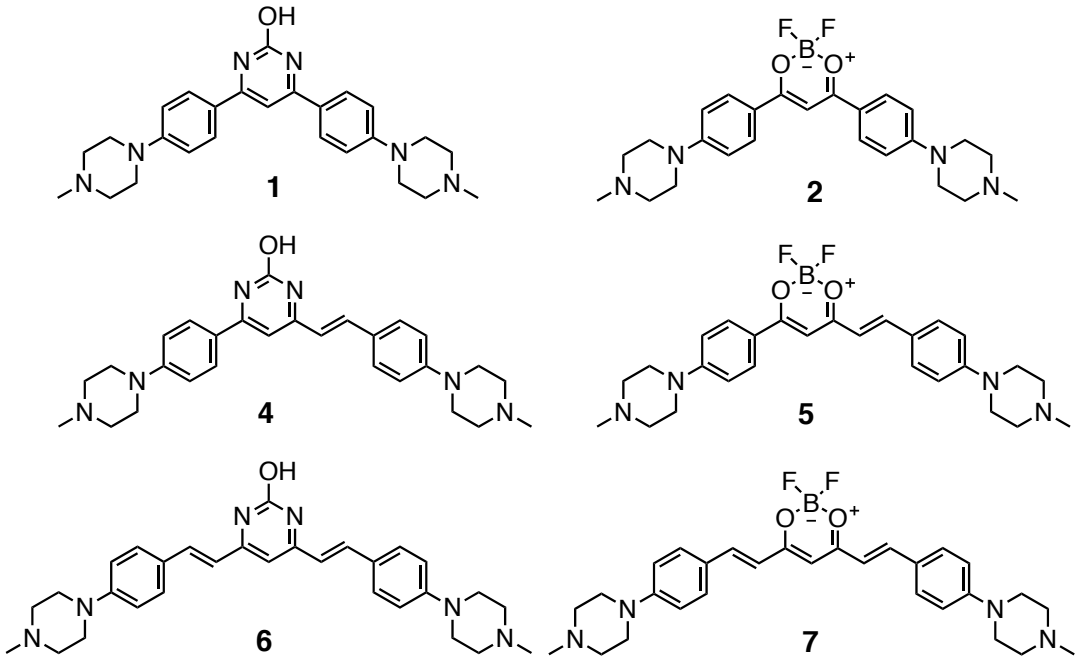

Figure 3.1. Chemical structures of parent DNA-binding dyes, **1**, **2**, and analogue compounds **4**-**7.**

between the electron-withdrawing core and the electron-donating aniline arms were explored. Optical spectroscopy reveals that **4** and **5** retain the high turn-on ratios of the parent compounds and furthermore, they can differentiate between DNA and other cellular binding sites through shifts in their excitation and/or emission spectra. Doubly substituted compounds **6** and **7** were also evaluated, but were found to not exhibit high turn-on ratios and did not demonstrate the ability to differentiate between DNA, RNA and/or other cellular targets. Confocal microscopy demonstrated that **4** and **5** are rapidly accumulated in live cells and broadly distributed throughout the cytosol and nucleus. Interestingly, the cytosolic and nuclear populations of **5**, and to a lesser extent, **4**, can be

separated into imaging channels, allowing two-color resolution of these cellular components. This attractive behavior can be linked to the ability of the dyes to respond to subtle changes in their chemical microenvironment. While a 'turn-on' response can result through interaction with RNA or any number of protein binding folds present in the cytosolic environment, probes bound to DNA exhibit redder excitation and emission spectra, which enables clear resolution of the nucleus. These dyes effectively combine the function of two separate dyes (i.e. a nuclear stain and a cytosolic stain) in a single probe. This behavior combined with their compatibility with standard laser lines (e.g. 458, 488, 514, 561 nm) or filter sets (e.g. GFP, FITC, YPF) suggests that these dyes should be useful probes for a number of imaging and screening applications.

3.2 Results and Discussion

3.2.1 Design and Synthesis

The parent compounds **1** and **2** were described in Chapter 1 and Chapter 2; these dyes are optimally excited with 405 and 514 nm laser lines, respectively. Many additional excitation sources are typically available on both epifluorescent and confocal microscopes and motivated the development of probes that would match excitation wavelengths in the blue to cyan portion of the spectrum (≈ 450 to 500 nm) as well as redder excitation sources beyond the 514 nm used for **2**. TD-DFT calculations at the 6-31G* level using the Gaussian quantum chemical suite[52] predicted that the optical transitions of these parent chromophores could be extended to redder wavelengths through the inclusion of one (**4**, **5**), or two vinyl groups (**6**, **7**) between the electron-donating arms and the electron-withdrawing core. The calculated spectra are shown in

Figure 3.2 suggest that the dyes should be compatible with excitation sources across the visible spectrum, including many common laser lines. The previously reported theoretical spectra for **1** and **2**, which are in good agreement with the experimentally observed spectra, are presented alongside the spectra for the analogue compounds, (**4**-**7**), as a reference.

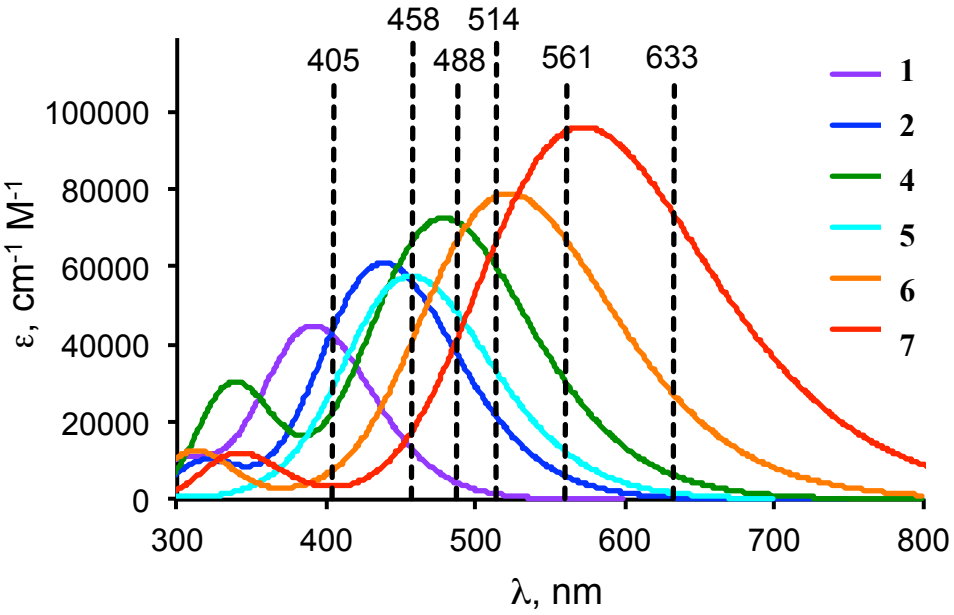

Figure 3.2. Predicted absorption spectra of **4**-**7** compared with **1** and **2**; with increased conjugation length, excitation energies are significantly red-shifted and a pronounced hyperchromic effect is also predicted. Dashed lines are common excitation sources available for confocal microscopy. TD-DFT calculations[52] were performed at the 6-31G* level, using the B3LYP basis set and Truhlar's SMD solvent model (MeOH).[53]

The synthesis of **4** and **5** relied on the common diketo intermediate, **8**, which was synthesized via condensation of 1-[-4-(4-methyl-1-piperazinyl)phenyl-ethanone with ethyl acetate (Figure 3.3). Cyclization of the diketo moiety with urea under acidic conditions produced **9**, with its electron-withdrawing hydroxypyrimidone core. Similarly, the electron-withdrawing core of **10** was prepared by reacting **8** with BF_3•Et_2O. Finally,

condensation of **9** or **10** with 4-(4-methyl-1-piperazinyl)-benzaldehyde produced **4** and **5**, respectively. Symmetrical dyes **6** and **7** were prepared in one step by condensation of 4-(4-methyl-1-piperazinyl)-benzaldehyde with 4,6-dimethyl-2(1H)-pyrimidone and difluoro-2-4-pentadionatoboron, respectively. The products were isolated in good to excellent yields as deeply colored solids that were readily soluble in polar organic solvents.

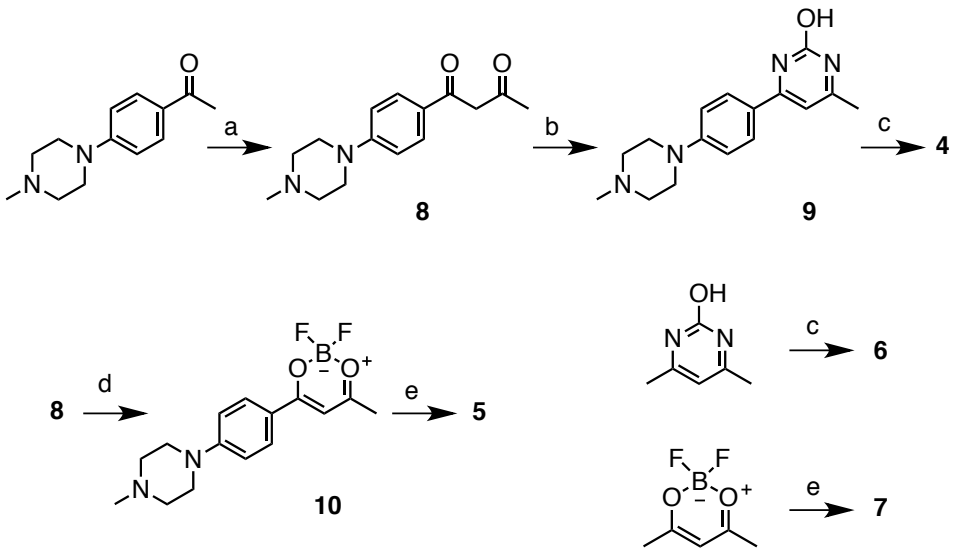

Figure 3.3. Synthesis of **4-7**. Reagents and conditions: a) NaH, EtOH, EtOAc, 0° C, 24h; b) urea, 10% HCl in EtOH, 80° C, 12 h; c) 4-(4-methyl-1-piperazinyl)-benzaldehyde, TMS-Cl, DMF, 90° C, 48 h; d) BF_3•Et2O, benzene, 25° C, 24 h; e) 4-(4-methyl-1-piperazinyl)-benzaldehyde, *t*Bu-NH_2, $B(OEt)_3$, toluene, 70° C, 48 h.

3.2.2 Optical Spectroscopy

The structures of **4-7**, with their donor-acceptor-donor motif, suggest that these dyes should be highly sensitive to the polarity of their microenvironment due to the formation of excited states with significant charge transfer (CT) character. Indeed, the fluorescence

of solutions of **4**-**7** in less polar solvents (e.g. CH_2Cl_2, EtOAc) can readily be detected by eye, while in more polar solvents; their emission is quenched (Figure 3.4). Binding to DNA may also induce enhancements in fluorescence, through reduction of the interactions with solvating water molecules as well as limiting twisting of the π system and reducing access to twisted intramolecular charge transfer (TICT) states. The optical properties of **4**-**7** in phosphate buffered saline (PBS) solutions, pH 7.2, in the absence and presence of ctDNA were evaluated.

The absorption and emission spectra of **4**-**7** are shown in Figure 3.4 with key photophysical parameters summarized in Table 3.1 and additional solvents are presented in Table 3.2. The most striking feature is the emission enhancement observed for the probes in the presence of ctDNA. For **4** and **5**, emission is increased 92- and 64-fold, respectively, with quantum yields of photoemission (Φ_{em}) of 0.44 for **4** and 0.13 for **5**. Moderate emission enhancements were observed for the probes in the presence of ctDNA for **6** and **7** when bound to DNA, with increases of approximately 10-fold for both dyes, while quantum yields remained relatively low, 0.02 for **6** and 0.003 for **7**. The poor optical performance of **6** and **7** is also observed in organic solvents (Table 3.2) and may be a result of their extended conjugation, which while achieving longer wavelength excitation and emission, could also lead to more polarized excited states and enhanced quenching.

Inspection of the absorption spectra also revealed marked changes **4** and **5**, with more moderate changes for **6** and **7**. Pronounced hyperchromicity and slight bathochromic shift were observed for the first pair of dyes. With molar absorptivities of

39,000 and 49,000 M^{-1} cm^{-1}, respectively, the overall brightness ($\varepsilon \bullet \Phi_{em}$) of the dyes are 17,000 M^{-1} cm^{-1} for **4** and 6,300 M^{-1} cm^{-1} for **5**. These values compares favorably with

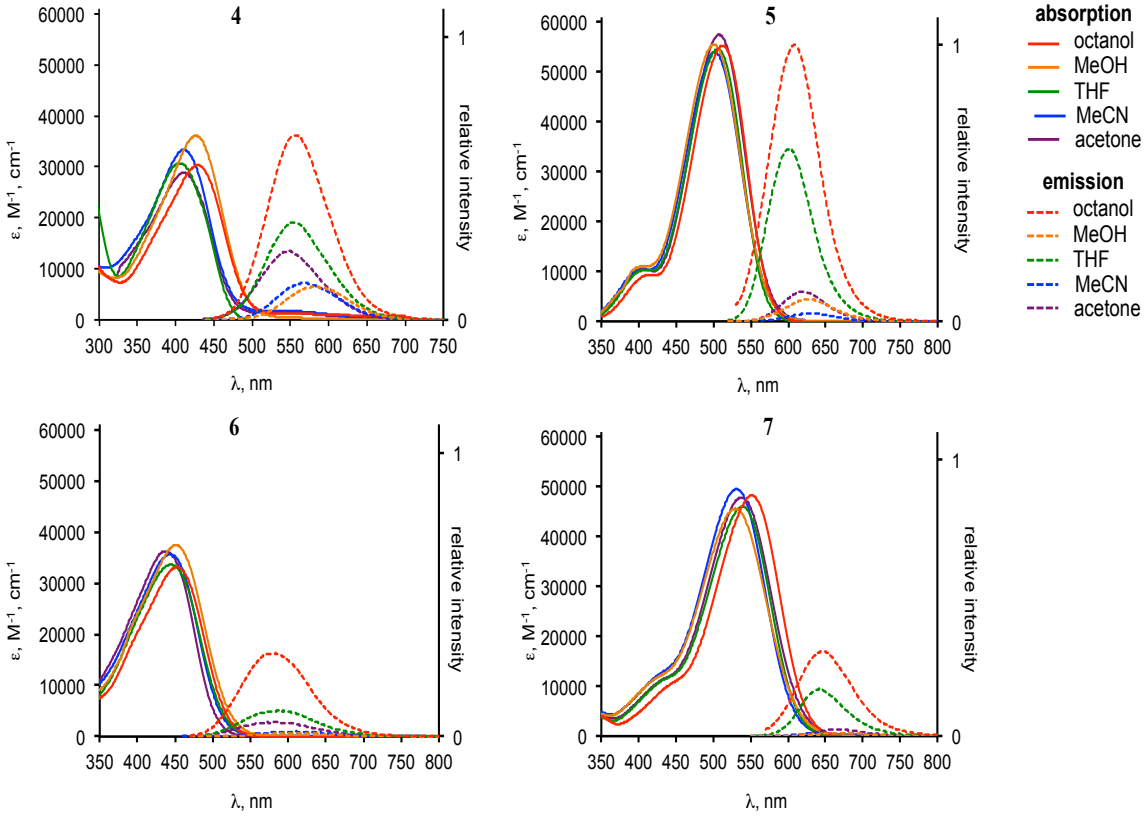

Figure 3.4. Absorption (solid line) and emission (dashed line) spectra of **1**-**4** in several protic (octanol, methanol) and aprotic (acetone, acetonitrile, THF) solvents. Emission intensity is highly sensitive to solvent polarity and viscosity with emission highest in octanol (red) and THF (green); this effect is consistent for both protic (octanol versusmethanol) and aprotic solvents (THF versus acetone/acetonitrile).

Table 3.1. Summary of optical parameters of DNA-bound dyes

cpd	$\lambda_{max, abs}$ (nm)	ε (M^{-1}, cm^{-1})	$\lambda_{max, em}$ (nm)	Φ_{em}[a]
4	452	39,000	582	0.44
5	532	49,000	636	0.13
6	557	16,000	617	0.02
7	449	23,000	683	0.003

[a] ± 10%

many commercially available probes such as DAPI[54] and the Hoechst family[55] of dyes. Though the molar absorptivities (Figure 3.2) of **6** and **7** were predicted to be higher than **4** or **5**, the observed values are much lower, and in the case of **7**, the appearance of a prominent peak at higher excitation energies (≈ 450 nm) suggests the formation of H-type aggregates.[56] For both **6** and **7**, solubility appears to be a limiting factor and aggregation may contribute to a lower observed molar absorptivity. Indeed, at concentrations approaching 5 μM, PBS solutions of **3** and **4** became slightly turbid, confirming that the dyes were aggregating. In organic solvents, such as methanol, the molar absorptivities are much closer to their predicted values and solubility is not an issue.

Table 3.2 Summary of photophysical parameters in organic solvents.

	1	**2**	**3**	**4**
acetone				
$l_{max, abs}$ / nm	410	507	436	538
e / cm^{-1} M^{-1}	28,800	57,500	36,200	47,900
$l_{max, em}$ / nm	552	624	585	661
ϕ	0.05	0.004	0.005	0.001
acetonitrile				
$l_{max, abs}$ / nm	410	501	444	531
e / cm^{-1} M^{-1}	33,300	54,000	35,600	49,500
$l_{max, em}$ / nm	570	627	613	652
ϕ	0.02	0.001	0.002	$\sim 10^{-4}$
tetrahydrofuran				
$l_{max, abs}$ / nm	405	506	445	539
e / cm^{-1} M^{-1}	30,700	54,600	33,600	46,000
$l_{max, em}$ / nm	558	602	598	638
ϕ	0.05	0.02	0.009	0.008
octanol				
$l_{max, abs}$ / nm	427	512	453	551
e / cm^{-1} M^{-1}	30,300	55,300	33,100	48,200
$l_{max, em}$ / nm	556	609	580	675
ϕ	0.14	0.04	0.03	0.01
methanol				
$l_{max, abs}$ / nm (calculated)	438	521	478	572
$l_{max, abs}$ / nm (observed)	426	500	452	529
e / cm^{-1} M^{-1}	36,100	55,600	37,400	45,600
$l_{max, em}$	579	628	627	675
ϕ	0.01	0.003	0.001	$\sim 10^{-4}$

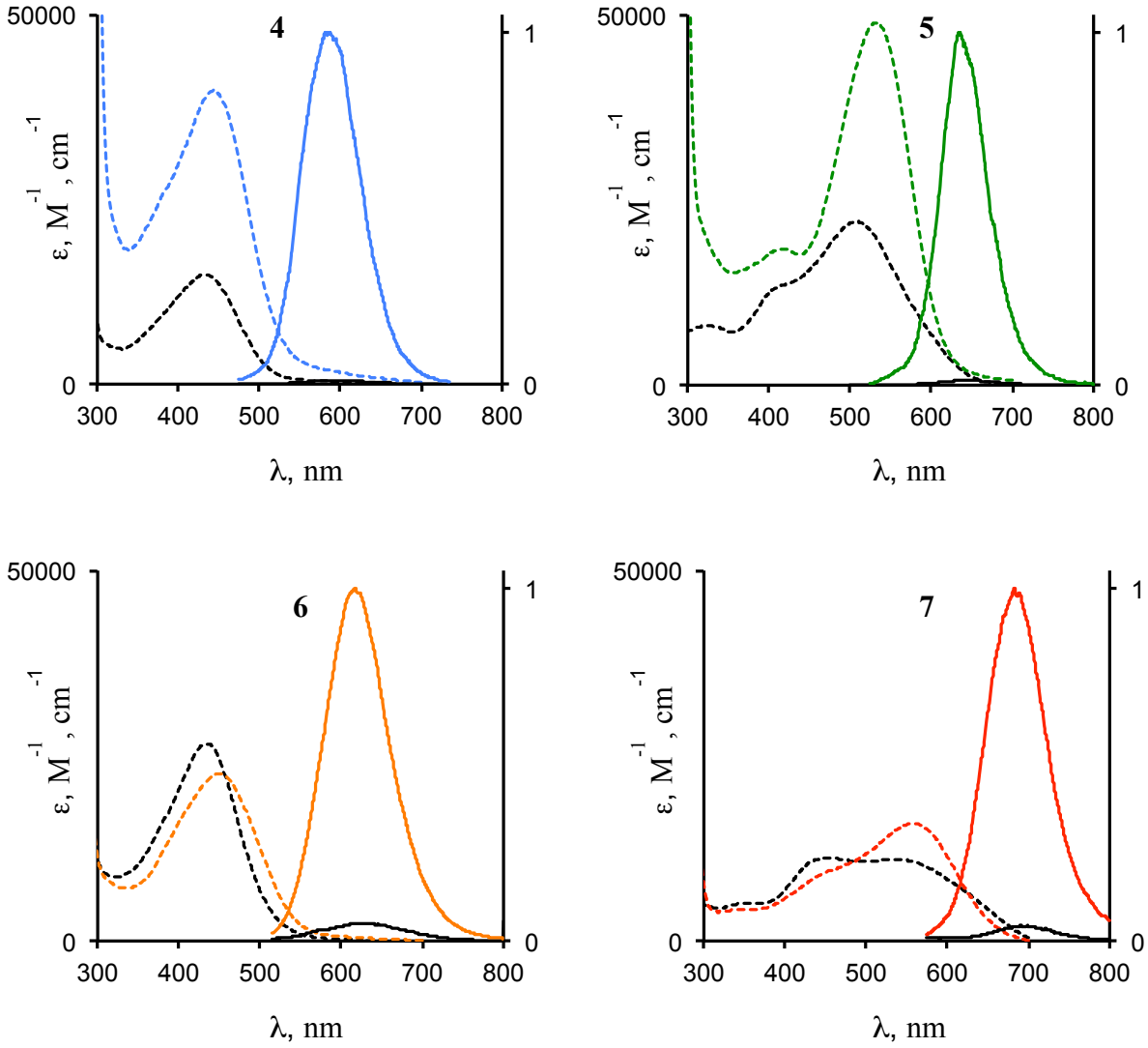

Figure 3.5. Absorption and emission spectra of 1 μM solutions of **4**-**7** (a-d, respectively) in PBS in the presence (colored lines) and absence (black lines) of ctDNA (500 μM). For **4** and **5** a significant hyperchromic effect is observed upon binding while emission enhancements are observed for all compounds binding to DNA. Quantum yields are noted in Table 3.1.

3.2.3 Confocal Microscopy

The fluorescence properties of the two promising dyes, **4** and **5** were examined, via confocal microscopy. Live adherent BT474, MCF7, and HEK293 cells were exposed to 2 μM of the probes by diluting 100x DMSO stock solutions directly into the cell culture media with rapid mixing; cell membranes were counterstained with CellMask Deep Red^{TM}. The probes rapidly accumulated in the cells and within 15 minutes, intracellular fluorescence could be observed. Given the spectral overlap with several laser lines, different excitation wavelengths for the dyes, including 405, 458, 476, and 488 nm were explored in the case of **5**. Interestingly, using two different excitation wavelengths and selecting specific emission windows, we observed that emission from different cellular components could readily be resolved into two channels, as depicted in Figure 3.6. In the case of **4**, the blue channel (figure 3.6a) revealed diffuse emission in the cytosol with nucleoli also visible; the green channel (Figure 3.6b) showed emission localized to the nucleus, with the nucleoli strongly fluorescent. Overlaying these two channels, and a third red channel corresponding to a plasma membrane dye (Figure 3.6c) reveals a clear contrast between the nuclear and cytosolic compartments, with emission from the nucleoli visible as cyan due to the overlap of the blue and green emission. For **5**, similar behavior was observed: the cytosol could be resolved into a blue channel (Figure 3.6d), while the nuclei were captured in the green channel (Figure 3.6e). In the case of **5**, staining of the nucleoli was not observed in either the blue or green channels, contrasting with the staining pattern of **4**. Additionally, the demarcation between the cytosol and nucleus is much clearer in the case of **5** as virtually no cyan fluorescence is visible to the eye in Figure 3.6f.

To gain some insight into the origin the two pools (blue and green channels) of fluorescent probes, we obtained the emission spectra from different regions of the cells, using the λ mode of the microscope, and compared them with possible cellular targets. Not surprisingly, the emission of both **4** and **5** from the nucleus corresponds very well with the emission spectra of the dyes in DNA solutions (Figure 3.7a and 3.7b). Nucleoli are centers of ribosome synthesis and we hypothesized that **4** may be interacting with RNA at these sites, yielding a complex with a different optical signature than that observe for **4** + DNA. The optical properties of **4** were then examined in the presence of RNA (Figure 3.7a) for comparison with the spectra of **4** + DNA and the emission of **4** from the nucleoli. Both the emission and excitation spectra of **4** + RNA show small (≈ 10 nm), but non-trivial blue shifts compared to the spectra of **4** + DNA. The emissions from the cytoplasm and from the nucleoli are also blue-shifted relative to the emission spectra observed for **4** + DNA or from the nucleus (excluding the nucleoli). The most important feature that distinguishes RNA and DNA spectra, is the presence of a broad "red" shoulder in the excitation spectrum of **4** + DNA (Figure 3.7a). At approximately 500 nm, this shoulder is half the height of the excitation maximum (450 nm); in the case of **4** + RNA, the height is only about 10% of the maximum value. The K_D values for **4** + DNA and **4** + RNA, obtained from saturating titrations (Figure 3.8), are very close at 2.5 and 2.9 μM, respectively. These results are consistent with the observed staining pattern with areas rich in both RNA and DNA overlapping in the blue and green channels.

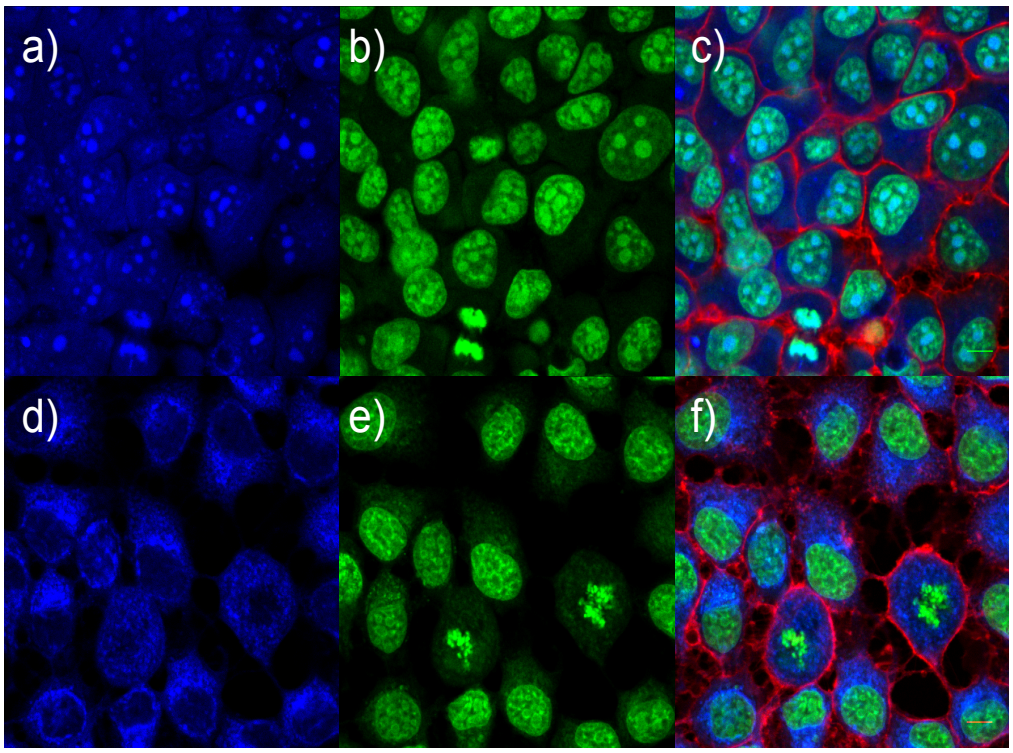

Figure 3.6. Confocal fluorescence microscopy of live BT474 cells treated with **4** (top row) and MCF7 cells treated with **5** (bottom row). Emission in the cytosol is resolved into the blue channel (a,d), while the nuclei are visualized in green (b,e). The overlays of the two channels, plus a red channel for the membrane stain are at the right (c,f). Excitation wavelengths and emission windows are shown in Figure 3.7. Scale bars are 10 μm.

Thus, **4** bound to DNA can be selectively excited with the 496 nm laser line and allowing clear resolution of the cell nuclei into green channel shown in Figure 3.6b. Excitation at 458 nm can result in emission from **4** interacting with RNA or DNA as well as complexes of **4** with any other possible binding folds present in the complex cellular milieu.

The lack of nucleoli staining with **5** suggested that RNA was not a major intracellular target of this dye. Indeed, while the K_D value for **5** + DNA was found to be 0.6 uM (Figure 3.8), the K_D for **5** + RNA could not accurately be measured due to inner filter effects at high concentrations and is greater than ~10 μM. Therefore, the possibility that **5** may interact with hydrophobic pockets of a protein to produce the blue channel shown in Figure 3.6d and the cytoplasmic emission shown in Figure 3.7 was examined. Human serum albumin (HSA) is a globular carrier protein with multiple binding sites[57] and is a suitable test protein for examining the binding mode of **5** to hydrophobic pockets. The emission of **5** in the presence of HSA is blue-shifted by 20 nm relative to the spectrum of **5** + DNA and matches very well with the emission obtained from the cytosol of cells treated with **5**. While the excitation spectra of **5** + DNA and **5** + HSA overlap significantly and excitation at 514 nm results in the emission from both populations, the emission spectrum of **5** + HSA has a strong blue edge that is not presented in the spectrum of **5** + DNA. This emission is captured in the blue channel and is limited to the cytosol. Conversely, excitation at 561 nm favors the DNA-bound population, which combined with the green channel capturing emission between 650-700 nm, leads to emission being almost exclusively from the nucleus.

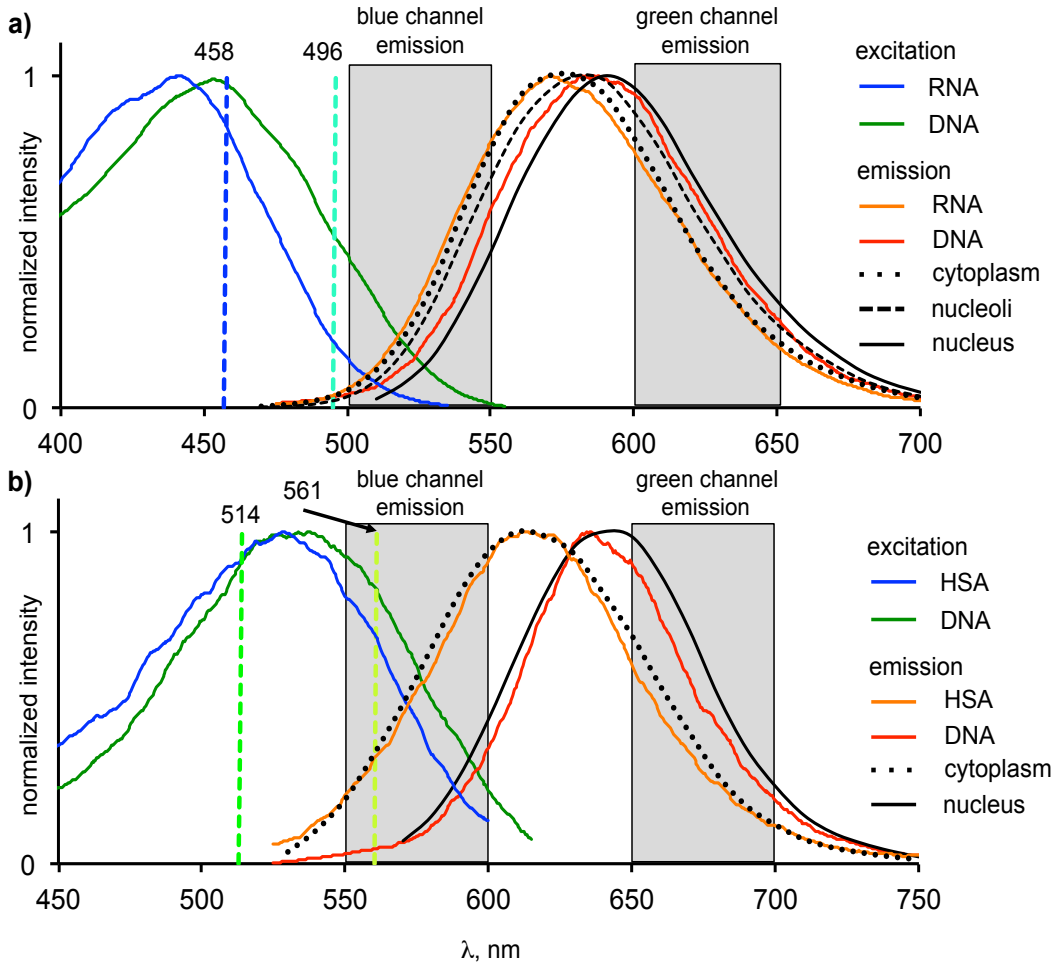

Figure 3.7. Comparison of excitation and emission spectra overlaid with imaging parameters for blue and green channels in Figure 3.6. **a)** Excitation and emission spectra of **4** in complex with RNA or DNA compared to emission from the cytoplasm, nucleoli and nucleus. **b)** Excitation and emission spectra of **5** in complex with HSA or DNA compared to emission from the cytoplasm and nucleus.

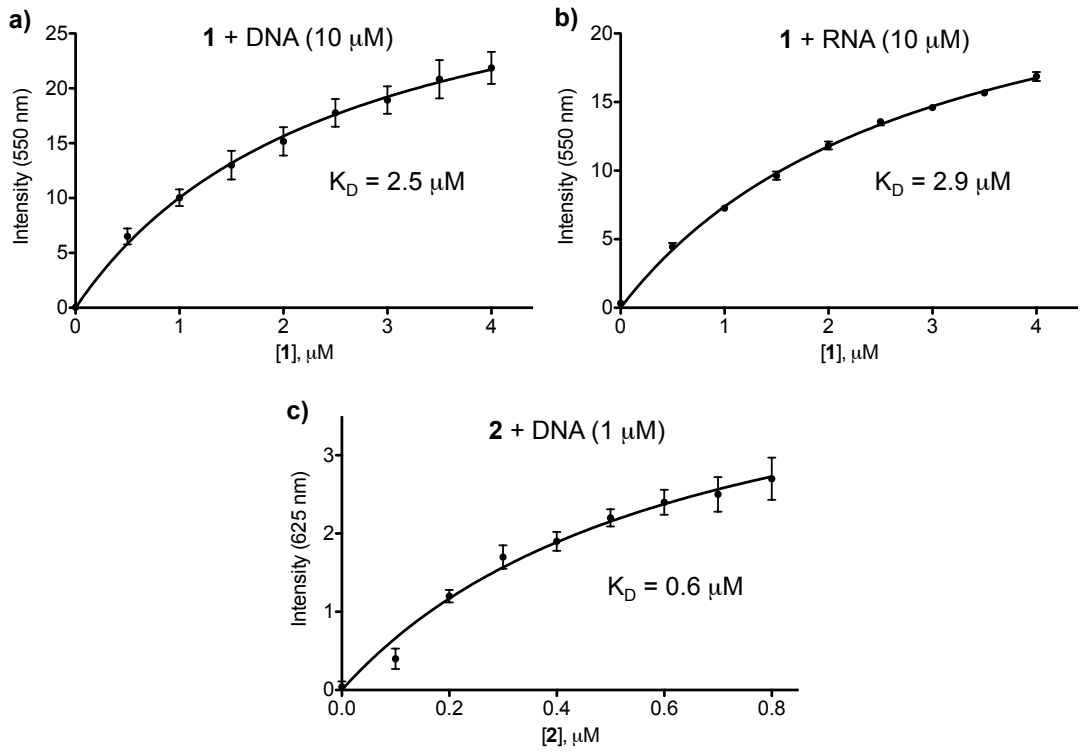

Figure 3.8. Determination of K_D values for a) **1** + DNA, b) **1** + RNA and c) **2** + DNA. Fluorescence was monitored at 550 nm for **1** and 625 nm for **2**. Data was plotted and analyzed with Prism 5. No saturation was observed for **2** + RNA over the concentration range tested; inner filter effects preclude measurements for [**2**] > 5 μM, as A > 0.2.

3.3 Conclusion

Orange and red emissive DNA-binding dyes, **4** and **5**, that exhibit high turn-on ratios and attractive staining patterns in live cells have been synthesized. Compared to commercially available nucleus stains, these new compounds offer a few advantages. First, they fill a spectroscopic gap between some of the most commonly employed nucleic acid dyes, such as the blue-emissive DAPI or Hoechst 33342 and red-emissive DRAQ5.[48] Second, in addition to staining cell nuclei, they can also serve as cytosolic stains, with each compartment easily resolved into a unique color captured in separate

imaging channels. While some commercially available compounds do stain both the nucleus and cytoplasm, they do not provide clear delineation of the two compartments, whereas **4** and **5** do. Acridine orange is one well-known dye that does exhibit two color staining, however, in lab testing with this dye uptake of acridine orange required longer exposure times (2 h) compared to **4** and **5**. Finally, these dyes demonstrate a more general property of fluorophores that can be employed to simultaneously image multiple targets in unique channels. Spectroscopic characterization of specific and "nonspecific" staining may reveal small, but non-trivial shifts in excitation or emission wavelengths that allows resolution of distinct populations of fluorescent probes.

Chapter 4

TWO-PHOTON SPECTROSCOPY AS A NEW METHOD FOR DETERMINING THE DNA BINDING MODE OF FLUORESCENT NUCLEAR DYES

4.1 Overview

Fluorophores that disp0lay enhanced fluorescence upon binding with DNA have been utilized in fluorescence microscopy as well as quantifying nucleic acids in gel electrophoresis and flow cytometry.[61] The binding interactions of external molecules with DNA often result in a significant change in their properties, which has an important impact on physiological functions.[62] Thus, the binding mode is crucial parameter for drugs targeted at DNA. DNA binding molecules interact with DNA through intercalation or groove binding as represented in Figure 4.1A and B, respectively. Common effects of DNA intercalative drugs inhibit cell growth, cell transformation, and cell death, which have applications as antitumor, antibacterial, and antiparasitic agents.[63] Several DNA groove binding drugs act by interfering with cellular processes, which target enzyme and protein access to DNA.[64] The mechanism of binding is key to the performance of both DNA-targeting therapies and fluorescent probes. While basic design principles are proposed, the binding modes of many dyes cannot be unambiguously assigned based on either structure or through the use of many well-established spectroscopic techniques. Therefore, distinguishing between an intercalator and groove binder is critical for the design of DNA-targeted drugs and fluorescent probes.

Qualitative methods have been employed to elucidate the binding modes of external molecules to DNA.[62] However, a combination of select methods must be used to

determine the DNA binding mode with certainty.[65] New methodologies, such as two-photon absorption (TPA), can provide a powerful tool to examine the photophysical properties of fluorescent organic molecules in biological systems.[66-68] TPA is a nonlinear technique that can be used with high sensitivity to understand the changes in the chromophore DNA binding environment, charge transfer character, and excited-dipoles.[69-71] The first results of two-photon spectroscopy to diagnose the DNA binding modes of small fluorescent molecules with ctDNA will be presented. The change in the TPA cross-section (σ) was examined to assess the binding mode based on the DNA electric field induced perturbation of the dye's transition dipole. A series of dyes (Figure 20) were investigated to demonstrate the methodology. These fluorophores illustrate a general scaffold for DNA binding dyes, which include linear, crescent, or planar structural motifs.

4.2 Synthesis and Steady State Spectroscopy

Reaction of 4,6-bis(4-fluorophenyl)pyrimidine[72] with N-methylpiperazine by nucleophilic aromatic substitution afforded **11** with an overall yield of 41% (Figure 4.2). The Biginelli reaction of 4-(4-methyl-1-piperazinyl)benzaldehyde, 4-(4-methyl-1-piperazinyl)acetophenone, and urea yielded **12**.[28] The steady-state absorption spectra, emission spectra, and quantum yield data of **1**, **11-15** were found when bound to ctDNA (Figure 4.3-4.8, and Table 4.1).

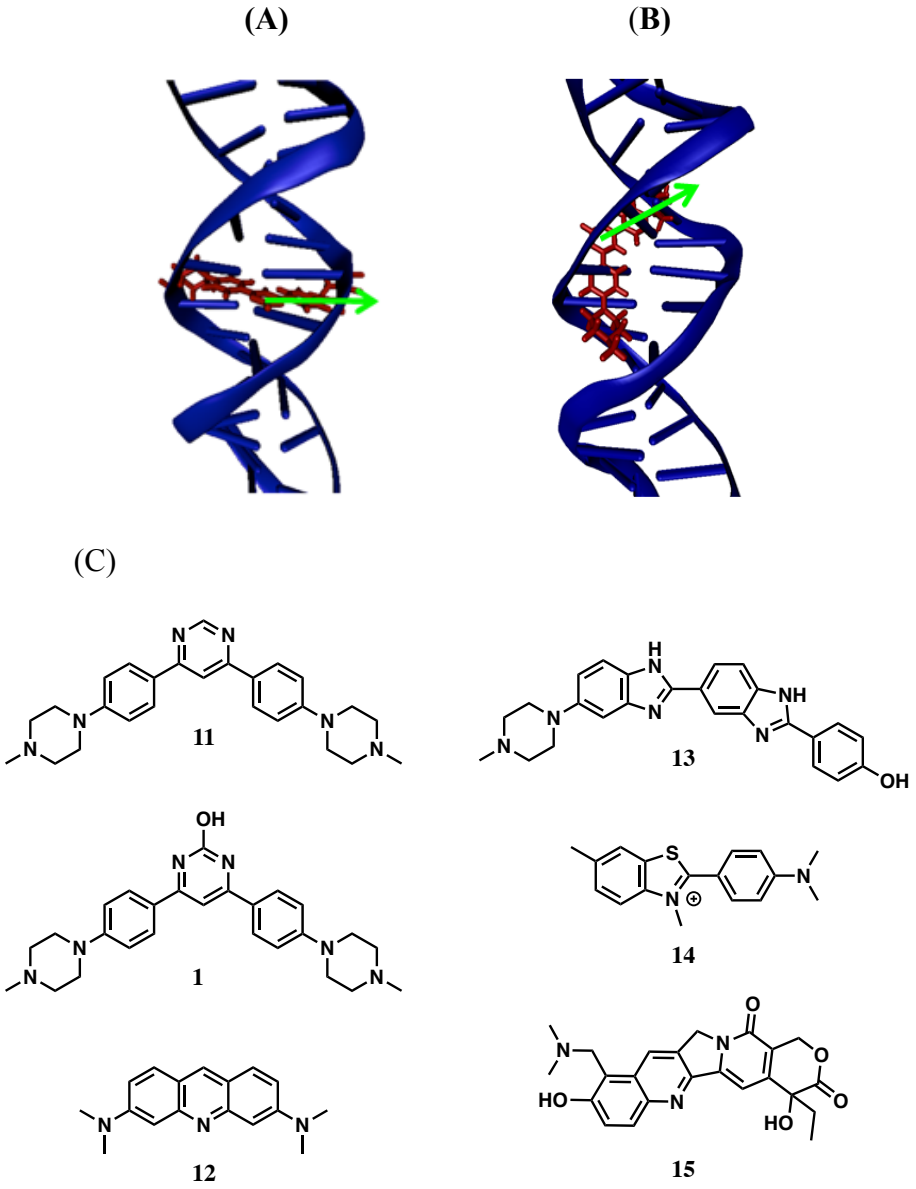

Figure 4.1. (A) Intercalative and (B) groove binding modes. Orientation of $S_0 \rightarrow S_1$ transition dipole is shown in green. (C) Chemical structures of 4,6-bis(4-(4-methylpiperazin-1-yl)phenyl) pyrimidine (**11**), 4,6-bis(4-(4-methylpiperazin-1-yl)phenyl) pyrimidin-2-ol (**1**), acridine orange (**13**), and Hoechst 33258 (**14**), thioflavin t (**15**), and topotecan (**16**).

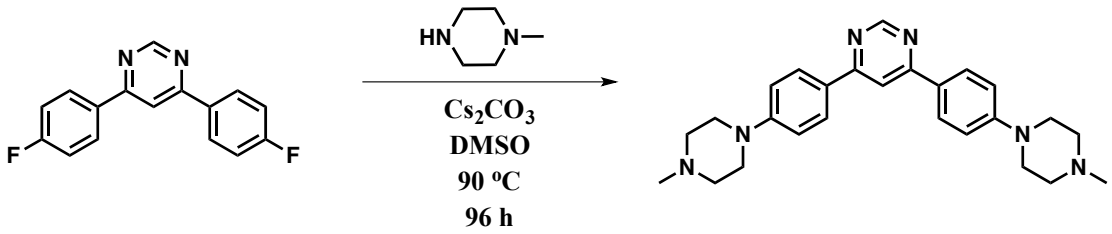

Figure 4.2. Synthesis of **11**

4.3 Two Photon Absorption Spectroscopy

It has been shown that the local electric fields have an influence on the TPA cross-section.[73-75] The TPA cross-section of triphenylamines with N-methyl benzimiadazolium moiety terminated branched dyes have been investigated, and it was reported that the TPA cross-section enhances 10-fold upon groove binding with DNA.[76,77] A TPA cross-section enhancement for the characterization of groove binding molecules similar to Dumat et al.[76] is also presented. However the TPA cross-section change can be attributed to the DNA electric field influence on the dipole of the binding molecule. The change in the TPA cross-section is analyzed to determine the DNA binding mode based on the orientation of the binding agent relative to the DNA helical axis. A groove binding molecule will have a dipole oriented more parallel to the DNA electric field resulting in an enhanced TPA cross-section upon binding. Contrarily, an intercalating molecule will have a dipole aligned more perpendicular to the DNA electric field leading to a decreased TPA cross-section upon binding. A groove binding molecule will exhibit an increased induced dipole, while an intercalating molecule will have a decreased induced dipole due to the DNA electric field perturbation. It was reported that DNA has the capacity to accumulate an electric field.[78,79] Additionally, it has been shown that tethered dsDNA

monomers, dimers, and trimmers exhibit different extension lengths when an external electric field is applied.[80-82] This suggests that the electric field (dipole) of DNA changes with increasing DNA concentration for a given system. Therefore, a change in the TPA cross-section of the dye upon binding with DNA is expected.

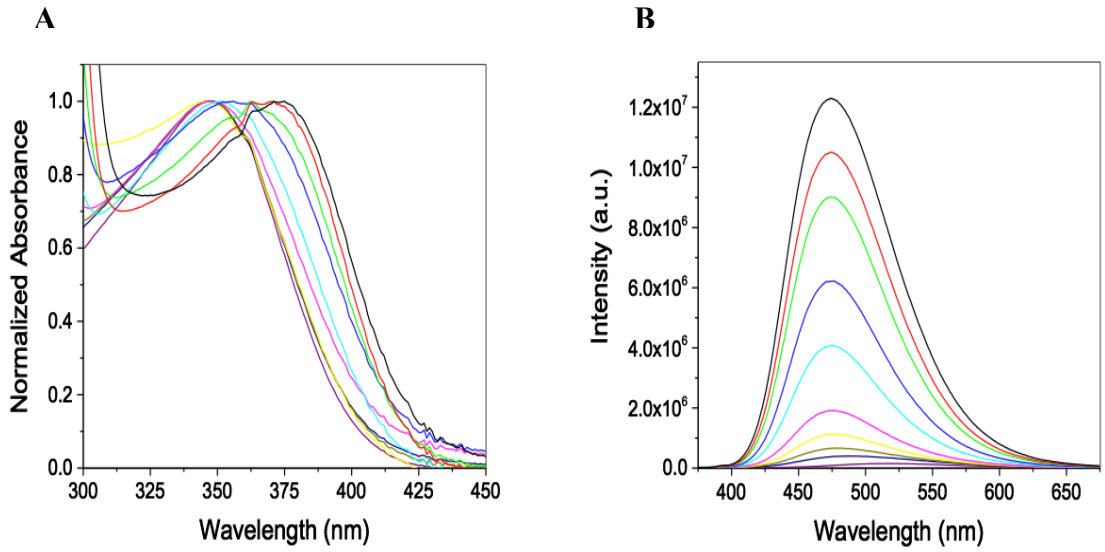

Figure 4.3. (A) Absorption and (B) emission spectra of **11**. Measurements were conducted at different DNA (base pairs) concentrations with units of μM (0, purple; 2, navy; 4, dark yellow; 7, yellow; 14, magenta; 32, cyan; 63, blue; 125, green; 250, red; 624, black).

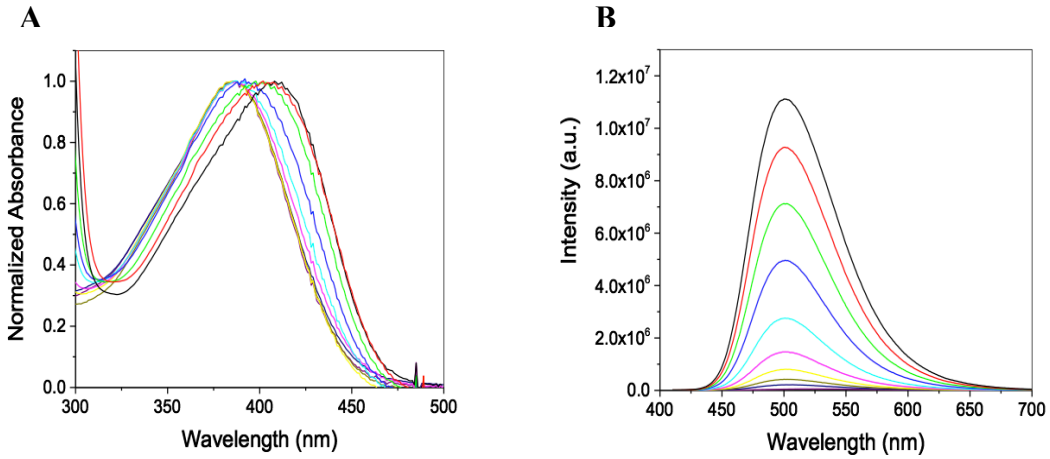

Figure 4.4. (A) Absorption and (B) emission spectra of **1**. Measurements were conducted at different DNA (base pairs) concentrations with units of μM (0, purple; 2, navy; 4, dark yellow; 7, yellow; 14, magenta; 32, cyan; 63, blue; 125, green; 250, red; 624, black).

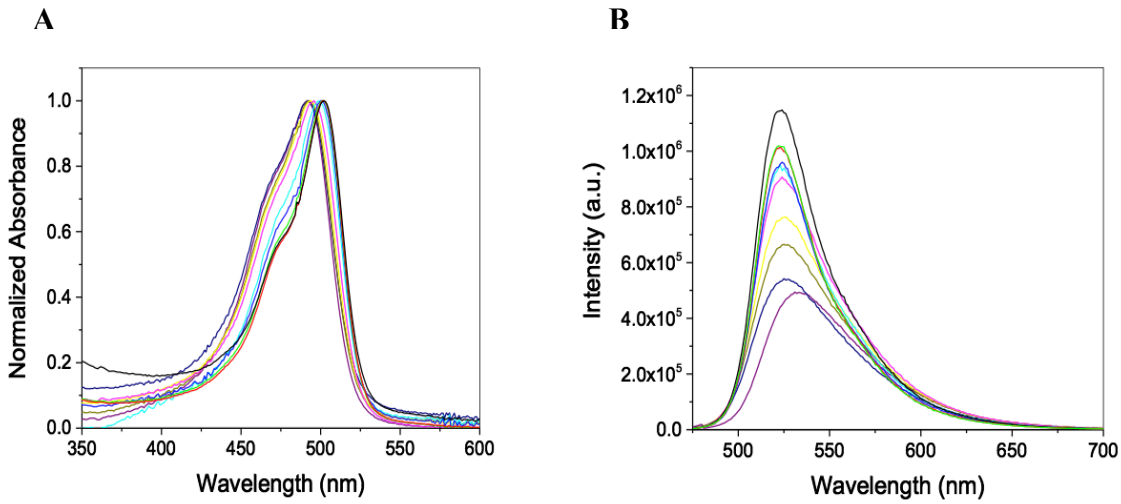

Figure 4.5. (A) Absorption and (B) emission spectra of **12**. Measurements were conducted at different DNA (base pairs) concentrations with units of μM (0, purple; 2, navy; 4, dark yellow; 7, yellow; 14, magenta; 32, cyan; 63, blue; 125, green; 250, red; 624, black).

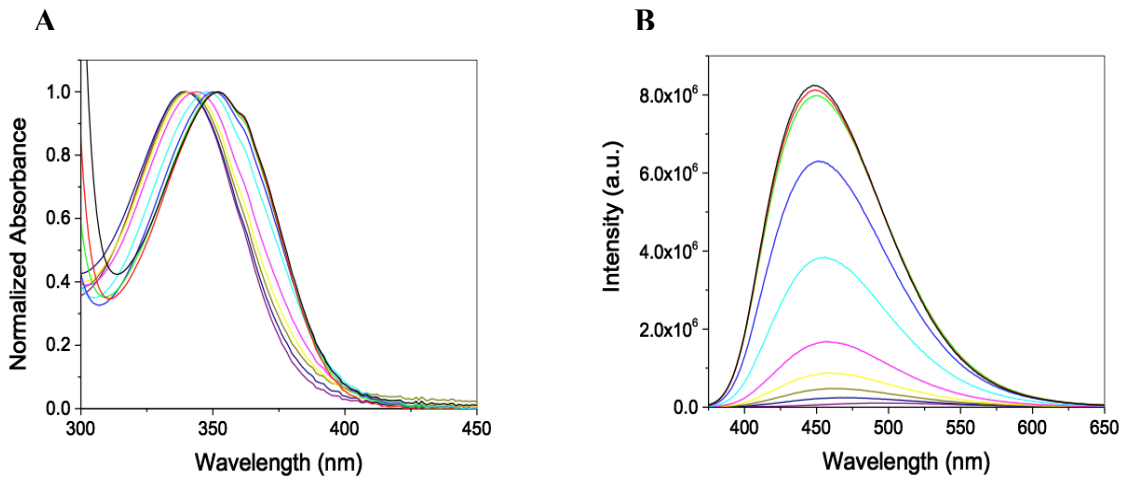

Figure 4.6. (A) Absorption and (B) emission spectra of **13**. Measurements were conducted at different DNA (base pairs) concentrations with units of μM (0, purple; 2, navy; 4, dark yellow; 7, yellow; 14, magenta; 32, cyan; 63, blue; 125, green; 250, red; 624, black).

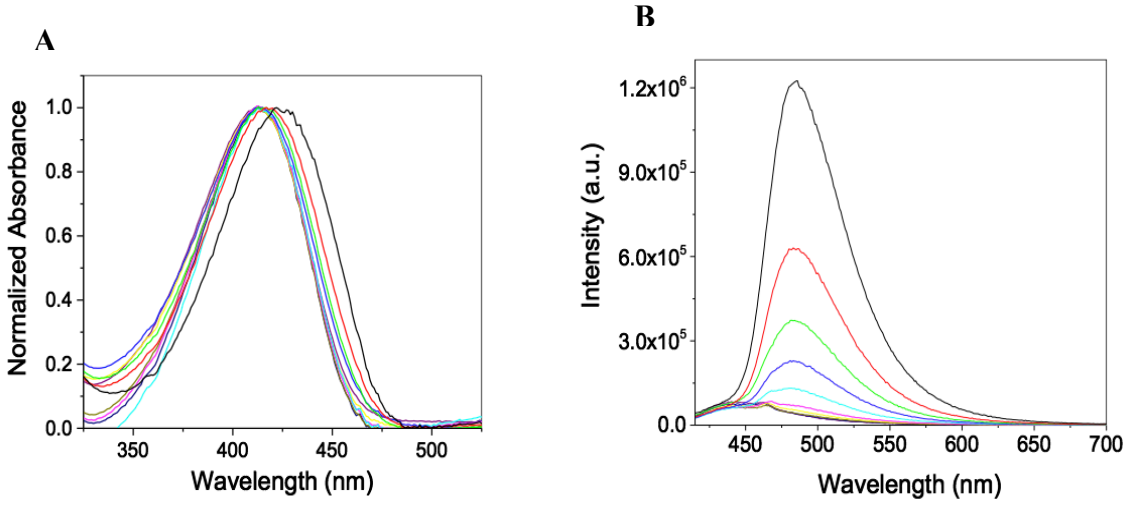

Figure 4.7. (A) Absorption and (B) emission spectra of **14**. Measurements were conducted at different DNA (base pairs) concentrations with units of μM (0, purple; 2, navy; 4, dark yellow; 7, yellow; 14, magenta; 32, cyan; 63, blue; 125, green; 250, red; 624, black).

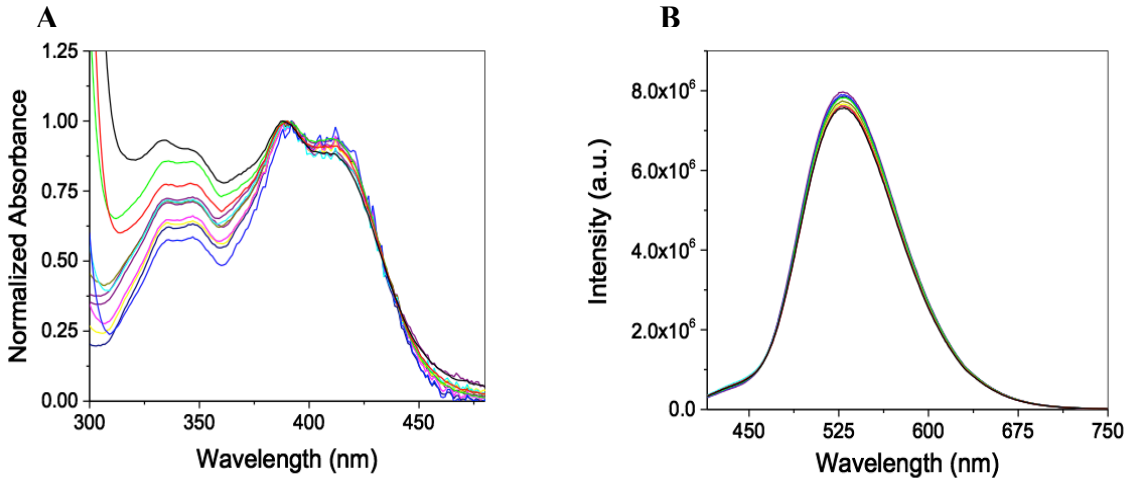

Figure 4.8. (A) Absorption and (B) emission spectra of **15**. Measurements were conducted at different DNA (base pairs) concentrations with units of μM (0, purple; 2, navy; 4, dark yellow; 7, yellow; 14, magenta; 32, cyan; 63, blue; 125, green; 250, red; 624, black).

Table 4.1 Fluorescence quantum yield of dyes at different calf thymus DNA concentrations

[DNA] (μM)	**11**	**1**	**12**	**13**	**14**	**15**
0	0.009	0.003	0.29	0.012	0.0026	0.29
2	0.029	0.008	0.31	0.018	0.0025	0.24
4	0.034	0.017	0.30	0.045	0.0021	0.24
7	0.048	0.033	0.47	0.082	0.0022	0.23
14	0.087	0.052	0.41	0.14	0.0026	0.23
32	0.19	0.11	0.42	0.30	0.0033	0.21
63	0.28	0.18	0.51	0.41	0.0049	0.22
125	0.37	0.25	0.66	0.46	0.0079	0.22
250	0.44	0.30	0.66	0.47	0.015	0.22
624	0.47	0.36	0.72	0.45	0.035	0.21

4.4 Results and Discussion

To demonstrate our methodology, **12** and **13** were used as standards. It is important to note that **12** has been reported as a intercalator,[83] and **13** has been reported as a groove binder.[84] The TPA cross-sections were measured utilizing the two-photon excited fluorescence (TPEF) method.[85] For **12**, a decrease in the TPA cross-section was observed as the DNA concentration was increased (Figure 4.9A) This can be rationalized by the orientation of **12** upon intercalating to DNA. The dipole of **12** is oriented more perpendicular to the DNA field (parallel to the bases) leading to a reduction in the induced dipole. The decreasing trend is evident of a DNA intercalative binding mode resulting in lengthening and unwinding of the DNA helix.[65] Important driving factors for intercalation are π–stacking, dispersive interaction, dipole-dipole interaction, and electrostatic factors with the aromatic nucleobases in DNA.[86] The TPA cross-section was also measured in the presence of $[poly(dG\text{-}dC]_2$ (Figure 4.10). The results confirm that the decreasing TPA cross-section trend is directly related to **12** intercalating at GC base pairs. Nafisi et. al previously reported that **12** intercalates at GC-rich sequences,[87] which corresponds with our results. Interestingly, the TPA cross-section was increased from 0.11 to 0.13 GM when the DNA concentration was increased from 0.11 to 0.13 GM when the DNA concentration was increased to 4 μM. This observation can be explained due to the dye-dye interactions at high dye-to-DNA ratios, which were also observed at 7 μM of DNA using circular dichroism (CD). The dyes from ordered aggregates at the surface of DNA[88] resulting in an enhanced dipole, which influences the TPA cross-section.

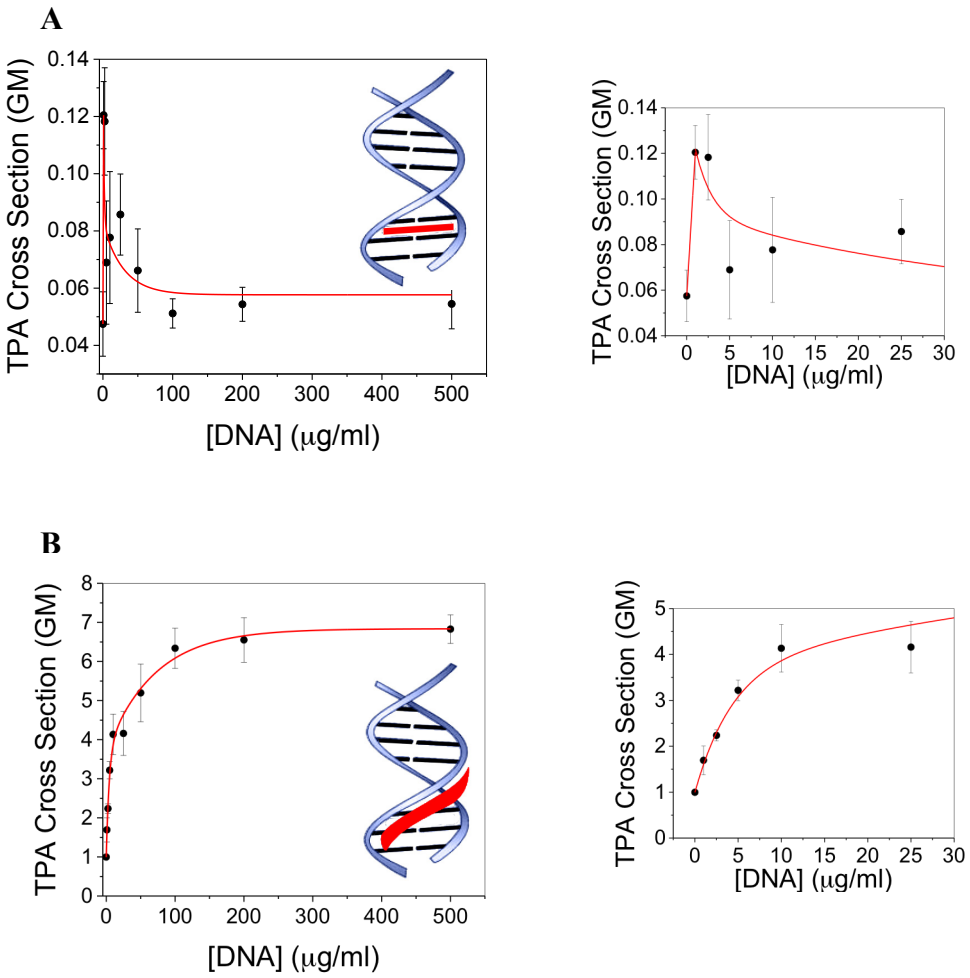

Figure 4.9. TPA cross-section of (A) **12** and (B) **13** plotted as a function of DNA (base pairs) concentration with [dye] = 5 μM. Results are the mean ± SD (n = 3)The red line is to guide the eye.

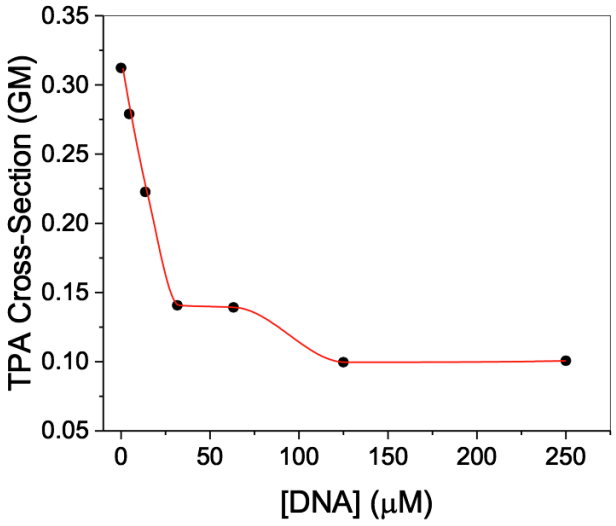

Figure 4.10. TPA cross-section of **12** plotted at different DNA (base pairs) concentrations of $[poly(dG\text{-}dC)]_2$. The red line is to guide the eye.

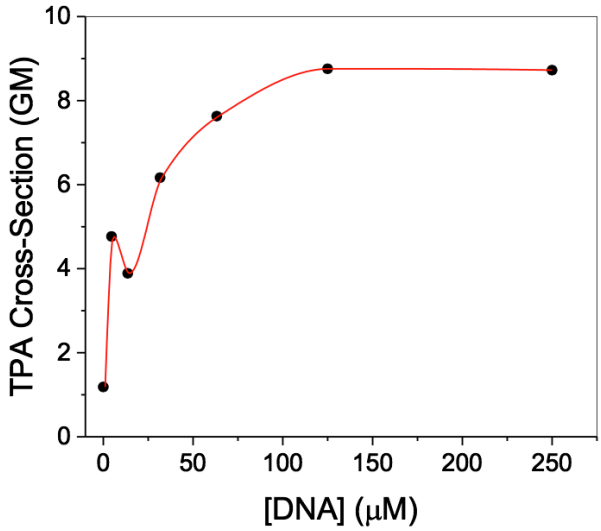

Figure 4.11. TPA cross-section of **13** plotted at different DNA (base pairs) concentrations of $[poly(dG\text{-}dC)]_2$. The red line is to guide the eye.

13 was investigated to demonstrate our methodology for a well-known groove binder. An interesting TPA cross-section trend was observed with increasing DNA concentrations (Figure 4.9B). A TPA cross-section enhancement of 6.9-fold was noted upon binding with DNA. The dipole of **13** is aligned more parallel to the DNA electric field when bound, resulting in an enhanced TPA cross-section. The increasing trend indicates a DNA groove binding mode, which is characterized by little to no perturbation of the DNA structure.[89] Groove binding molecules require conformational flexibility that allows the molecule to fit into the groove and functional groups that interact with the nucleobases with minimal steric hinderance.[62]The TPA cross-section of **13** was measured in the presence of $[poly(dA\text{-}dT)]_2$ (Figure 4.11). A TPA cross-section enhancement of 7.4-fold was observed upon binding at the AT base pairs. The findings confirm that the TPA cross-section enhancement is directly related to **13** groove binding at AT-rich sequences. **13** was reported to groove bind along AT-rich sequences while occupying four base pairs[90] through van der Waals and hydrogen bonding interactions.[91]

CD measurements were applied to compare were applied to compare with the TPA analysis. Positive and negative induced circular dichroism (ICD) signals were observed near 480 and 465 nm, respectively, for **12** (Figure 4.12). The positive band is due to the interaction between the transition dipoles of two or more ordered dyes and reduces when DNA concentrations are increased.[88] The negative ICD signal near 465 nm is attributed to the intercalated dye.[92] Contrarily, a strong positive ICD signal was observed at approximately 360 nm for the interaction of **13** with DNA (Figure 4.13). The positive band is ascribed to **13** groove binding with DNA.[93]

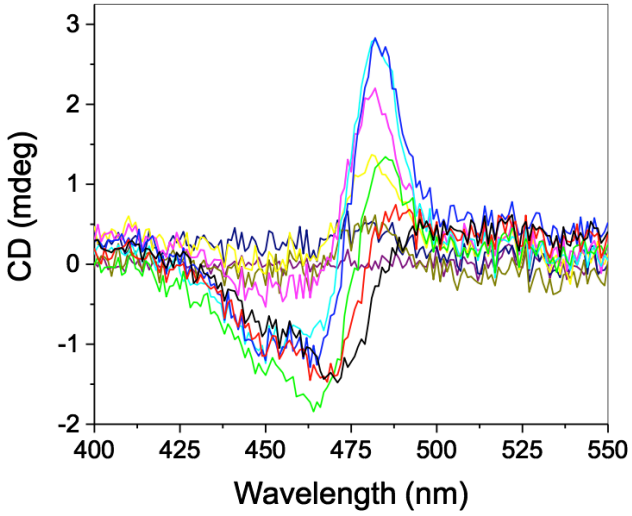

Figure 4.12. CD spectra of **12** at different DNA concentrations. Measurements were conducted at different DNA (base pairs) concentrations with units of μM (0, purple; 2, navy; 4, dark yellow; 7, yellow; 14, magenta; 32, cyan; 63, blue; 125, green; 250, red; 624, black).

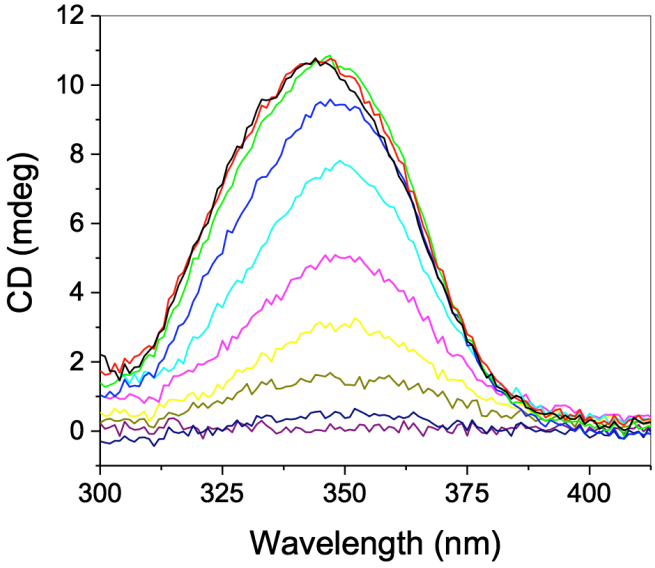

Figure 4.13. CD spectra of **13** at different DNA concentrations. Measurements were conducted at different DNA (base pairs) concentrations with units of μM (0, purple; 2, navy; 4, dark yellow; 7, yellow; 14, magenta; 32, cyan; 63, blue; 125, green; 250, red; 624, black).

TPA was employed to study the binding mode of thioflavin t (**14**). It was previously reported that **14** intercalates with dsDNA.[94-96] **14** undegoes a twisted internal charge-transfer (TICT), which is responsible for the quenched fluorescence in the absence of DNA. When bound with DNA, the internal rotation of the dye is restricted due to steric hindrance resulting in enhanced fluorescence.[97] Presented in Figure 4.14, the decreasing trend is indicative of an intercalative binding mode. This suggests that the dipole of **14** is oriented more perpendicular with the DNA electric field upon binding. **14** had a TPA cross-section decreased of 40.0 GM in the absence of DNA. The TPA cross-section decreased to 11.4 GM at 624 μM of DNA. The decrease in the TPA cross-section can be attributedto the DNA electric field induced perturbation of the dye's transition dipole rather than the conformational change of the dye upon intercalation since **1, 11,** and **13** undergo a conformational change upon groove binding. Similar to **12**, the TPA cross-section increased at low DNA concentrations. The TPA cross-section increased to 53.7 GM at 4 uM of DNA, which can be attributed to the formation of simers that bind at the DNA grooves under excess dye conditions.[98] CD was used to compare with the TPA experiments. However, an ICD signal was not detected at our experimental conditions (Figure 4.15). This demonstrates that TPA is more sensitive at low dye concentrations as compared to CD. Bathochromic shifts of 8 and 48 nm were observed in the absorption and emission spectra, respectively at 624 μM of DNA, indicating the dye is bound with DNA (Figure 4.16).

The binding mode of topotecan (**15**), a clinically approved anticancer drug, was investigated using TPA. There has been controversely regarding the binding mode of **15**.

The binding mechanism is of interest because therapeutic importance can be improved. Yang et al.[99] reported an intercalating binding mode in the absence of topoisomerase I.

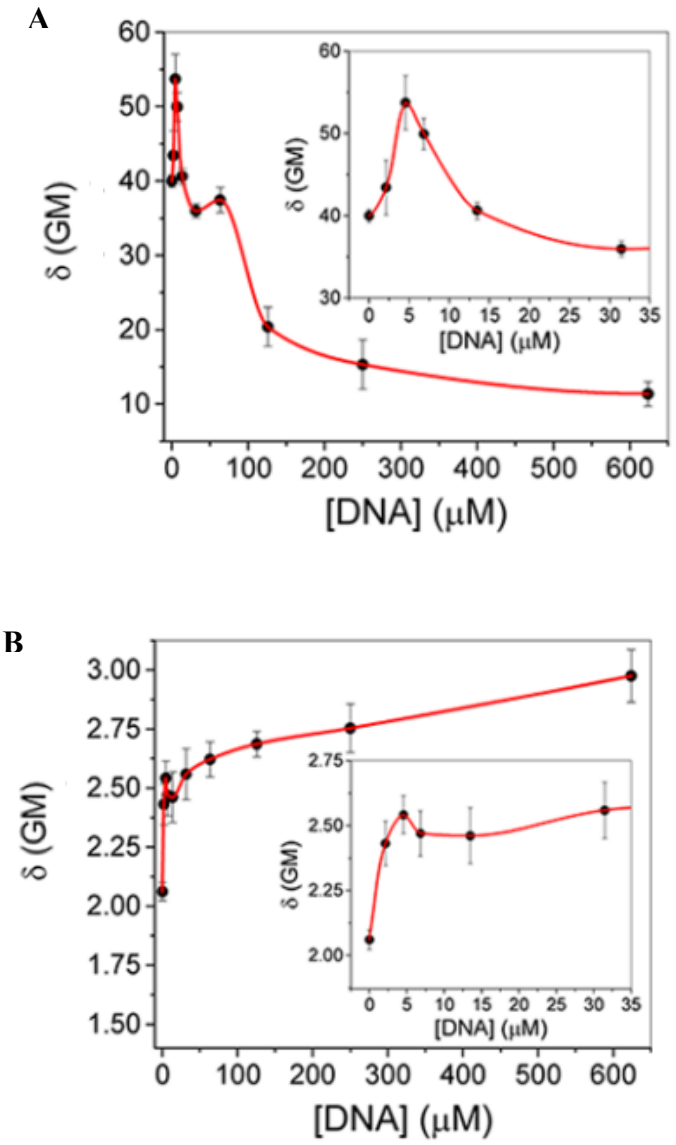

Figure 4.14. TPA cross-section of (A) **14** and (B) **15** plotted as a function of DNA (base pairs) concentration with [dye] = 5 μM. Inset graph: enlargement at low DNA concentration. Result are the mean ± SD (n = 3). The red line is to guide the eye.

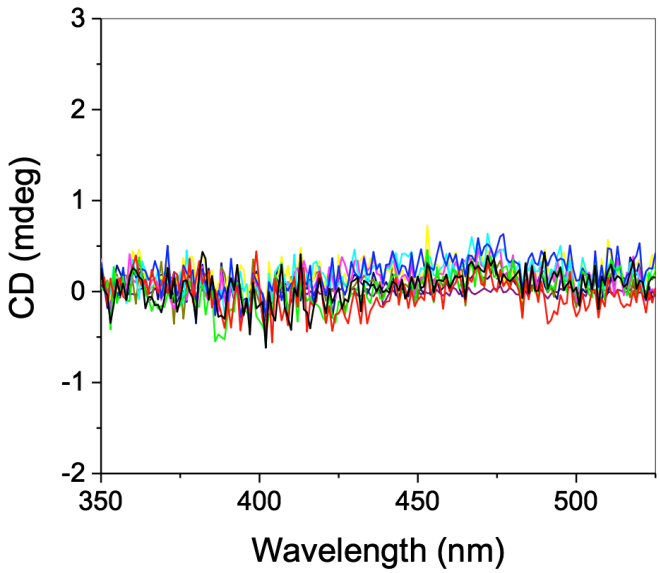

Figure 4.15. CD spectra of **14** at different DNA concentrations. Measurements were conducted at different DNA (base pairs) concentrations with units of μM (0, purple; 2, navy; 4, dark yellow; 7, yellow; 14, magenta; 32, cyan; 63, blue; 125, green; 250, red; 624, black).

However, Streltsov et al.[100] and Joshi et al.[101] concluded that **15** binds to DNA through a groove binding mechanism. Our TPA analysis suggest that **15** groove binds with DNA, as shown in Figure 4.14B. The TPA cross-sectionenhancement can be attributed to **15** groove binding at GC-rich sequences.[100,101] Quenching in both the steady-state and two-photon excited emission was observed (Figure 4.17). This can be ascribed to the photoinduced electron transfer (PET) between the drug and DNA nucleobases.[101] A TPA cross-section enhancement of 1.5-fold was noted upon binding with DNA. The low enhancement can be attributed to orientation of the binding agent relative to the DNA helical axis. **15** was reported to be oriented nearly 55^{o} to the DNA helical axis, which is approximate to a groove binder (<55^{o}) but less than a classical intercalator (62-76^{o}).[100,101]

Comparatively, **13** had a TPA cross-section enhancement of 6.9-fold with 45° angle of orientation.[102] The difference in the TPA cross-section enhancement at low and high

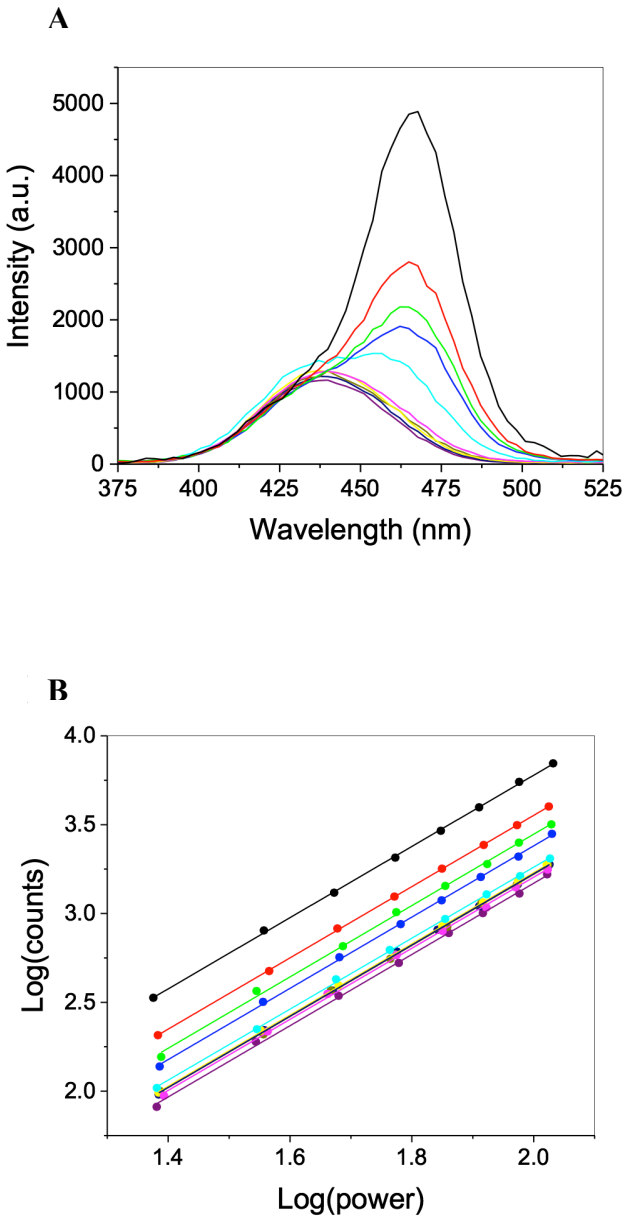

Figure 4.16. (A) Two-photon excited fluorescence and (B) Log-Log plot of **14** with slope equals ~2. Measurements were conducted at different DNA (base pairs) concentrations with units of μM (0, purple; 2, navy; 4, dark yellow; 7, yellow; 14, magenta; 32, cyan; 63, blue; 125, green; 250, red; 624, black).

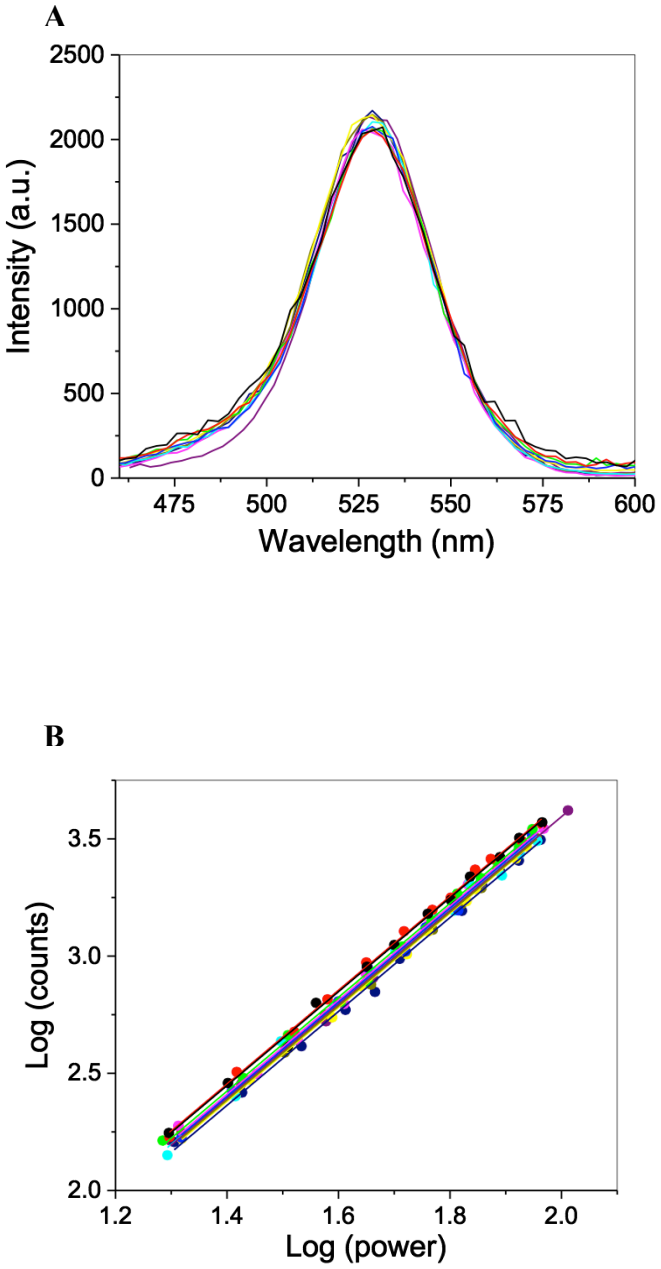

Figure 4.17. (A) Two-photon excited fluorescence and (B) Log-Log plot of **15** with slope equals ~2. Measurements were conducted at different DNA (base pairs) concentrations with units of μM (0, purple; 2, navy; 4, dark yellow; 7, yellow; 14, magenta; 32, cyan; 63, blue; 125, green; 250, red; 624, black).

DNA concentrations can be ascribed to the DNA electric field induced enhancement of the dye's transition dipole. The low TPA cross-section enhancement suggests that the binding angle of topotecan is between an intercalator and groove binder. A larger TPA cross-section enhancement is expected if the dipole of the binding molecule is oriented more parallel with the DNA electric field.

The binding mode **11** was studied utilizing TPA and CD. The TPA cross-section of the unbound dye was 2.1 GM. Shown in Figure 4.18A, the TPA cross-section increased to 28.7 GM at 624 μM of DNA. A significant TPA cross-section enhancement of 13.6-fold was observed upon binding with DNA, which was the largest enhancement noted. The TPA cross-section enhancement indicates that **11** undergoes a groove binding mechanism in the presence of DNA. The crescent shape of **11** allows the molecule to groove bind at AT-rich sequences. CD was used to investigate the system. **11** exhibits a positive ICD signal near 370 nm in the presence of DNA, which is consistent of a groove binding mode (Figure 4.18B). The positive band corresponds to the $S_0 \rightarrow S_1$ transition, which suggests that the transition dipole of **11** is oriented along the groove.[103] Interestingly, a weak negative band is observed near 325 nm at 32 μM of DNA or greater. The bisignate ICD signal is attributed to the formation of dimers at the surface or in the groove of the DNA.[104] In agreement with CD, the TPA cross-section enhancement indicates that the transition dipole of **11** is oriented more parallel to the DNA electric field.

TPA and CD were employed to investigate the binding mode of **1**. Presented in Figure 4.19A, the TPA cross-section is plotted as a function of DNA concentration. The TPA cross-section increased from 3.4 to 14.0 GM from 0 to 624 uM of DNA. A TPA

cross-section enhancement 4.1-fold was observed. Compared with **11**, this suggests that a larger TPA cross-section enhancement is noted when a less electron withdrawing heterocyclic central core is incorporated into the donor-acceptor-donor π-system. In addition, the hydroxyl substituent from **1** may interact with the DNA nucleobases and surrounding water molecules resulting in a lower TPA cross-section enhancement.[105] The increasing trend indicates that **1** interacts with DNA though a groove binding mechanism. CD was used to examine the binding mode of **1** (Figure 4.19B). A positive ICD signal was recorded in the presence of DNA near 400 nm, which corresponds to the $S_0 \rightarrow S_1$ transition. The negative band at approximately 350 nm corresponds to the $S_0 \rightarrow S_2$ transition. **1** was previously reported to groove bind with DNA using linear dichroism (LD),[28] which agrees with the TPA analysis. Additionally, it was shown that **1** interacts with DNA through hydrogen bonding interactions at the AT base pairs, occupying three base pairs. However, the fluorescence is nearly quenched from GC sequences, which is most likely due to the PET from guanine to the excited chromophore.[51]

A direct comparison of TPA and CD demonstrates superior sensitivity compared to CD. It is important to note an ICD signal was not observed for **14** and **15**; however, a change was detected utilizing TPA. This indicates that our method has superior sensitivity at low dye and DNA concentrations. AN ICD signal was not observed at DNA concentrations less than 7 uM for **1, 11** and **12**. However, an ICD signal was detected at 4 uM of DNA for **13**. TPA detected a significant environmental change in the presence of 2 uM of DNA for all compounds, which demonstrates that the methodology has potential use at biologically relevant concentrations while avoiding problems with background absorption of common buffers.[106] For example, the TPA cross-section increased from

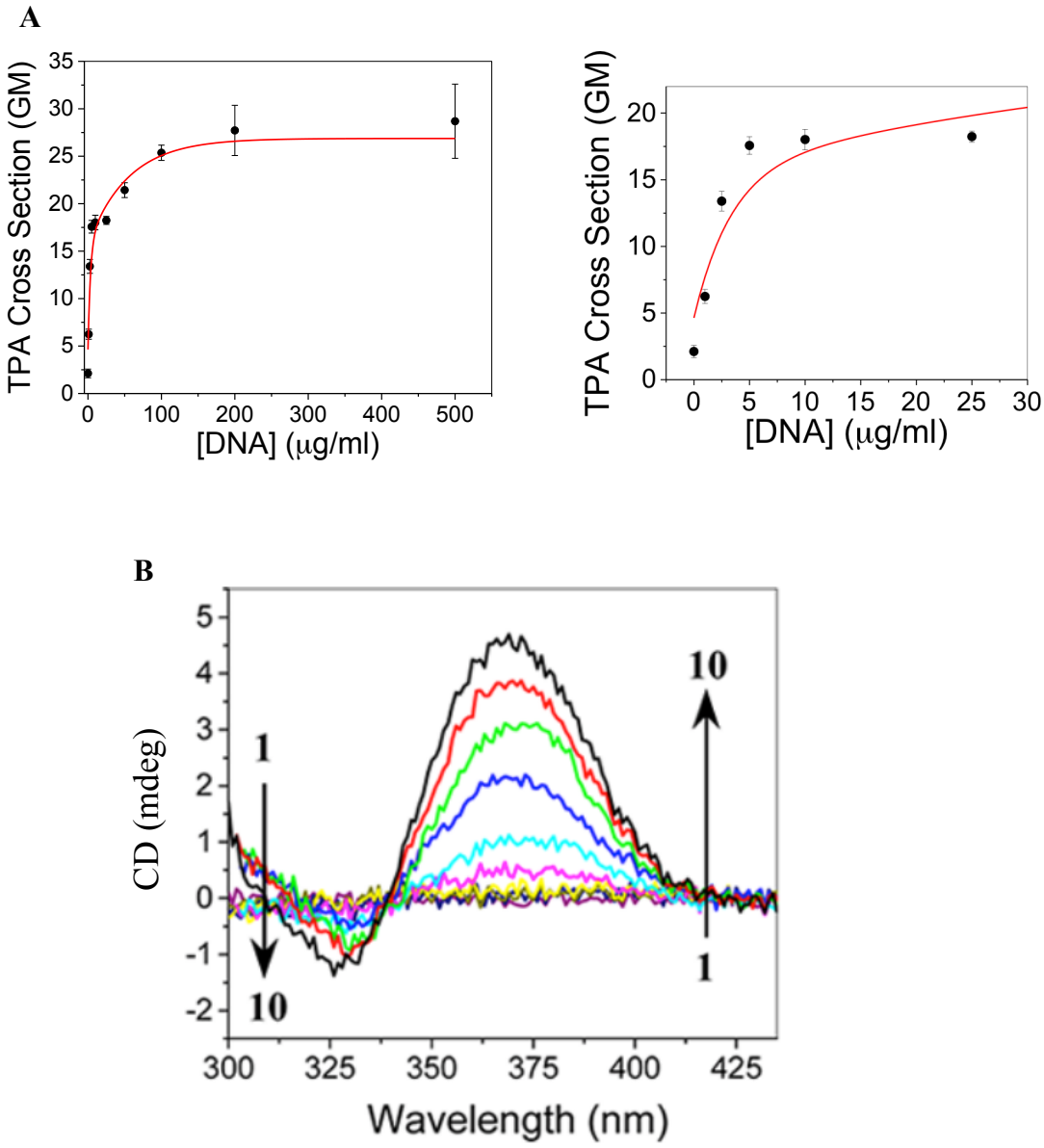

Figure 4.18. (A) TPA cross section of **11** (5 μM) plotted as a function of DNA (base pairs) concentration. Results are the mean ± SD (n = 3). The red line is to guide the eye. (B) CD spectra at different DNA concentrations. 1 → 10 represents DNA (base pairs) concentrations 0, 2, 4, 7, 14, 32, 63, 125, 250, and 624 μM, respectively.

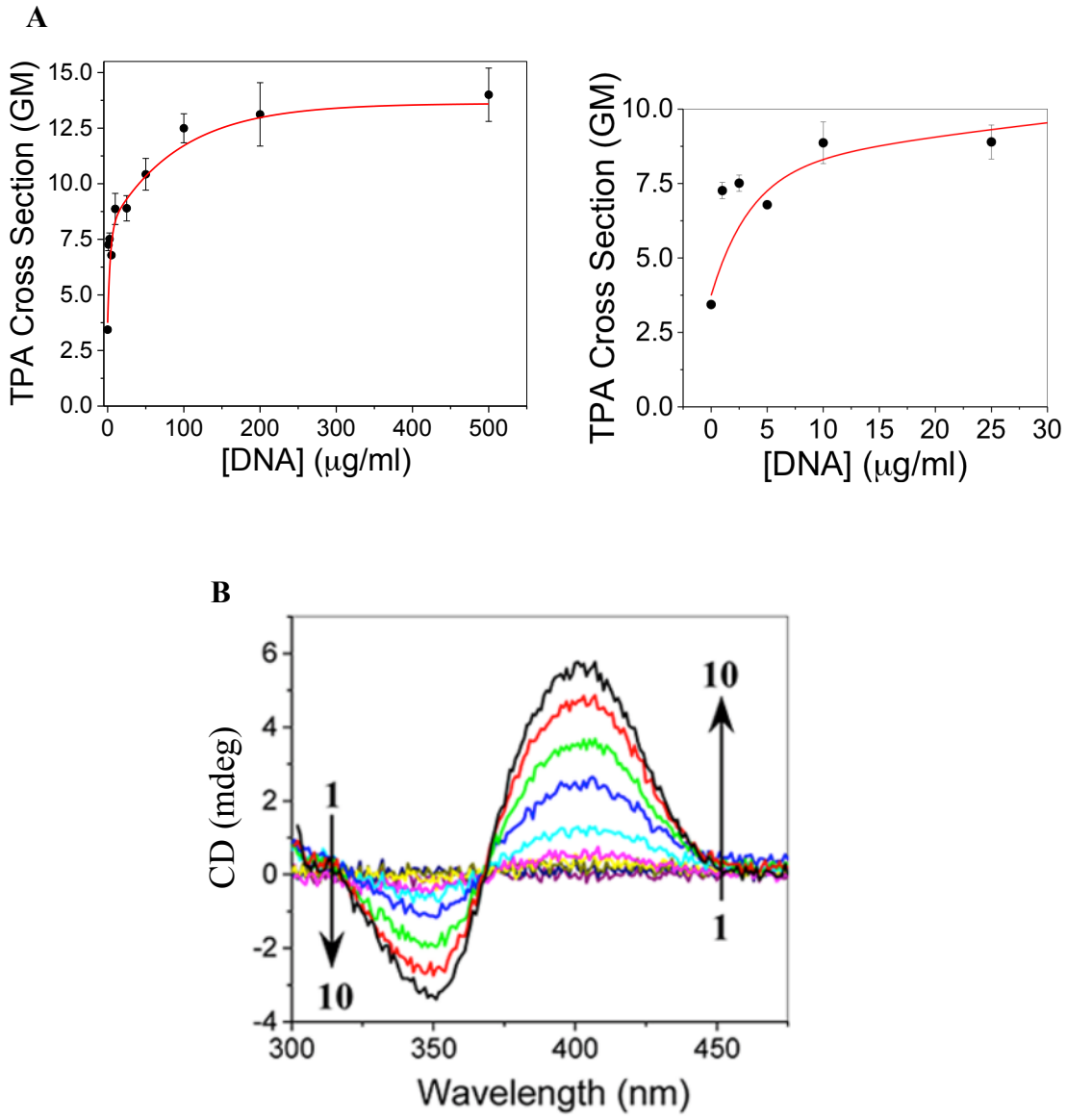

Figure 4.19. (A) TPA cross section of **1** (5 μM) plotted as a function of DNA (base pairs) concentration. Results are the mean ± SD (n = 3). The red line is to guide the eye. (B) CD spectra at different DNA concentrations 1 → 10 represents DNA (base pairs) concentrations 0, 2, 4, 7, 14, 32, 63, 125, 250, and 624 μM, respectively.

2.1 to 6.2 GM when the DNA concentration was increased to 2 μM for **11**. The findings are significant, as it suggests that two photon spectroscopy can provide detailed information at dilute concentrations of DNA and differentiate between the DNA binding modes of external molecules, which are inaccessible with single-phopton excited fluorescence. Furthermore, two-photon excitation microscopy (TPEM) can be used for cellular studies. Since the TPA process is quadratically intensity dependent, TPEM can provide superior spatial resolution with reduced photobleaching and photodamage as well as autofluorescence for bioimaging at low concentrations.

4.5 Conclusion

In conclusion, we developed a new highly sensitive methodology to diagnose the DNA binding mode of external molecules. This is the first example of TPA cross-section being applied to determine the DNA binding mode of fluorescent nuclear dyes and DNA-targeted drugs. The TPA cross-sections of intercalating and groove binding dyes are influenced by the electric field of the DNA backbone upon binding. An increasing TPA cross-section trend is indicative of a groove binding mode, while a decreasing TPA cross-section trend suggest an intercalative binding mode. A comparison of our TPA studies with CD demonstrates that TPA exhibits superior sensitivity at DNA concentrations of 4 uM and lower by more than an order of magnitude. These findings may facilitate the biological studies of DNA interactions with other external molecules as well as applications for bioimaging.

Chapter 5

EXPERIMENTAL TECHNIQUES

5.1 Materials

All chemicals and solvents were obtained from commercial suppliers and used without further purification, unless otherwise indicated. Calf thymus DNA (ctDNA), [poly(dA-dT)]2, [poly(dG- dC)]2, and topotecan were purchased from Sigma Aldrich and used as received. ^{1}H NMR and ^{13}C NMR spectra were recorded on 500 MHz spectrometer.

5.2 Quantum Chemical Calculations

Quantum chemical calculations on **1-7** were carried out utilizing the Gaussian '09 suite of electronic structure modeling software.[52] Ground state geometries of the dyes with were optimized by DFT with the B3LYP/6-31G(d) method using Truhlar's SMD solvation model.[107] Vertical transition energies and associated transition dipoles were obtained by TD- DFT calculations with the B3LYP/6-31G(d) method. Molecular orbitals and transition dipoles were visualized using the GaussView 5 program.

5.3 Quantum Yield Measurements

The fluorescence quantum yields in chapter 4 were measured using the Williams comparative method. The optical density was measured below 0.10 to avoid reabsorption and internal filter effects. The absorption and fluorescence were measured for four samples with decreasing concentrations. The quantum yield was calculated using the following equation

$$\Phi_x = \Phi_{Std} \frac{Grad_x}{Grad_{std}} \frac{\eta^2_x}{\eta^2_{std}}$$

where is Φ the quantum yield, η is the refractive index of the solvent, and $Grad$ is the slope obtained from plotting the fluorescence versus absorbance. The quantum yields were measured for **1** and **11** using Coumarin 307 (Φ = 0.56)[108] dissolved in methanol as the standard; **12** using Coumarin 153 (Φ = 0.54)[109] dissolved in methanol as the standard; **13**, **14**, and **15** using Coumarin 30 (Φ = 0.35)[110] dissolved in methanol as the standard. The quantum yields were measured at the maximum absorption for each complex. Extra precaution was taken when measuring the quantum yields as it can significantly influence the TPA cross- section.

5.4 Spectroscopy

5.4.1 Absorption and Steady State Fluorescence

UV-vis absorption spectra were obtained for chapter 1-3 on a Perkin-Elmer Lambda 35 UV-vis spectrometer using chromophore solutions of 10 μM unless otherwise noted in the text; path lengths were 1 cm. For chapter 4, absorption spectra were measured on an Agilent 8341 spectrophotometer. In chapter 1-3 fluorescence studies were performed on a Perkin- Elmer LS55 Fluorometer using probe concentrations of 1 μM or less. For chapter 4 emission spectra were collected on a Fluoromax-2 fluorimeter with slits set at 3 nm and an integration time of 0.100 s. For determination of Φ_{em}, solutions were prepared to an optical density of less than 0.05 in order to minimize inner filter effects. Perylene in cyclohexane was used as a reference for quantum yields.[111]

Time-resolved emission measurements were performed using a time correlated single photon counting (TCSPC) setup. The excitation light was provoded by a 405 nm diode laser from Picoquant, GmbH, model LDH-P-C-405 and a PDL 800B pulsed laser diode driver from Picoquant, GmbH. The emitted photons were collected by a thermoelectrically cooled microchannel plate photomultiplier tube (R3809U-50, Hamamatsu). The signal was digitalized using a multichannel analyzer with (SPC-300, Edinburgh Analytical Instruments). Emission was recorded at 504 and 533 nm for **1** and **2**, respectively. Fluorescence decay curves of the sample were then fitted to a single exponential decay expression by using the IgorPro software from Wavemetrics, Inc. (moved pulse-limited sentence).

5.4.2 Flow Aligned Linear Dichroism and Circular Dichroism

LD spectra were measured on a Chirascan CD spectropolarimeter equipped with an LD.3 linear dichromism detector (Applied Photophysics), run in linear dichroism mode. Sample orientation is achieved by shear fllow in an outer rotating cylinder quartz Couette cell. A nonoriented sample was used as baseline. LD spectra were recorded at 1 dye per 5 base pairs in 0.5x TBE buffer.

CD spectra were measured on an Aviv model 202 circular dichroism spectrometer using a wavelength step of 1 nm and a bandwidth of 1.0 nm. The CD scans were averaged with n = 3. Quartz cells with 10 mm path lengths were used for all measurements. All optical measurements were carried out at 25 ^{o}C.

5.4.3 Two Photon Spectroscopy

Two-photon spectroscopy was performed using a Kapteyn Murnane Laboratories diode-pumped mode-locked Ti:sapphire laser with pulses of ~30 fs. All emission scans were recorded at 800 nm excitation, scanning from 350 – 750 nm. TPA cross-sections were measured utilizing the two-photon excited fluorescence (TPEF) method.[112] The input power from the laser was varied using a variable neutral density filter. The fluorescence was collected perpendicular to the incident beam. A focal-length plano-convex lens was used to direct the fluorescence into a monochromator whose output was coupled to a photomultiplier tube. A counting unit was used to convert the photons into counts. Coumarin 307 dissolved in methanol was used as a standard ((φδ)800 nm = 15 GM).[112]

Disadvantages of TPA. There are several drawbacks when using TPA. First, the quantum yield is required to calculate the TPA cross-section using the TPEF method. Inaccurate quantum yield measurements can significantly influence the TPA cross-section, therefore affecting the results. In order to measure the TPA cross-section accurately, the quantum yield must be measured with precaution. It is important to use proper technique and keep the optical density below 0.10 to avoid reabsorption and internal filter effects. The quantum yield and TPA measurements were conducted with three trials and averaged to give a TPA cross-section value. Another disadvantage of TPA is that it is a destructive technique since a high density of photons is required for two-photon excitation. It is important to monitor the degradation of the sample by measuring the absorption and fluorescence before and after the experiment. Sample degradation can be reduced by minimizing the output power used to excite the sample. Finally, the TPEF technique cannot be used if the sample does not display two-photon excited fluorescence.

In this case, a nonlinear transmission method, such as Z-scan would have to be employed to measure the TPA cross-section. Measurements using the TPEF technique are more accurate and precise than nonlinear transmission techniques. When using a nonlinear transmission technique, there will be more variation in the TPA data. Such variations can be reduced by minimizing false nonlinear optical processes including thermal lensing as well as stimulated emission and scattering.[113]

5.5 Confocal Microscopy

Imaging was performed on a Leica SP5 confocal microscope housed within the UM Biology Imaging Core Facility. Time-course images were obtained in xyt mode with line averaging. Identical settings (photodiode gain, offset, etc.) were used when comparing brightness of the dyes. Images were analyzed using Fiji/ImageJA software (NIH, USA).

5.5.1 Cell Culture

HEK-293, BT474 and MCF7 cells were maintained in DMEM (Dulbecco's Modification of Eagle's Medium with 4.5 g/L glucose, without L-glutamine and sodium pyruvate) or RPMI (Roswell Park Memorial Institute medium) containing 10% dialyzed FBS, 2 mM glutamine, 100 units/ml penicillin, 100 μg/ml streptomycin, and 250 μg/ml Geneticin at 37°C and 5% CO_2 atmosphere. For imaging, cells were seeded at a density of 10^5 cell/cm^2 in 96 microwell plates or 35 mm imaging dishes and incubated for at least 48 hours until a visible monolayer was established. Prior to imaging, DMEM or RPMI was removed and L-15 (Leibovitz's L-15 modified, pH 7.3) was added to each well. 100 μM stock solutions of **1**-**7**, DAPI and Hoechst 33342 were prepared in L15 media with 5%

FBS and added to imaging wells or dishes to achieve the appropriate final concentration. Cells maintained a normal morphology during the course of the experiments and remained adhered to the imaging surface . For cell viability and growth studies, cells were plated at a density of 10^5 cell/cm^2 in 96 microwell plates. Confluence was initially 50% with readings taken every 24 hours until 100% confluence was reached; six sample wells were used for each dye concentration (10, 5, 1, 0.5, 0.1 μM) and the control cells.

5.6 Electrochemistry

Measurements were performed on a BAS100B potentiostat in dry acetonitrile using a single compartment cell fitted with a glassy carbon working electrode (0.071 cm^2), a platinum auxillary electrode, and an Ag/AgCl reference electrode. Fc/Fc^+ was the internal reference, and 100 mM $TBAPF_6$ was supporting electrolyte; dye concentrations were 0.3 mM. the low solubility of **1** necessitated the use of a dimethylamino derivative, **3**. As the relevant molecular orbitals are confined to the aromatic core, this change in peripheral groups does not expected to alter the oxidation or reduction potentials.

5.7 Experimental Procedures

Synthesis of 1. 2.04 g (10.0 mmol) of 4-(4-methyl-1-piperazinyl)-benzaldehyde[114] was combined with 1.80 g (30.0 mmol) of urea and 35 mL of 10% HCl/ethanol in a pressure tube (65 mL) with a magnetic stirbar and stirred at room temperature. After 2 h, 2.18 g (10.0 mmol) of 1-(4-(4-methyl-1-piperazinyl)- phenyl)-ethanone[115] was added to the reaction mixture (3.0 mmol), which was capped heated at 100 ^oC for 24 h with vigorous

stirring; after several hours, a yellow precipitate was observed. After 24 h, the reaction mixture was cooled to room temperature; the precipitate was isolated by filtration and rinsed with saturated of $NaHCO_3$ solution. **1** was crystallized from isopropanol, isolated as yellow flakes by filtration and dried under vacuum. Yield: 960 mg, 22%; m.p; 210 ^oC (dec.); IR ν_{max} (cm^{-1}): 789.18, 823.95, 887.56, 1227.9, 1580.45, 1623.71, 2930.72; 1H NMR (500 MHz, DMSO−d_6), δ (ppm): 2.88 (6H, s), 3.15 (4H, s), 3.21-3.24 (4H, d, *J* = 12.6 Hz), 3.56-3.58 (4H, d *J* = 10.9 Hz), 4.27-4.30 (4H, d *J* = 12.7 Hz), 7.20-7.22 (4H, d *J* = 8.7 Hz), 7.57 (1H, s), 8.21-8.22 (4H, d *J* = 8.6 Hz), 10.18 (2H, s); ^{13}C NMR (125 MHz, DMSO−d_6, TFA), δ (ppm): 42.46, 44.05, 52.27, 97.39, 114.49, 118.13, 131.54, 150.31, 153.80, 161.20; HRMS (ESI) calculated for $C_{26}H_{33}N_6O^+$ ($M+H^+$): 445.2710, found: 445.2718.

Synthesis of 2. 782 mg (3.0 mmol) of 1,3-bis(4-fluorophenyl)-1,3-propanedione was placed in an argon-purged 25 mL Schlenk flask charged with a stirbar. The flask was capped, cooled to 0 ^oC and 4.0 mL (32.0 mmol) of boron trifluoride diethyl etherate was added by syringe. The reaction was heated to 75 ^oC and stirred for 24 h. Excess boron trifluoride diethyl etherate and was evacuated and the resultant solid was tritrurated with methanol to produce 1,3-bis(4-fluorophenyl)-1,3-propanedionato-κ*O*, κ*O*']difluoroborane as a precipitate that was collected by filtration, dried under vacuum and directly reacted with 1.0 mL of N-methylpiperazine at 120 ^oC for 24 h. The reaction mixture was cooled, directly loaded on a neutral alumina column and the product eluted using a 1:1 mixture of ethyl acetate and methanol. After removal of the solvents under reduced pressure, **2** was isolated as an orange-red powder. Yield: 124 mg (10.6%); m.p. 305 ^oC (dec.); IR ν_{max}:

cm^{-1} 799.88, 1199.69, 1340.14, 1591.69, 1621.26, 2941.25, 3396.21; ^{1}H NMR (500 MHz, DMSO−d_6), δ (ppm): 3.70 (6H, s), 4.36-4.38, (4H, d, *J* = 8.9 Hz), 5.08-5.10 (4H, d, *J* = 10.0 Hz), 7.97-7.99 (4H, d, *J* = 8.9 Hz), 8.39 (1H, s), 9.03-9.05 (4H, d, *J* = 8.8 Hz) ^{13}C NMR (125 MHz, DMSO−d_6, TFA), δ (ppm): 40.75, 44.03, 52.31, 91.55, 112.93, 121.10,

131.70, 154.33, 178.33. HRMS (ESI) calculated for $C_{25}H_{32}BF_2N_4O_2^+$ ($M+H^+$): 469.2581, found: 469.2540.

Synthesis of 3. 4-Dimethylaminobenzaldehyde (2.5 g; 10.0 mmol) was combined with 3.0 g (30.0 mmol) of urea and 35 mL of 10% HCl/isopropanol in a pressure tube (65 mL) with a magnetic stir bar and stirred at room temperature. After 2 h, 2.5 g (10.0 mmol) of 1-[4-(dimethylamino)phenyl]ethanone was added to the reaction mixture, which was then capped and heated at 100 °C for 24 h with vigorous stirring; after several hours, a yellow precipitate was observed. After 24 h, the reaction mixture was cooled to room temperature; the precipitate was isolated by filtration and rinsed with saturated NaHCO3 solution. **3** was crystallized from isopropanol, isolated as yellow flakes by filtration, and dried under vacuum. Yield: 2.57 g (77%); ^{1}H NMR (500 MHz, DMSO−d_6): δ (ppm) 3.00 (s, 12H), 6.77−6.78 (d, 4H, J = 8.2 Hz), 7.13 (s, 1H), 8.00−8.01 (d, 4H, J = 8.02 Hz); ^{13}C NMR (125 MHz, MeOD-d4, TFA) δ (ppm) 38.7, 94.9, 111.8, 114.2, 130.0, 149.1, 154.9, 160.0; IR ν_{max} (cm^{-1}): 785.7, 799.9, 822.7, 947.0, 1121.0, 1166.4, 1199.7, 1258.4, 1340.1, 1393.7, 1515.5, 1591.7, 1621.3, 2941.3, 3396.2. HRMS (ESI) $C_{20}H_{23}N_4O$ [M + H^+]: calculated, 335.1866; found, 335.1846.

Synthesis of 4. ((E)-4-(4(-4-methylpiperazin-1-yl)phenyl)6-(4-(4- methylpiperazin-1-yl)styryl)pyrimidin-2-ol): 0.30 g (1.0 mmol) of 4-methyl-6-(4-(4-methylpiperazin-1-yl)phenyl)pyrimidin-2- ol, 0.27 g (1.3 mmol) of 4-(4-methyl-1-piperazinyl)-benzaldehyde, 2.40 g (19.0 mmol) of TMS-Cl, and 10 ml of anhydrous dimethylformamide were mixed in a 25 mL pressure tube with a magnetic stirbar. After heating at 90 ^{o}C for 2 days, the reaction was cooled to room temperature and quenched with concentrated sodium hydroxide; the precipitate was isolated by filtration. **4** was crystallized from isopropanol, resultant orange flakes were filtered and dried under vacuum. (0.20 g, 40%); mp 400 °C (decomp.); IR ν_{max} (cm^{-1}): 3672.1, 2978.1, 2903.2, 1604.4, 1549.2, 1448.5, 1236.6, 1076.0, 1066.2, 1054.7, 820.5, 791.7; ^{1}H NMR (500 MHz, DMSO-d_6, TFA): δ 2.87 (s, 3H), 3.15, (broad s, 4H), 3.23-3.25 (d, 4H, J = 10.0 Hz), 3.56 (broad s, 4H), 4.12-4.14 (d, 2H, J = 10.0 Hz), 4.26-4.29 (d, 2H, J = 15.0 Hz), 6.94-6.97 (d, 1 H, J = 15.0 Hz), 7.15-7.16 (d, 2H, J = 10.0 Hz), 7.20-7.22 (d, 2H, J = 10.0 Hz), 7.61-7.63 (d, 2H, J = 10.0 Hz), 8.11-8.13 (d, 2H, J = 10.0 Hz), 8.30-8.33 (d, 1H, J = 15.0 Hz), 10.12-10.19 (d, 2H, J = 35.0 Hz); ^{13}C NMR (125 MHz, DMSO-d_6, TFA): δ 42.19, 44.05, 44.51, 52.64, 52.74, 97.03, 113.13, 114.68, 115.05, 118.80, 125.70, 130.37, 131.21, 147.47, 148.84, 152.38, 153.79, 161.45, 161.48; HR-ESI (Q- TOF) m/z: calc'd for $C_{28}H_{34}N_6O^+$ $[M+H]^+$: 471.6285, found: 471.2897.

Synthesis of 5. ((E)-4-(4(-4-methylpiperazin-1-yl)-phenyl)6-(4-(4- methylpiperazin-1-yl)styryl)-1,3-propanedionato-κO, κO']difluoroborane): 1.00 g (3.2 mmol) of 2, 0.73 g (3.55 mmol) of 4-(4-methyl-1-piperazinyl)-benzaldehyde, 0.82 g (3.6 mmol) of tributyl

borate, 0.03 g (0.35 mmol) of tert-butylamine and 10 mL of toluene were mixed in a 25 mL round bottom flask with a stirbar and heated to 70 ^{o}C. After 48 h, the reaction was cooled and concentrated under reduced pressure. The resulting residue was purified over alumina (1:1 Ethyl acetate to methanol eluent), followed by triturated with methanol to produce a red powder as a precipitate that was collected by vacuum filtration. (73.0 mg, 5%); mp 327-330 °C; IR ν_{max} (cm^{-1}): 3133.2, 1600.5, 1521.5, 1557.7, 1397.8, 1036.2, 973.3, 925.6; ^{1}H NMR (500 MHz, DMSO-d_6): δ 2.22 (s, 3H), 2.43 (broad s, 8H), 3.5 (broad s, 8H), 6.85-6.88 (d, 1H, J = 15.0 Hz), 7.01-7.03 (d, 2H, J = 10.0 Hz), 7.08-7.10 (d, 2H, J = 10.0 Hz), 7.64-7.65 (d, 2H, J = 5.0 Hz), 7.83-7.86 (d, 2H, J = 15.0 Hz), 7.96-7.98 (d, 2H, J = 10.0 Hz); ^{13}C NMR (125 MHz, DMSO- d_6): δ 46.01, 46.08, 46.51, 46.95, 54.65, 54.71, 96.14, 113.69, 114.62, 117.06, 119.35, 124.14, 131.48, 131.57, 145.38, 153.41, 155.42, 177.56, 177.90; HR-ESI (Q-TOF) m/z: calc'd for $C_{27}H_{33}BF_2N_4O_2^+$ $[M+H]^+$: 494.3938, found: 495.4013.

Synthesis of 6. **(4,6-bis(4-(4-methylpiperazin-1-yl)styryl)pyrimidin-2-ol)**

0.37 mg (3.0 mmol) of 4,6-dimethylpyrimidone, 1.50 g (7.3 mmol) of 4-(4-methyl-1-piperazinyl)-benzaldehyde, 2.40 g (19.0 mmol) of TMS-Cl, and 10 ml of anhydrous dimethylformamide were mixed in a 25 mL pressure tube with a magnetic stirbar. After heating at 90 ^{o}C for 2 days, the reaction was cooled to room temperature and quenched with concentrated sodium hydroxide; the precipitate was isolated by filtration. **6** was crystallized from isopropanol, resultant yellow flakes were filtered and dried under vacuum. (0.41 g, 82%); mp 400 °C (decomp.); IR ν_{max} (cm^{-1}): 3678.1, 2974.9, 1741.2, 1630.7, 1601.4, 1543.9, 1294.3, 1142.0, 1007.5, 973.4, 825.0; ^{1}H NMR (500 MHz,

DMSO-d_6, TFA): δ 1.99 (s, 6H), 3.13-3.16 (broad d, 4H J = 15.0 Hz), 3.19-3.22 (broad d, 4H, J =15.0 Hz) 3.51-3.53 (d, 4H, J = 10.0 Hz), 4.10-4.13 (d, 4H, J = 15.0 Hz), 6.92-6.95 (d, 2H, J = 15.0 Hz), 7.14-7.15 (d, 4H, J = 5.0 Hz) 7.524 (s, 1H), 7.60-7.62 (d, 4H, J = 10.0 Hz), 8.19-8.22 (d, 4H, J = 15.0 Hz), 10.570 (broad s, 1H); ^{1}H NMR (500 MHz, MeOD-d_4, TMS-Cl): δ 2.37 (s, 6H), 2.63-2.64 (d, 8H, J = 5.0 Hz), 6.80-6.83 (d, 2 H, J = 15.0 Hz), 6.953 (s, 1H), 7.00-7.02 (d, 4H, J = 10.0 Hz), 7.57-7.59 (d, 4H, J = 10.0 Hz), 7.76-7.79 (d, 2H, J = 15.0 Hz); ^{13}C NMR (125 MHz, MeOD-d_4,): δ 23.15, 45.00, 54.51, 101.43, 115.46, 124.15, 127.80, 128.21, 134.59, 151.31, 165.30, 169.78, 179.12. HR-ESI (Q-TOF) m/z: calc'd for $C_{30}H_{36}N_6O^+$ $[M+H]^+$: 497.6654, found: 497.3043.

Synthesis of 7. **(4,6-bis(4-(4-methylpiperazin-1-yl)-styryl)-1,3-propane- dionato-κO, κO']-difluoroborane)**: 3.10 g (15.1 mmol) of 4- (4-methyl-1-piperazinyl)-benzaldehyde, 1.10 g (7.5 mmol) difluro-2,4-pentanedianatoboron, 1.73 g (7.5 mmol of tributyl borate, 0.110 g (1.5 mmol) of tert-butylamine and 15 ml of toluene were mixed in a 25 mL round bottom flask with a stirbar and heated at 70 ^{o}C. After 48 h the reaction was cooled and the precipitate filtered and rinsed with toluene. The precipitate was then recrystallized in isopropanol. (160 mg, 40%); mp 325-329 °C; IR ν_{max} (cm^{-1}): 3579.2, 2741.4, 1595.3, 1543.4, 1492.5, 1392.7, 1057.9, 995.7, 974.5, 822.4; ^{1}H NMR (500 MHz, DMSO-d_6,): δ 2.858 (s, 6H), 3.12-3.16 (t, 8H, J =20.0 Hz) 3.52-3.53 (d, 8H, J = 10.0 Hz), 4.12-4.15 (t, 8H, J = 15.0 Hz), 6.386 (s, 1H), 6.97-7.00 (d, 2H, J = 15.0 Hz) 7.09- 7.11 (d, 4H, J = 10.0 Hz), 7.77-7.79 (d, 4H, J = 10.0 Hz), 7.89- 7.92 (d, 2H, J = 15.0 Hz): ^{13}C NMR (125 MHz, DMSO-d_6, TFA): δ 40.86, 42.52, 44.53, 52.39, 101.83, 115.28, 117.61, 125.30, 132.09,

146.54, 152.31, 178.56 HR-ESI (Q-TOF) m/z: calc'd for $C_{29}H_{36}BF_2N_4O_2^+$ $[M+H]^+$: 521.4393, found: 521.2905.

Synthesis of 8. **(1-(4-(4-methylpiperazyn-1-yl)phenyl)-butane-1-3- dione)**: To a nitrogen-purged 25 mL Schlenk flask charged with a stirbar and containing 0.25 g of sodium hydride, 10 mL of anhydrous ethanol was added by syringe at 0 ^oC. To this mixture, 2.0 g of anhydrous ethyl acetate (20.5 mmol) was added while stirring. After 5 min, 3.0 g (13.7 mmol) of 4-(4- methyl-1-piperazinyl)-ethanone dissolved in anhydrous THF were added by syringe. After stirring for 24 h at room temperature, the mixture was quenched with the addition of 5% HCl solution, extracted three times with ethyl acetate, dried over anhydrous MgSO4. Crystallization from isopropanol produced 2.50 g (70%) of **8** as a beige powder; mp. 324-326 °C (decomp.); IR ν_{max} (cm^{-1}): 3357.7, 2975.4, 2941.1, 1568.1, 1380.5, 1289.1, 1201.4, 785.8; ^1H NMR (500 MHz, DMSO-d_6 TFA) (major tautomer): δ 2.19 (s, 3H), 2.81 (s, 3H), 3.26 (broad s, 8H), 6.46 (s, 1H), 7.07-7.08 (d, 2H, J = 5.0 Hz), 7.88- 7.86 (d, 2H, J = 10.0 Hz); ^{13}C NMR (125 MHz, DMSO-d_6, TFA): δ 25.07, 31.08, 44.63, 52.43, 95.93, 114.64, 124.68, 129.37, 130.97, 158.57, 184.42, 191.20; HR-ESI (Q-TOF) m/z: calc'd for $C_{15}H_{21}N_2O_2^+$ $[M+H]^+$: 261.3445, found 261.1609.

Synthesis of 9. **(1-(4-(4-methylpiperazin-1-yl)phenyl)-1,3-propane- dionato-κO, κO']difluoro-borane)**: 1.0 g (3.8 mmol) of 1-(4- (4-methylpiperazyn-1-yl)phenyl)butane-1-3-dione was placed in a nitrogen-purged 25 mL Schlenk flask charged with a stirbar. The flask was then capped and 10 mL of anhydrous benzene

followed by 5 ml (40.5 mmol) of boron trifluoride diethyl etherate were added by syringe. The reaction was then stirred at room temperature for 24 h. Excess boron trifluoride diethyl etherate was evacuated and benzene solvent evaporated, the resultant orange slurry was then triturated with ethyl acetate to produce 6 as an orange precipitate that was collected by vacuum filtration. (0.862 g, 72%); mp 242-244 °C (decomp.); IR ν_{max} (cm^{-1}): 3672.9, 2978.9, 1559.9, 1055.4, 976.3; ^{1}H NMR (500 MHz, DMSO-d_6): δ 2.21 (s, 3H), 2.29 (s, 3H), 2.41-2.42 (t, 4H J = 5.0 Hz), 3.51-3.53 (t, 4H, J = 10.0 Hz), 6.95 (s, 1H), 7.06-7.08 (d, 2H, J = 10.0 Hz), 7.99-8.01 (d, 2H, J = 10.0 Hz); ^{13}C NMR (125 MHz, DMSO-d_6): δ 24.25, 42.51, 43.89, 52.35, 96.63, 114.27, 119.22, 132.25, 154.94, 180.21, 188.97; HR-ESI (Q-TOF) m/z: calc'd for $C_{15}H_{20}BF_2N_2O_2^+$ $[M+H]^+$: 309.1433, found: 309.1601.

Synthesis of 10. (**4-methyl-6-(4-(4-methylpiperazin-1-yl)phenyl)- pyrimidin-2-ol)**: 1.0 g (3.8 mmol) of 5, 1.38 g (23 mmol) of urea, 2.0 mL of HCl and 10.0 mL of isopropanol were mixed in a 20 mL pressure tube with a magnetic stirbar. After monitoring the reaction by TLC, the reation was cooled to room temperature and quenched with concentrated sodium hydroxide; the resultant yellow precipitate was then filtered and dried under vacuum. (0.37 g, 34%); mp 325-330 °C; IR ν_{max} (cm^{-1}): 3680.3, 2983.9, 2899.8, 1643.1, 1619.1, 1584.3, 1240.9, 1203.0, 1065.9, 814.0; ^{1}H NMR (500 MHz, DMSO-d_6): 2.22 (s, 6H), 2.42-2.44 (t, 4H, J = 10.0 Hz), 3.29-3.31 (t, 4H, J = 10.0 Hz), 6.791 (s, 1H), 7.00-7.02 (d, 2H, J = 10.0 Hz), 7.95-7.97 (d, 2H, J = 10.0 Hz); ^{13}C NMR (125 MHz, DMSO-d_6, TFA): δ 19.65, 42.44, 44.52, 52.29, 100.02, 114.92, 123.84,

130.08, 152.77, 155.48, 161.25, 167.43; HR-ESI (Q-TOF) m/z: calc'd for $C_{16}H_{20}N_4O^+$ $[M+H]^+$: 285.3705, found: 285.1734.

The synthesis of **11** was reported,[116] however, only elemental analysis was reported. Here we report a new route to **11** and provide full characterization data.

(4,6-bis(4-(4-methylpiper-azin-1-yl)phenyl)-pyrimidine). 4,6-Bis(4-fluorophenyl)pyrimidine[116,117] (450 mg, 1.68 mmol), Cs_2CO_3 (1 g, 3.0 mmol), N-methylpiperazine (3.0 mL, 27.0 mmol) and 1.0 mL of DMSO were placed in a 15 mL pressure tube with a stir bar, then heated at 90 °C for 96 h. The progress of the reaction was monitored every 12 h by TLC until the 4,6-bis(4-fluorophenyl)pyrimidine and mono-substituted product were completely consumed. The cooled, crude reaction mixture was poured into 100 mL of water, extracted with 3 x 50 mL of EtOAc and 1 x 50 mL of CH_2Cl_2. The organic fractions were combined with the solvents removed under reduced pressure; as the volume reduced, a yellow precipitate was observed. This was collected by filtration to yield 298 mg of 1 (41% yield). mp 468 - 472 °C (decomp.); IR ν_{max} (cm_{-1}): 2967.25, 2930.95, 2840.30, 27966.66, 1606.34, 1570.55, 1499.84, 1223.38, 816.92, 792.64; 1H NMR (500 MHz, DMSO-d_6, TFA): d 2.896 (s, 6H), 3.151 (broad s, 8H), 3.542 (broad s, 4H), 4.053 (broad s, 4H), 7.129-7.147 (d, 4H, J = 9 Hz), 8.262-8.280 (d, 4H, J = 9 Hz), 8.382 (s, 1H), 9.085 (s, 1H), 10.539 (broad s, 2H); ^{13}C NMR (125 MHz, DMSO-d_6, TFA): d 42.52, 45.01, 52.47, 110.22, 115.46, 117.73, 127.26, 128.95, 151.89, 163.18; HR-ESI (Q-TOF) m/z: calcd for C15H21N2O2+ [M+H]+ calcd 429.2761, found 429.2754.

REFERENCES

1. 1. T. Jia, J.; Xiang, J.; Wand, P.; Guo, and J. Yu. *Org. Biomol. Chem*. **2013**, 11, 5512-5520.

2. A. Manna and S. Chakravorti. *J. Phys. Chem. B*., **2012**, 116, 5226-5233.

3. Ploeger, L.S.; Dullens, H.F.; Huisman, A.; van Diest, P. *J. Biotech. Histochem*. **2008**, 83, 63-69

4. Glaser, K.; Wilke, K.; Wepf, R.; Biel, S. S. *Skin Res. Technol*. **2009**, 14, 324-326.

5. Nocker, A.; Sossa-Fernandez, P.; Burr, M. D.; Camper, A. K. *Appl. Environ. Microbiol*. **2007**, 73, 5111-5117.

6. Zhao, H.; Traganos, F.; Dobrucki, J.; Wlodkowic, D.; Darzynkiewicz, Z. *Cytometry A*, **2009**, 75, 510-519

7. Huang, X.; King, M. A.; Halicka, H. D.; Traganos, F.; Okafuji, M.; Darzynkiewicz, Z. *Cytometry A***. 2004**, 62, 1-7.

8. Suzuki, T.; Fujikura, K.; Higashiyama, T.; Takata, K. J. *Histochem. Cytochem*. **1997**, 45, 49-53.

9. Darzynkiewizc, Z. *Current Protocols in Cytometry*; John Wiley and Son: 2010; Ch. 7.

10. Gunther, K.; Mertig, M.; Seidel, R. *Nucleic Acids Res*. **2010**, 38, 6526-6532.

11. Persson, F.; Westerlund. F.; Tegenfeldt, J. O.; Kristensen, A. *Small* **2009**, 5, 190-193.

12. Armitage, B. A. *Top. Curr. Chem*. **2005**, 253, 55-76.

13. Hirons, G. T.; Fawcett, J. J.; Crissman, H. A. *Cytometry* **1994**, 15, 129-140.

14. Bink, K.; Walch, A.; Feuchtinger, A.; Eisenmann, H.; Hutzler, P.; Hofler, H.; Werner, M. Histochem. *Cell. Biol*. **2001**, 115, 293-299.

15. Adjaye-Mensah, E.; Gonzalez, W. G.; Busse, D. R.; Captain, B.: Mikosovska, J.; Wilson, J. N. *J. Phys. Chem. A* **2012**, 116, 8671-8677.

16. Dhuguru, J.; Gheewala, C.; Kumar, N. S. S.; Wilson, J. N. *Org. Lett*. **2011**, 13, 4188-4191.

17. Zucchero, A.J.; McGrier, P.L.; Bunz, U. H. F. *Acc. Chem. Res*. **2010**, 43, 397-408.

18. Wilson, J.N.; Brown, A. S.; Babinchak, W. M.; Ridge, C.D.; Walls, J. D. *Org. Bionol. Chem.* **2012**, 10, 8710-8719.

19. Norben, B.; Kubista, M.; Kurucsec, T. Q. *Rev. Biophys*. **1992**, 25, 51-170.

20. Larsson, A.; Akerman, B.; Jonsson, M. *J. Phys. Chem*. **1996**, 100, 3252-3263.

21. Carlsson, C.; Larsson, A.; Jonsson, M.; Albinsson, B.; Norben, B. *J. Phys. Chem*. **1994**, 98, 10313-10321.

22. Eriksson, S.; Kim, S. K.; Kubista, M.; Norden, B. *Biochemistry* **1993**, 32, 2987-2998.

23. Kim, S. K.; Eriksson, S.; Kubista, M.; Norden, B. *J. Am. Chem. Soc*. **1993**, 115, 3441-3447.

24. Cosa, G.; Focsaneanu, K. S.; McLean, J. R.; McNamee, J. P.; Scaiano, J. C. *Photochem, Photobiol*. **2001**, 73, 585.

25. Wilson, J. N.; Cho, Y. Y.; Tan, S.; Cuppoletti, A.; Kool, E. T. *ChemBioChem*. **2008**, 9, 279-285.

26. Ihmels, H.; Faulhaber, K.; Wissel, K.; Viola, G.; Vedaldi, D. *Org. Biomol. Chem*. **2003**, 1, 2999-3001.

27. Vummidi, B. R.; Alzeer, J.; Luedtke, N. W. *ChemBioChem*. **2013**, 14, 540-558.

28. Pitter, D. R. G.; Wigenius, J.; Brown, A. S.; Baker, J. D.; Westerlund, F.; Wilson, J. N. *Org Lett.* **2013**, 15, 1330-1333.

29. Suzuki, T.; Fujikura, K.; Higashiyama, T.; Takata, K. *J. Histochem. Cytochem*. **1997**, 45, 49-53.

30. Glaser, K.; Wilke, K.; Wepf, R.; Biel, S. S. *Skin Res. Technol*. **2008**, 14, 324-326.

31. Banerjee, D.; Pal, S. K. *J. Phys. Chem. B*. **2008**, 112, 1016-1021.

32. Schweitzer, C.; Scaiano, J. C. *Phys. Chem. Chem. Phys.* **2003**, 5, 4911-4917.

33. Marky, L.A.; Blumenfeld, K. S.; Kozlowski, S.; Breslauer, K. J. *Biopolymers* **1983**, 22, 1247-1257.

34. Nakano, S.; Kirihata, T.; Fujii, S.; Sakai, H.; Kuwahara, M.; Sawai, H.; Sugimoto, N. *Nucleic Acids Res*. **2007**, 35, 486-494.

35. Seidel, C. A. M.; Schulz, A.; Sauer, M. H. M. *J. Phys. Chem*. **1996**, 100, 5541-5553.

36. Pakku, Y.; Hill, G. *J. Phys. Chem. A* **2011**, 115, 4804-4810.

37. Steenken, S.; Reynisson, J. *Phys. Chem. Chem. Phys*. **2010**, 12, 9088-9093.

38. Hsu, S. C. N.; Wang, T. P.; Kao, C. L.; Chen, H. F.; Yang, P. Y.; Chen, H. Y. *J. Phys. Chem. B* **2013**, 117, 2096-2105.

39. Caruso, T.; Carotenuto, M.; Vasca, E.; Peluso, A. *J. Am. Chem. Soc*. **2005**, 127, 15040-15041.

40. Wigenius, J.; Andersson, M. R.; Esbjorner, E. K.; Westerlund, F. *Biochem. Biophys. Res. Commun*. **2011**, 408, 115-119.

41. Murphy, C. J.; Arkin, M. R.; Ghatlia, N. D.; Bossmann, S.; Turro, N. J.; Barton, J. K. *Proc. Natl. Acad. Sci*. U.S.A. **1994**, 91, 5315-5319.

42. Garo, F.; Haner, R. *Bioconjugate Chem*. **2012**, 23, 2015-2113.

43. Somsen, O. J. G.; van Hoek, A.; van Amerongen, H. *Chem. Phys. Lett*. **2004**, 402, 61-65.

44. Goncalves, M. S. *Chem. Rev*. 2009, 109, 190-212.

45. Sinkeldam, R. W.; Greco, N. J.; Tor, Y. *Chem. Rev*. **2010**, 110, 2579-2619.

46. Giepmans, B. N. B.; Adams, S. R.; Ellisman, M. H.; and Tsien, R. Y. *Science*, **2006**, 312, 217-224.

47. Armitage, B. A.; *Curr. Opin. Chem. Biol*. **2011**, 15, 806-812.

48. Smith, P. J.; Wiltshire, M.; Davies, S.; Patterson, L. H.; Hoy, T. *J. Immunol. Methods*, **1999**, 229, 131-139.

49. Kapuscinski, J. *Histochem. Cytochem*. **1990**, 38, 1323-1329.

50. Vlodkowic, D.; Skommer, J.; Darzynkiewicz, Z. *Cytometry A*. **2008**, 73A, 496-507.

51. Wilson, J. N.; Wigenius, J.; Pitter, D. R. G.; Qui, Y.; Abrahamsson, M.; Westerlund, F. *J. Phys. Chem. B*. **2013**, 117, 12000-12006.

52. Frisch, M. J.; Trucks, G. W.; Schlegel, H. B.; Scuseria, G. E.; Robb, M. A.; Cheeseman, J. R.; Scalmani, G.; Barone, V.; Mennucci, B.; Petersson, G. A.; Nakatsuji, H.; Caricato, M.; Li, X.; Hratchian, H. P.; Izmaylov, A. F.; Bloino, J.; Zheng, G.; Sonnenberg, J. L.; Hada, M.; Ehara, M.; Toyota, K.; Fukuda, R.; Hasegawa, J.; Ishida, M.; Nakajima, T.; Honda, Y.; Kitao, O.; Nakai, H.; Vreven, T.; Montgomery Jr., J. A.; Peralta, J. E.; Ogliaro, F.; Bearpark, M.; Heyd, J. J.; Brothers, E.; Kudin, K. N.; Staroverov, V. N.; Kobayashi, R.; Normand, J.; Raghavachari, K.; Rendell, A.; Burant, J. C.; Iyengar, S. S.; Tomasi, J.; Cossi, M.; Rega, N.; Millam, J. M.; Klene, M.; Knox, J. E.; Cross, J. B.; Bakken, V.; Adamo, C.; Jaramillo, J.; Gomperts, R.; Stratmann, R. E.; Yazyev, O.; Austin, A. J.; Cammi, R.; Pomelli, C.; Ochterski, J. W.; Martin, R. L.; Morokuma, K.; Zakrzewski, V. G.; Voth, G. A.; Salvador, P.; Dannenberg, J. J.; Dapprich, S.; Daniels, A. D.; Farkas, Ö.; Foresman, J. B.; Ortiz, J. V.; Cioslowski, J.; Fox, D. J. *Gaussian 09, Revision A.1*, Gaussian, Inc., Wallingford, CT, **2009**.

53. A. V. Marenich, C. J. Cramer and D. G. Truhlar, *J. Phys. Chem. B*, 2009, **113**, 6378-6396.

54. Cavatoria, P.; Masotti, L.; and Szabo, A.G. *Biophys. Chem*. **1985**, 22, 11-16

55. Comings, D. E. *Chromasoma*, **1975**, 52, 229-243.

56. Eisfeld, A. and Briggs, J. S. *Chem. Phys*. **2006**, 324, 376-384.

57. Fassano, M.; Currt, S.; Terreno, E.; Galliano, M.; Fanali, G.; Narciso, P.; Notari, S.; Ascenzi, P. *Life*, **2005**, 57, 787-796.

58. Berlman, I. *Handbook of Fluorescence Spectra of Aromatic Molecules*, Academic Press, New York, 2nd edn, **1971**.

59. Park, E.; Baron, R. and Landgraf, R. *Biochem*., **2008**, 47, 11992-12005.

60. Wang, J. Nucleic Acids Res. **2008**, 28, 3011-3016.

61. Benvin, A. L.; Creeger, Y.; Fisher, G. W.; Ballou, B.; Waggoner, A. S.; Armitage, B. A. *J. Am. Chem. Soc*. **2007**, 129, 2025-2034.

62. Ihmels, H.; Otto, D. *Top. Curr. Chem*. **2005**, 258, 161-204.

63. Berman, H. M.; Young, P. R. *Ann. Rev. Biophys. Bioeng.* **1981**, *10*, 87-114.

64. Mukherjee, A.; Lavery, R.; Bagchi, B.; Hynes, J. T. *J. Am. Chem. Soc*. **2008**, *130*, 9747–9755.

65. Suh, D.; Chaires, J. B. *Bioorg. Med. Chem.* **1995**, *3*, 723-728.

66. Clark, T. B.; Ziółkowski, M.; Schatz, G. C.; Goodson III, T. *J. Phys. Chem. B* **2014**, 118, 2351-2359.

67. McLean, A. M.; Socher, E.; Varnavski, O.; Clark, T. B.; Imperiali, B.; Goodson III, T. *J. Phys. Chem. B* **2013**, *117*, 15935-15942.

68. Wang, Y.; Clark, T. B.; Goodson, T. *J. Phys. Chem. B*. **2010**, 114, 7112-7120.

69. Wang, Y.; He, G. S.; Prasad, P. N.; Goodson, T. *J. Am. Chem. Soc.* **2005**, 127, 10128-10129.

70. Flynn, D. C.; Ramakrishna, G.; Yang, H. B.; Northrop, B. H.; Stang, P. J.; Goodson III, T. *J. Am. Chem. Soc.* **2010**, *132*, 1348-1358.

71. Bhaskar, A.; Ramakrishna, G.; Lu, Z.; Twieg, R.; Hales, J. M.; Hagan, D. J.; Stryland, E. V.; Goodson, T. *J. Am. Chem. Soc.* **2006**, *128*, 11840-11849.

72. Wheelhouse, R. T.; Jennings, S. A.; Phillips, V. A.; Pletsas, D.; Murphy, P. M.; Garbett, N. C.; Chaires, J. B.; Jenkins, T. C. *J. Med. Chem.* **2006**, *49*, 5187-5198.

73. Drobizhev, M.; Makarov, N. S.; Tillo, S. E.; Hughes, T. E.; Rebane, A. *Nat. Methods* **2011**, *8*, 393-399.

74. Drobizhev, M.; Tillo, S.; Makarov, N. S.; Hughes, T. E.; Rebane A. *J. Phys. Chem. B* **2009**, *113*, 12860-12864.

75. Bairu, S.; Ramakrishna, G. *J. Phys. Chem. B*. **2013**, 117, 10484-10491.

76. Dumat, B.; Bordeau, G.; Faurel-Paul, E.; Mahuteau-Betzer, F.; Saettel, N.; Metge, G.; Fiorini-Debuisschert, C.; Charra, F.; Teulade-Fichou, M. P. *J. Am. Chem. Soc*. **2013**, 135, 12697-12706.

77. Allain, C.; Schmidt, F.; Lartia, R.; Bordeau, G.; Fiorini-Debuisschert, C.; Charra, F.; Tauc, P.; Teulade-Fichou M. P. *ChemBioChem* **2007**, 8, 424-433.

78. Takashima, S. *J. Mol. Biol*. **1963**, 7, 445-468.

79. Saxena, V. K.; Van Zandt, L. L. *Phys. Rev. A: At., Mol., Opt. Phys*. **1992**, 45, 7610-7620.

80. Stigter, D. *Biophys. Chem*. **2002**, 101-102, 447-459.

81. Stigter, D.; Bustamante, C. *Biophys. J*. **1998**, 75, 1197-1210.

82. Ferree, S.; Blanch, H. W. *Biophys. J*. **2003**, 85, 2539-2546.

83. Armstrong, R. W.; Kurucsev, T.; Strauss, U. P. *J. Am. Chem. Soc*. **1970**, 92, 3174-3181.

84. Furse, K. E.; Corcelli, S. A. *J. Am. Chem. Soc*. **2008**, 130, 13103-13109.

85. Xu, C.; Webb, W. *J. Opt. Soc. Am. B*. **1996**, 13 481-491.

86. Reynisson, J.; Schuster, G. B.; Howerton, S. B.; Williams, L. D.; Barnett, R. N.; Cleveland, C. L.; Landman, U.; Harrit, N.; Chaires, J. B. *J. Am. Chem. Soc*. **2003**, 125, 2072-2083.

87. Nafisi, S.; Saboury, A. A.; Keramat, N,; Neault, J. F.; Tajmir-Riahi, H. A. *J. Mol. Struct.* **2007**, 827, 35-43.

88. Zama, M.; Ichimura, S. *Biopolymers*. **1970**, 53-63.

89. Mallena, S.; Lee, M. P.; Bailly, C.; Neidle, S.; Kumar, A.; Boykin, D. W.; Wilson, W. D. *J. Am. Chem. Soc*. **2004**, 126, 13659-13669.

90. Fornander, L. H.; Wu, L.; Billeter, M.; Lincoln, P.; Norben, B. *J. Phys. Chem. B*. **2013**, 117, 5820.-5830.

91. Wan, K. X.; Shibue, T.; Gross, M. L. *J. Am. Chem. Soc*. **2000**, 122, 300-307.

92. Mason, S. F.; McCaffery, A.J. *Nature*. **1964**, 204, 468-470.

93. Willis, B.; Arya, D. P. *Biochemistry*. **2006**, 45, 10217-10232.

94. Canete, M.; Villanueva, A.; Juarranz, A.; Stockert, J. C. *Cell Mol. Biol*. **1987**, 33, 191-199.

95. Zsila, F. *Int. J. Bio. Macromol*. **2015**, 72, 1034-1040.

96. Murudkar, S.; Mora, A. K.; Jakka, S.; Singh, P.K.; Nath, S. *J. Photochem. Photobiol., A* **2014**, 295, 17-25.

97. Stsiapura, V. I.; Maskevich, A.A.; Kuzmitsky, V. A.; Turoverov, K. K.; Kuztnetsova, I. M. *J. Phys. Chem. A*. **2007**, 111, 4829-4835.

98. Biancardi, A.; Biver, T.; Burgalassi, A.; Mattonai, M.; Secco, F.; Venturini, M. *Phys. Chem. Chem. Phys.* **2014**, 16, 20061-20072.

99. Yang, D.; Strode, J. T.; Spielmann, H. P.; Wang, A. H. J.; Burke, T. G. *J. Am. Chem. Soc*. **1998**, 120, 2979-2980.

100. Streltsov, S.; Sukhanova, A.; Mikheikin, A. ; Grokhovsky, A.; Zhuze, A., Kudelina, I.; Mochalov, L.; Olienikov, V.; Jardillier, J. C.; Nabiev, I. *J. Phys. Chem. B*. **2001**, 105, 9643-9652.

101. Joshi, H.; Sengupta, A.; Gavvala, K.; Hazra, P. *RSC Adv*. **2014**, 4, 1015-1024.

102. Moon, J. H.; Kim, S. K.; Sehlstedt, U.; Rodger, A.; Norden, B. *Biopolymers*. **1996**, 38, 593-606.

103. Wilson, W. D.; Tanious, F.A.; Ding, D.; Kumar, A.; Boykin, D. W.; Colson, P.; Houssier, C.; Bailly, C. *J. Am. Chem. Soc*. **1998**, 120, 10310-10321.

104. Seifert, J.; Connor, R.; Kushon, S. A.; Wang, M.; Armitage, B. A. *J. Am. Chem. Soc*. **1999**,121, 2987-2995.

105. Liu, Z.; Shao, P.; Huang, Z.; Liu, B.; Chen, T.; Qin, J. *Chem. Commun*. **2008**, 19, 2260-2292.

106. Greenfield, N. J. *Nat. Protoc*. **2007**, 1, 2876-2890.

107. Marenich, A. V.; Cramer, C. J.; Truhlar, D. G. *J. Phys. Chem. B* 2009, 113, 6378−6396.

108. Reynolds, G. A.; Drexhage, K. H. *Opt. Comm*. 1975, 13, 222-225.

109. Rurack, K.; Spieles, M. *Anal. Chem*. 2011, 83, 1232-1242.

110. Jones II, G.; Jackson, W. R.; Choi, C.; Bergmark, W. R. *J. Phys. Chem*. 1985, 89, 294.

111. Berlman, I., *Handbook of Fluorescence Spectra of Aromatic Molecules*. 2nd ed.; Academic Press: New York, 1971

112. Xu, C.; Webb, W. W. *J. Opt. Soc. Am. B* 1996, 13, 481-491.

113. Oulianov, D. A.; Tomov, I. V.; Dvornikov, A. S.; Rentzepis, P. M. *Opt. Commun.* 2001, 191, 235-243.

114. Lieber, S.; Scheer, F.; Meissner, W.; Naruhn, S.; Adhikary, T.; Müller-Brüsselbach, S.; Diederich, W. E.; Müller R. *J. Med. Chem.* **2012**, *55*, 2858-2868.

115. Yadav, N.; Dixit, S. K.; Bhattacharya, A.; Mishra, L. C.; Sharma, M.; Awasthi, S. K.; Bhasin, V. K. *Chem. Biol. Drug Des.* **2012**, *80*, 340-347.

116. Wheelhouse, R. T.; Jennings, S. A.; Phillips, V. A.; Pletsas, D.; Murphy, P. M.; Garbett, N. C.; Chaires, J. B.; Jenkins, T. C. *J. Med. Chem*. 2006, 49, 5187.

117. Qing, F.-L.; Wang, R.; Li, B.; Zheng, X.; Meng, W.-D. *J. Fluorine Chem*. 2003, 120, 21.

Appendix A

SYNTHESIS AND OPTICAL PROPERTIES OF NOVEL TURN-ON, FLUORESCENT NUCLEAR STAINS WITH LIVE CELL COMPATIBILITY

The following compounds were synthesized using the general synthetic methods of compounds **1-11**.

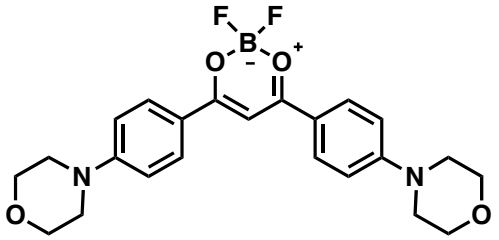

Synthesis of 1,3-bis(4-morpholinophenyl)-1,3-propanedionato-κO, κO')difluoroborane: (500 mg, 60%); m.p. 320-322°C; IR ν_{max} (cm^{-1}): 2960.43, 2854.00, 1604.03, 1546.39, 1496.85, 1440.09, 1354.19, 1229.41, 1016.15, 923.07, 809.67; ^{1}H NMR (500 MHz, DMSO-d_6,): δ 3.45-3.47 (t, 8H, J = 5.0 Hz) 3.74-3.76 (t, 8H, J = 5.0 Hz), 7.07-7.09 (d, 4H, J = 10.0 Hz), 7.49 (s, 1H), 8.17-8.19 (d, 4H, J = 10.0 Hz): ^{13}C NMR (125 MHz, DMSO-d_6, TFA): δ 46.75, 66.24, 91.10, 113.47, 120.30, 131.55, 155.51, 177.83.

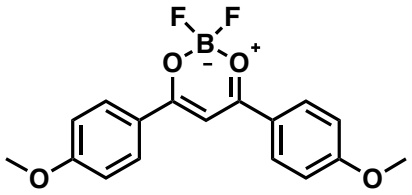

Synthesis of 1,3-bis(4-methoxyphenyl)-1,3-propanedionato-κO, κO')difluoroborane: (215 mg, 60%); m.p. 286-290 °C; IR ν_{max} (cm^{-1}): 2945.07, 1604.56, 1584.75, 1547.50, 1422.03, 1376.23, 1314.34, 1267.25, 1034.95, 1018.70, 794.34, 703.34 ^{1}H NMR (500 MHz, DMSO-d_6,): δ 3.94 (s, 6H), 7.19-7.21 (d, 4H, J =10.0 Hz) 7.75 (s, 1H), 8.36-3.38

(d, 4H, J = 10.0 Hz: ^{13}C NMR (125 MHz, DMSO-d_6): δ 56.38, 92.85, 115.30, 124.18, 132.21, 165.78, 180.54

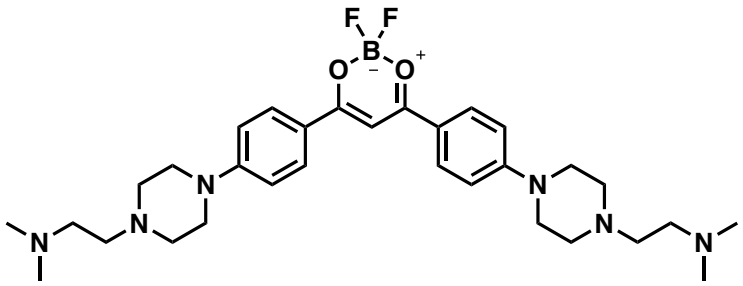

Synthesis of 1,3-bis(1-(4-(4-(2-dimethylamino)ethyl)piperazin-1-yl)phenyl)-1,3-propanedionato-κO, κO')difluoroborane: (68 mg, 20%); m.p. 225-227°C; IR ν_{max} (cm^{-1}): 27772.2, 1674.79, 1445.92, 1389.10, 1227.58, 1199.41, 1000.05, 804.65, 735.76; ^{1}H NMR (500 MHz, DMSO-d_6,): δ 2.148 (s, 6H), 2.36-2.38 (t, 4H, J = 5.0 Hz), 2.42-2.44 (t, 4H, J = 5.0 Hz), 2.53 (broad s, 8H), 3.46 (broad s, 8H), 7.05-7.07 (d, 4H, J = 10 Hz), 7.44 (s, 1H), 8.13-8.15 (d, 4H, J = 10.0 Hz): ^{13}C NMR (125 MHz, DMSO-d_6): δ 46.04, 46.63, 53.19, 56.16, 57.13, 90.97, 113.49, 119.79, 131.55, 155.24, 177.53: HR-ESI (Q-TOF) m/z: calc'd for $C_{31}H_{46}BF_2N_6O_2^+$ $[M+H]^+$: 583.5553, found: 583.5526.

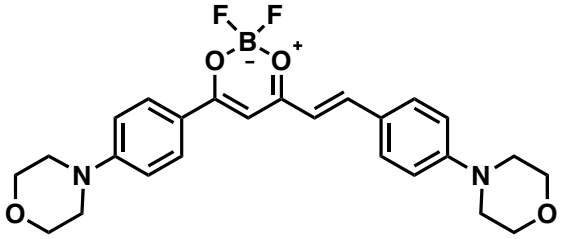

Synthesis of (E)-4-(4-morpholino)phenyl)-6-(4-morpholino)styryl)-1,3-propanedionato-κO, κO')difluoroborane: (440 mg, 55%); m.p. 350 °C decomp; IR

ν_{max} (cm^{-1}): 2947.15, 1600.83, 1542.25, 1498.26, 1440.10, 1364.52, 1344.91, 1251.93, 1218.82, 1022.86, 978.95, 923.52; ^{1}H NMR (500 MHz, DMSO-d_6,): δ 3.32-3.45 (t, 4H, J = 5.0 Hz) 3.47-3.49 (t, 4H, J = 5.0 Hz), 3.74 (s, 8H), 6.89-6.92 (d, 2H, J = 15.0 Hz), 7.03-7.05 (d, 2H, J = 10.0 Hz), 7.04 (s, 1H), 7.10- 7.12 (d, 2H, J = 15.0 Hz), 7.67-7.69 (d, 2H, J = 10.0 Hz), 7.87-7.90 (d, 2H, J = 15.0 Hz), 8.00-8.02 (d, 2H, J = 10.0 Hz): ^{13}C NMR (125 MHz, DMSO-d_6): δ 46.68, 47.21, 66.21, 66.30, 96.27, 113.59, 114.49, 117.26, 119.70, 124.55, 131.45, 131.57, 145.54, 153.63, 155.65, 177.69, 178.00 HR-ESI (Q-TOF) m/z: calc'd for $C_{25}H_{27}BF_2N_2NaO_4^+$ $[M+Na]^+$: 491.2970, found: 491.1901.

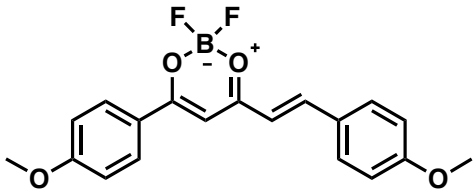

Synthesis (E)-4-(4-methoxy)phenyl)-6-(4-methoxy)styryl)-1,3-propanedionato-κO, κO')difluoroborane of: (250mg, 53%); m.p. 286-290 °C; IR ν_{max} (cm^{-1}): 32979.90, 2849.96, 1600.37, 1538.75, 1499.96, 1377.62, 1195.92, 1165.67, 1124.84, 915.76, 825.47; ^{1}H NMR (500 MHz, DMSO-d_6,): δ 3.85 (s, 3H), 3.92 (s, 3H) 7.08-7.10 (d, 2H, J = 10.0 Hz), 7.19-7.21 (d, 8H, J = 10.0 Hz), 7.254 (s, 1H), 7.81-7.83 (d, 2H, J = 10.0 Hz) 8.07-8.10 (d, 2H, J = 15.0 Hz), 8.16-8.18 (d, 2H, J = 10.0 Hz): ^{13}C NMR (125 MHz, DMSO-d_6): δ 56.04, 56.44, 97.16, 115.38, 115.53, 119.31, 124.03, 127.31, 131.80, 132.03, 147.01, 163.03, 165.76, 179.86, 180.38.

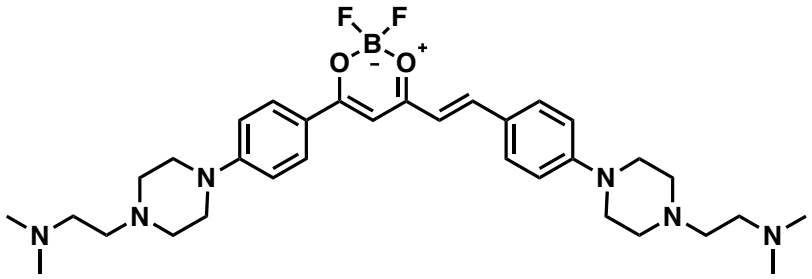

Synthesis of (E)1-(4-(4-dimethyamino)ethyl)piperazin-1-yl)phenyl)-6-(1-(4-(4-dimethylamino)ethyl)piperazin-1-yl)styryl)-1,3-propanedionato-κO, κO')difluoroborane: (350 mg, 60%); m.p. 320 °C decomp.; IR ν_{max} (cm^{-1}): 3137.03, 2832.96, 1627.59, 1602.91, 1553.31, 1377.23, 1361.23, 1243.93, 1198.23, 1055.37, 815.40; ^{1}H NMR (500 MHz, DMSO-d_6,): δ 2.6 (s, 6H), 2.66 (broad s, 4H, Hz) 2.8 (s, 6H), 3.23 (broad s, 4H), 3.41 (broad s, 4H), 3.55 (s, 4H) 6.87-6.90 (d, 2H, J = 15.0 Hz), 7.0 (s, 1H), 7.04-7.06 (d, 2H, J = 10.0 Hz), 7.12-7.14 (d, 2H, J = 10.0 Hz), 7.66-7.68 (d, 2H, J = 10.0 Hz), 7.85-7.88 (d, 2H, J = 15.0 Hz), 7.98-8.0 (d, 2H, J = 10.0 Hz): ^{13}C NMR (125 MHz, DMSO-d_6): δ 43.20, 46.40, 46.84, 51.94, 52.07, 52.43, 52.50, 53.45, 96.21, 113.72, 114.66, 117.06, 119.33, 124.20, 131.51, 131.63, 145.41, 153.33, 155.33, 177.51, 177.87 HR-ESI (Q-TOF) m/z: calc'd for $C_{34}H_{49}BF_2N_5O_2^+$ $[M+H]^+$: 609.5933, found: 609.3894.

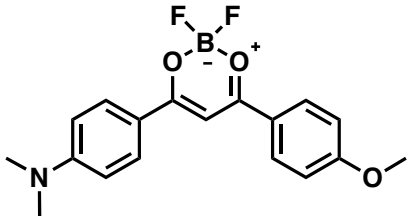

Synthesis of 4-(4-(dimethylamino)phenyl)-6-(4-methoxyphenyl)-1,3-propanedionato-κO, κO')difluoroborane: (340 mg, 58%); m.p. 298-300 °C; IR ν_{max} (cm^{-1}): 2926.67,

2648.30, 1610.46, 1532.04, 1453.44, 1424.16, 1362.37, 1307.05, 1086.88, 1018.98, 803.29, 701.84; ^{1}H NMR (500 MHz, DMSO-d_6,): δ 3.16 (s, 6H), 3.91 (s, 3H) 6.86-6.88 (d, 2H, J = 10.0 Hz), 7.14-7.16 (d, 2H, J = 10.0 Hz), 7.53 (s, 1H), 8.19-8.21 (d, 2H, J = 10.0 Hz) 8.25-8.27 (d, 2H, J = 10.0 Hz): ^{13}C NMR (125 MHz, DMSO-d_6, TFA): δ 56.11, 91.66, 114.32, 114.97, 116.61, 125.25, 131.13, 132.35, 155.65, 164.69, 176.60, 179.64: HR-ESI (Q-TOF) m/z: calc'd for $C_{18}H_{19}BF_2NO_3^+$ $[M+H]^+$: 346.1597, found: 346.1434.

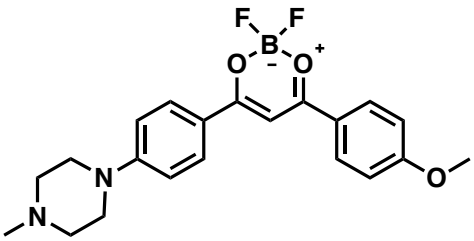

Synthesis of 4-(4-methoxyphenyl)-6-(4-(4-methylpiperazin-1-yl)-1,3-propanedionato-κO, κO')difluoroborane: (162 mg, 60%); m.p. 318-320 °C; IR ν_{max} (cm^{-1}): 3566.04, 3126.75, 1602.61, 1552.53, 1530.60, 1498.25, 1366.96, 1241.20, 100.14, 946.97, 844.43; ^{1}H NMR (500 MHz, DMSO-d_6,): δ 2.87 (s, 3H), 3.14-3.18 (t, 4H, J = 10.0 Hz), 3.54-3.56 (d, 4H, J = 10.0 Hz), 3.92 (s, 3H), 4.29-4.32 (d, 4H, J = 15.0 Hz), 7.16-7.18 (d, 2H, J = 10.0 Hz), 7.18- 7.20 (d, 2H, J = 10.0 Hz), 7.64 (s, 1H), 8.26- 8.28 (d, 2H, J = 10.0 Hz), 8.30-8.32 (d, 2H, J = 10 Hz): ^{13}C NMR (125 MHz, DMSO-d_6): δ 42.55, 43.97, 52.43, 56.33, 92.19, 114.25, 115.20, 120.61, 124.54, 131.72, 132.18, 154.70, 165.28, 178.61, 179.89: HR-ESI (Q-TOF) m/z: calc'd for $C_{21}H_{24}BF_2N_2O_3^+$ $[M+H]^+$: 401.2403, found: 401.1853.

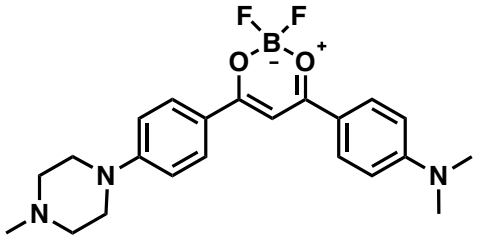

Synthesis of 4-(4-(dimethylamino)phenyl)-6-(4-(4-methylpiperazin-1-yl)-1,3-propanedionato-κO, κO')difluoroborane: (743 mg, 65%); m.p. 286-288 °C; IR ν_{max} (cm^{-1}): 2960.38, 1604.20, 1547.73, 1497.59, 1497.59, 1444.62, 1322.70, 1109.78, 1096.73, 1053.33, 1016.54, 923.51, 869.08, 810.11; ^{1}H NMR (500 MHz, DMSO-d_6,): δ 2.88 (s, 3H), 3.14 (s, 6H) 3.52-3.53 (d, 4H, J = 10.0 Hz), 4.22-4.25 (broad d, 4H, J = 15.0 Hz), 6.84-6.86 (d, 2H, J = 10.0 Hz), 7.15-7.17 (d, 2H, J = 10.0 Hz) 7.45 (s, 2H, J = 10.0 Hz), 8.16-8.18 (d, 2H, J = 10.0 Hz), 8.18-8.20 (d, 2H, J = 10.0 Hz): ^{13}C NMR (125 MHz, DMSO-d_6): δ 42.55, 44.18, 52.45, 90.93, 111.99, 114.43, 117.77, 121.83, 131.05, 131.96, 153.86, 155.32, 172.49, 176.57, 178.52; HR-ESI (Q-TOF) m/z: calc'd for $C_{22}H_{27}BF_2N_3O_2^+$ $[M+H]^+$: 414.2833, found: 414.2149.

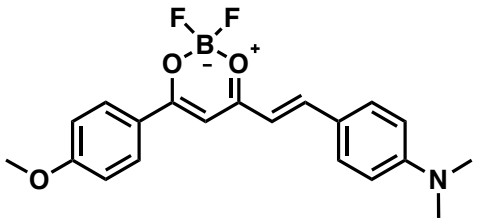

Synthesis of (E)-4-(4-(dimethylamino)styryl)-6-(4-methoxyphenyl)-1,3-propanedionato-κO, κO')difluoroborane: (140 mg, 23%); m.p. 272-274 °C; IR ν_{max} (cm^{-1}): 2931.22, 1599.10, 1531.90, 1487.75, 1373.10, 1257.06, 1099.26, 814.25, 807.05, 785.76; ^{1}H NMR (500 MHz, DMSO-d_6,): δ 3.08 (s, 6H), 3.90 (s, 6H) 6.80-6.82 (d, 2H, J

= 10.0 Hz), 6.83-6.86 (d, 1H, J = 15.0 Hz), 7.09 (s, 1H), 7.15-7.17 (d, 2H, J = 10.0 Hz) 7.69-7.71 (d, 2H, J = 10.0 Hz), 8.03-8.06 (d, 1H, J = 15.0 Hz), 8.09-8.11 (d, 2H, J = 10.0 Hz): ^{13}C NMR (125 MHz, DMSO-d_6): δ 56.29, 96.45, 112.59, 114.11, 115.32, 122.40, 124.73, 131.05, 132.93, 148.94, 153.75, 164.97, 177.02, 180.20; HR-ESI (Q-TOF) m/z: calc'd for $C_{20}H_{21}BF_2NO_3^+$ $[M+H]^+$: 372.1983, found: 372.1575.

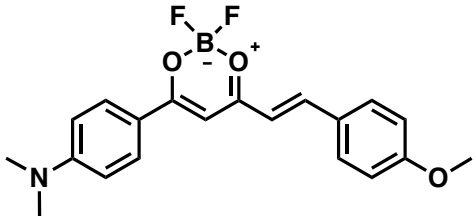

Synthesis of (E)-4-(4-(dimethylamino)phenyl)-6-(4-methoxystyryl)-1,3-propanedionato-κO, κO')difluoroborane: (180 mg, 23%); m.p. 268-270 °C; IR ν_{max} (cm^{-1}): 2936.62, 1614.62, 1605.69, 1511.71, 1414.01, 1362.19, 1228.43, 977.66, 818.05, 803.85; ^{1}H NMR (500 MHz, DMSO-d_6,): δ 3.08 (s, 6H), 3.84 (s, 3H), 6.87-6.89 (d, 2H, J = 10.0 Hz), 6.96-6.99 (d, 1H, J = 15.0 Hz), 7.02 (s, 1H), 7.05-7.07 (d, 2H, J = 10.0 Hz), 7.74-7.66 (d, 2H, J = 10.0 Hz), 7.83-7.86 (d, 1H, J = 15.0 Hz), 8.00-8.02 (d, 2H, J = 10.0 Hz); ^{13}C NMR (125 MHz, DMSO-d_6): δ 55.95, 96.50, 112.32, 115.24, 117.28, 119.96, 127.66, 128.67, 129.37, 131.25, 132.00, 143.39, 155.70, 162.32, 176.02, 179.03; HR-ESI (Q-TOF) m/z: calc'd for $C_{20}H_{21}BF_2NO_3^+$ $[M+H]^+$: 372.1977, found 372.2661.

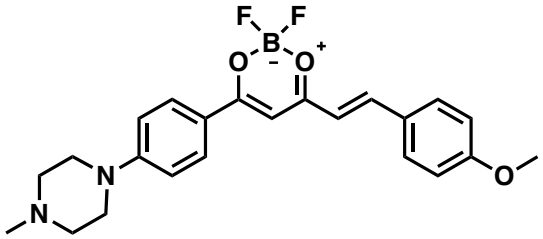

Synthesis of (E)-4-(4-(methoxy)styryl)-6-(4-(4-methylpiperazin-1-yl)-1,3-propanedionato-κO, κO')difluoroborane: (360 mg, 41%); mp 268-270 °C; IR ν_{max} (cm^{-1}): 2841.27, 1597.87, 1504.73, 1246.45, 1001.44, 977.31, 920.68, 828.42, 791.04, 722.50: ^{1}H NMR (500 MHz, DMSO-d_6,): δ 2.27 (s, 3H), 3.05 (broad s, 2H) 3.55 (broad s, 2H), 3.84 (s, 3H), 6.97-7.00(d, 1H, J = 15.0 Hz), 7.00-7.07 (d, 2H, J = 10.0 Hz), 7.07 (s, 1H), 7.10- 7.12 (d, 2H, J = 10.0 Hz), 7.58-7.78 (d, 42, J = 10.0 Hz), 7.88- 7.91 (d, 2H, J = 15.0 Hz), 8.00-8.02 (d, 2H, J = 10.0 Hz): ^{13}C NMR (125 MHz, DMSO-d_6): δ 45.76, 46.25, 54.47, 55.97, 96.66, 113.69, 115.27, 118.89, 119.79, 121.57, 131.42, 131.96, 144.23, 155.62, 162.48, 177.08, 179.02; HR-ESI (Q-TOF) m/z: calc'd for $C_{23}H_{26}BF_2NO_3^+$ $[M+H]^+$: 427.2783, found: 427.2714.

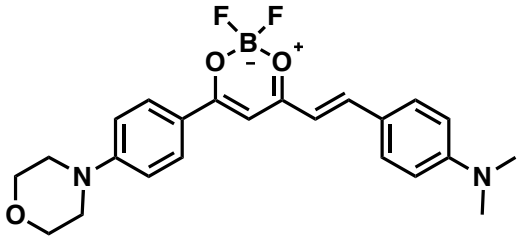

Synthesis of (E)-4-(4-(dimethylamino)styryl)-6-(4-morpholinophenyl)-1,3-propanedionato-κO, κO')difluoroborane: (315 mg, 45%); m.p. 258 °C decomp. ; IR ν_{max} (cm^{-1}): 2846.44, 1599.69, 1526.88, 1508.93, 1483.30, 1431.49, 1365.38, 1127.19, 1077.67, 808.66: ^{1}H NMR (500 MHz, DMSO-d_6,): δ 3.06 (s, 6H), 3.44-3.46 (t, 4H, J =

5.0 Hz) 3.73-3.75 (t, 4H, J = 5.0 Hz), 6.78-6.80 (d, 2H, J = 10.0 Hz), 6.79-6.83 (d, 1H, J = 15.0 Hz) 6.91 (s, 1H), 7.08-7.10 (d, 2H, J = 10.0 Hz) 7.64-7.66 (d, 2H, J = 10.0 Hz), 7.88-7.91 (d, 1H, J = 15.0 Hz), 7.98- 8.00 (d, 2H, J = 10.0 Hz): ^{13}C NMR (125 MHz, DMSO-d_6, TFA): δ 46.74, 66.22, 95.79, 112.17, 115.43, 120.40, 122.40, 128.70, 129.80, 131.13, 132.01, 146.60, 153.22, 155.47, 117.22, 177.98; HR-ESI (Q-TOF) m/z: calc'd for $C_{23}H_{26}BF_2N_2O_3^+$ $[M+H]^+$: 427.2783, found: 427.1998.

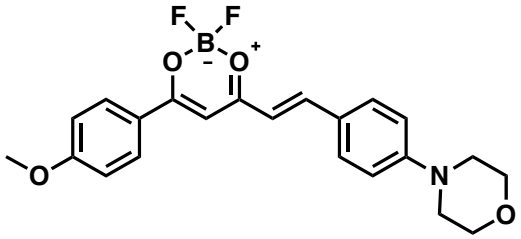

Synthesis of (E)-4-(4-(methoxy)phenyl)-6-(4-morpholino)styryl)-1,3-propanedionato-κO, κO')difluoroborane: (50mg, 12%); m.p. 266 °C decomp. ; IR ν_{max} (cm^{-1}): 2946.32, 1599.91, 1537.64, 1493.53, 1267.84, 1111.63, 1050.54, 845.15, 814.11, 783.72; ^{1}H NMR (500 MHz, DMSO-$d_{6,}$): δ 3.35-3.37 (t, 4H, J = 5.0 Hz) 3.73-3.74 (t, 4H, J = 5.0 Hz), 3.91 (s, 3H), 6.93-6.96 (d, 1H, J = 15.0 Hz), 7.04-7.06 (d, 2H, J = 10.0 Hz) 7.15- 7.18 (d, 2H, J = 10.0 Hz), 7.168 (s, 1H), 7.71-7.73 (d, 2H, J = 10.0 Hz), 8.03- 8.06 (d, 2H, J = 15.0 Hz), 8.12-8.14 (d, 2H, J = 10.0 Hz): ^{13}C NMR (125 MHz, DMSO-d_6): δ 47.10, 56.36, 66.27, 96.72, 114.37, 115.40, 116.59, 124.19, 124.38, 131.34, 132.22, 148.01, 154.02, 165.30, 178.20, 180.32; HR-ESI (Q-TOF) m/z: calc'd for $C_{22}H_{22}BF_2NO_4^+$ $[M+H]^+$: 414.2301, found: 414.1680.

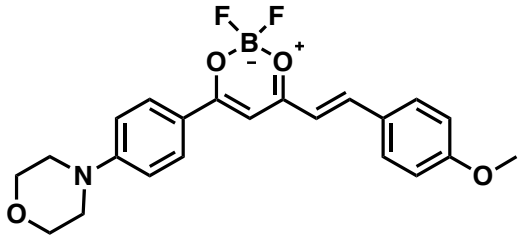

Synthesis of (E)-4-(4-(methoxy)styryl)-6-(4-morpholinophenyl)-1,3-propanedionato-κO, κO')difluoroborane: (245 mg, 36%); m.p. 238-240 °C; IR ν_{max} (cm^{-1}): 2979.78, 2856.01, 1599.89, 1547.29, 1488.92, 1415.07, 1165.88, 1107.41, 1097.19, 967.61, 936.82; ^{1}H NMR (500 MHz, DMSO-d_6,): δ 3.5-3.51 (t, 4H, J =5.0 Hz), 3.73-3.75 (t, 4H, J = 5.0 Hz) 6.97-7.01 (d, 1H, J = 15.0 Hz), 7.05-7.07 (d, 2H, J = 10.0 Hz), 7.08 (s, 1H), 7.10-7.12 (d, 2H, J = 10.0 Hz) 7.76- 7.78 (d, 2H, J = 10.0 Hz), 7.89-7.92 (d, 1H, J = 15.0 Hz), 8.02- 8.04 (d, 2H, J = 10.0 Hz): ^{13}C NMR (125 MHz, DMSO-d_6): 46.67, 55.96, 66.20, 96.70, 113.55, 115.27, 119.32, 119.75, 127.55, 131.46, 131.86, 144.44, 155.91, 162.52, 177.33, 179.14; HR-ESI (Q-TOF) m/z: calc'd for $C_{23}H_{26}BF_2NO_4^+$ $[M+H]^+$: 414.2347, found: 414.1677.

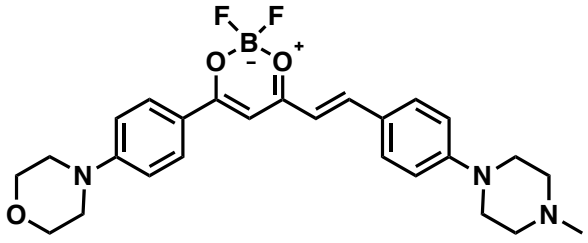

Synthesis of (E)-4-(4-(morpholinophenyl)-6-(4-(4-methylpiperazin-1-yl)styryl)-1,3-propanedionato-κO, κO')difluoroborane: (207 mg, 26%); m.p. 278-280 °C; IR ν_{max} (cm^{-1}): 2937.14, 1599.47, 1540.11, 1497.69, 1378.98, 1344.46, 1103.99, 1022.99, 973.97, 863.10, 678.07; ^{1}H NMR (500 MHz, DMSO-d_6,): δ 2.22 (s, 3H), 2.42-2.44 (t, 4H, J = 5.0

Hz) 3.36-3.38 (t, 4H, J = 5.0 Hz), 3.46-3.48 (t, 4H, J = 5.0 Hz), 3.73-3.75 (t, 4H, J = 5.0 Hz), 6.86-6.89 (d, 1H, J = 15.0 Hz) 7.02- 7.04 (d, 3H, J = 10.0 Hz), 7.09-7.11 (d, 2H, J = 10.0 Hz), 7.64-7.66 (d, 2H, J = 10.0 Hz), 7.86-7.89 (s, 1H, J = 15.0 Hz), 7.99-8.01 (d, 2H, J = 10.0 Hz): ^{13}C NMR (125 MHz, DMSO-d_6): δ 21.63, 47.25, 55.22, 66.23, 96.21, 113.62, 114.60, 119.84, 124.06, 128.67, 129.37, 131.38, 131.68, 138.06, 145.69, 153.50, 155.63, 177.82, 177.89: HR-ESI (Q-TOF) m/z: calc'd for $C_{26}H_{31}BF_2N_3O_3^+$ $[M+H]^+$: 482.3583, found: 482.2431.

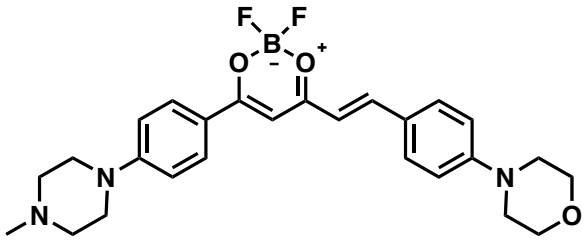

Synthesis of (E)-4-(4-(morpholino)styryl)-6-(4-(4-methylpiperazin-1-yl)phenyl)-1,3-propanedionato-κO, κO')difluoroborane: (120 mg, 24%); m.p. 240-242 °C; IR ν_{max} (cm^{-1}): 2930.15, 1601.10, 1541.33, 1499.22, 1375.80, 1365.90, 1273.62, 813.50, 791.89, 730.00; ^{1}H NMR (500 MHz, DMSO-d_6,): δ 2.23 (s, 3H), 2.43-2.45 (t, 4H, J = 5.0 Hz) 3.31-3.33 (t, 4H, J = 5.0 Hz), 3.50-3.52 (t, 4H, J = 5.0 Hz), 3.73-3.75 (t, 4H, J = 5.0 Hz), 6.88-6.91 (d, 2H, J = 15.0 Hz) 7.01 (s, 1H) 7.02- 7.04 (d, 2H, J = 10.0 Hz), 7.09-7.11 (d, 2H, J = 10.0 Hz), 7.66- 7.68 (d, 2H, J = 10.0 Hz), 7.85-7.88 (t, 1H, J = 15.0 Hz), 7.97-7.99 (d, 2H, J = 10.0 Hz): ^{13}C NMR (125 MHz, DMSO-d_6): δ 46.04, 46.47, 46.47, 47.27, 54.65, 66.31, 96.22, 113.68, 114.51, 117.39, 119.20, 124.62, 131.48, 131.56, 145.24, 153.58, 155.46, 177.43, 177.99; HR-ESI (Q-TOF) m/z: calc'd for $C_{26}H_{31}BF_2N_3O_3^+$ $[M+H]^+$: 482.3583, found: 482.2423.

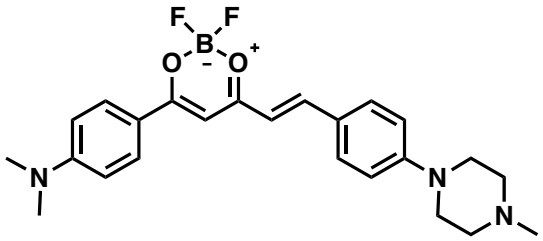

Synthesis of (E)-4-(4-(dimethylaminophenyl)-6-(4-(4-methylpiperazin-1-yl)styryl)-1,3-propanedionato-κO, κO')difluoroborane: (270 mg, 40%); m.p. 276-278 °C; IR ν_{max} (cm^{-1}): 2940.97, 1616.43, 1602.59, 1486.92, 1371.85, 1330.97, 1201.39, 116.09, 1133.59, 1009.73, 815.45; ^{1}H NMR (500 MHz, DMSO-d_6,): δ 2.21 (s, 3H), 2.41-2.453(t, 4H, J = 5.0 Hz), 3.05 (s, 6H), 3.46-3.48 (t, 4H, J = 5.0 Hz), 6.79-6.81 (d, 1H, J = 10.0 Hz)), 6.85-6.87 (d, 2H, J = 10.0 Hz), 6.85-6.88 (d, 1H, J = 15.0 Hz) 6.95 (s, 1H), 7.01-7.03 (d, 2H, J = 10.0 Hz), 7.63- 7.65 (d, 2H, J = 10.0 Hz), 7.79-7.82 (d, 1H, J = 15.0 Hz), 7.97- 7.99 (d, 2H, J = 10.0 Hz): ^{13}C NMR (125 MHz, DMSO-d_6, TFA): 42.53, 44.70, 52.37, 96.24, 112.20, 115.50, 117.43, 117.83, 118.50, 125.67, 131.19, 131.76, 143.88, 151.82, 155.51, 176.26, 178.43; HR-ESI (Q-TOF) m/z: calc'd for $C_{24}H_{29}BF_2N_3O_2^+$ $[M+H]^+$: 440.3213, found 440.3415.

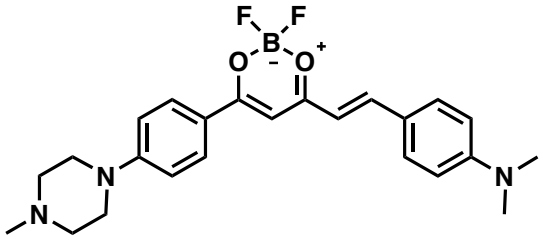

Synthesis of (E)-4-(4-(dimethylamino)styryl)-6-(4-(4-methylpiperazin-1-yl)phenyl)-1,3-propanedionato-κO, κO')difluoroborane: (67 mg, 14%); m.p. 278-280 °C; IR ν_{max}

(cm^{-1}): 2940.26, 1602.35, 1529.62, 1487.58, 1289.76, 1248.08, 1134.04, 1030.51, 975.20, 952.68, 815.; ^{1}H NMR (500 MHz, DMSO-d_6,): δ 2.23 (s, 3H), 2.43-2.45 (t, 4H, J = 5.0 Hz), 3.06 (s, 6H), 3.48-3.50 (t, 4H, J = 5.0 Hz), 6.79-6.81 (d, 1H, J = 10.0 Hz)), 6.80-6.83 (d, 1H, J = 15.0 Hz), 6.96 (s, 1H), 7.08-7.10 (d, 2H, J = 10.0 Hz), 7.64-7.66 (d, 2H, J = 10.0 Hz), 7.87-7.90 (d, 1H, J = 15.0 Hz), 7.96-7.98 (d, 2H, J = 10.0 Hz): ^{13}C NMR (125 MHz, DMSO-d_6, TFA): δ 42.56, 44.11, 52.33, 96.05, 112.53, 114.49, 121.19, 122.06, 131.03, 132.22, 147.24, 153.40, 154.12, 158.75, 159.00, 177.04, 178.63; HR-ESI (Q-TOF) m/z: calc'd for $C_{24}H_{29}BF_2N_3O_2^+$ $[M+H]^+$: 440.3213, found: 440.3415

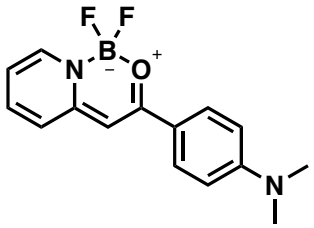

Synthesis of 1-(4-(dimethylamino)phenyl)-2-(2-pyridinyl-κN)ethanonato-κO)difluroborane: (90 mg, 30%); m.p. 248-250 °C; IR ν_{max} (cm^{-1}): 2915.09, 1633.94, 1596.98, 1442.74, 1117.09, 1095.45, 1075.00, 1025.24, 914.14, 820.80, 788.73; ^{1}H NMR (500 MHz, DMSO-d_6,): δ 3.02 (s, 6H), 6.64 (s, 1H) 6.77-6.79 (d, 2H, J = 10.0 Hz), 7.37-7.39 (dd, 1H, J = 5.0 Hz), 7.51-7.53 (d, 1H, J = 10.0 Hz), 7.76-7.78 (d, 2H, J = 10.0 Hz) 8.07-8.10 (dd, 1H, J = 5.0 Hz), 8.35-8.37 (d, 2H, J = 10.0 Hz): ^{13}C NMR (125 MHz, DMSO-d_6): δ 90.77, 111.96, 120.42, 120.86, 122.82, 128.0, 139.65, 142.47, 151.83, 152.44, 162.15: HR-ESI (Q-TOF) m/z: calc'd for $C_{15}H_{16}BF_2N_2O^+$ $[M+H]^+$: 289.1123, found: 289.1325.

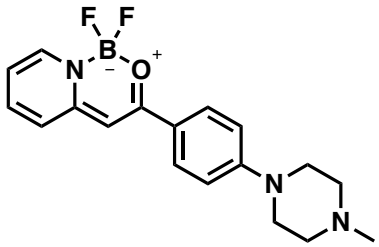

Synthesis of 1-(4-(4-(methypiperazin-1-yl)phenyl)-2-(2-pyridinyl-κN)ethanonato-κO)difluroborane:: (120 mg, 40%); m.p. 300 °C decomp; IR ν_{max} (cm^{-1}): 33149.44, 1629.69, 1606.05, 1520.64, 1390.11, 1221.93, 1073.31, 1031.94, 980.42, 924.50, 803.57; ^{1}H NMR (500 MHz, DMSO-d_6,): δ 2.88 (s, 3H), 3.05-3.10 (t, 2H, J = 10.0 Hz), 3.15-3.17 (d, 2H, J = 10 Hz), 3.53-3.55 (d, 4H, J = 10.0 Hz), 4.05-4.07 (d, 4H, J = 10.0 Hz), 6.76 (s, 1H), 7.10-7.12 (d, 2H, J = 10.0 Hz), 7.45-7.48 (dd, 1H, J = 5.0 Hz), 7.57-7.59 (d, 1H, J = 10.0 Hz), 7.84- 7.86 (d, 2H, J = 10.0 Hz), 8.14-8.17 (dd, 1H, J= 5.0 Hz), 8.42-8.44 (d, 1H, J = 10.0 Hz) 9.58 (s, 1H): ^{13}C NMR (125 MHz, DMSO-d_6): δ 42.57, 44.98, 52.56, 92.09, 115.27, 121.24, 123.10, 124.70, 127.90, 139.90, 142.91, 151.53, 151.61, 161.12: HR-ESI (Q-TOF) m/z: calc'd for $C_{18}H_{21}BF_2N_3O^+$ $[M+H]^+$: 344.1923, found: 344.4562.

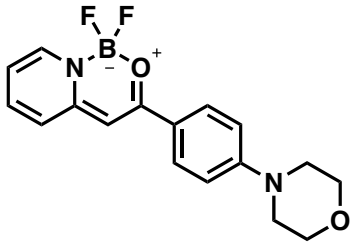

Synthesis of 1-(4-(morpholino)phenyl)-2-(2-pyridinyl-κN)ethanonato-κO)difluroborane:: (130 mg, 45%); m.p. 248-250 °C; IR ν_{max} (cm^{-1}): 2955.24, 1630.56, 1603.06, 1541.47, 1489.75, 1383.01, 1347.16, 1218.38, 1153.81, 941.36, 916.13, 812.41; ^{1}H NMR (500 MHz, DMSO-d_6,): δ 3.26-3.28 (t, 4H, J = 5.0 Hz), 3.74-3.76 (t, 4H, J = 5.0

Hz), 6.712 (s, 1H), 7.02-7.04 (d, 2H, J = 10.0 Hz), 7.42-7.45 (dd, 1H, J = 5.0 Hz), 7.55-7.57 (d, 1H, J = 10.0 Hz) 7.80-7.82 (d, 2H, J = 10.0 Hz), 8.11-8.14 (dd, 1H, J = 5.0 Hz), 8.40-8.42 (d, 2H, J = 10.0 Hz): ^{13}C NMR (125 MHz, DMSO-d_6): δ 47.63, 66.37, 91.67, 114.29, 120.96, 123.00, 123.69, 127.84, 139.83, 151.64, 153.19, 161.50: HR-ESI (Q-TOF) m/z: calc'd for $C_{17}H_{18}BF_2N_2O_2^+$ $[M+H]^+$: 331.1493, found: 331.4132

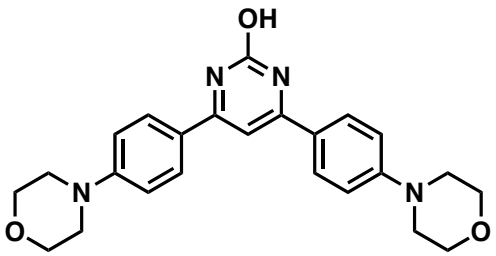

Synthesis of 4,6-bis(4-morpholinophenyl)pyrimidin-2-ol: (500 mg, 52%); m.p. 340 °C decomp; IR ν_{max} (cm^{-1}): 2960.40, 1622.72, 1587.71, 1510.78, 1428.80, 1339.11, 1225.70, 1201.76, 925.89, 879.68, 821.86; ^{1}H NMR (500 MHz, DMSO-d_6,): δ 3.23-3.25 (t, 4H, J = 5.0 Hz), 3.75-3.77 (t, 4H, J = 5.0 Hz) 7.00-7.02 (d, 4H, J = 10.0 Hz), 7.12 (s, 1H), 8.01-8.03 (d, 4H, J = 10.0 Hz): ^{13}C NMR (125 MHz, DMSO-d_6, TFA): δ 46.65, 66.11, 96.71, 112.37, 124.67, 131.39, 149.85, 155.05, 160.53; HR-ESI (Q-TOF) m/z: calc'd for $C_{24}H_{26}N_4O_3^+$ $[M+H]^+$: 419.5045, found: 419.2075.

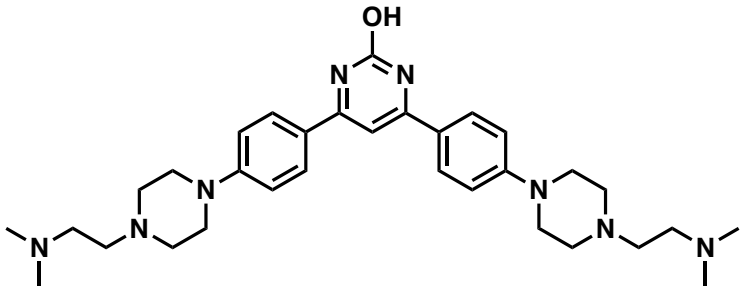

Synthesis of 4,6-bis(4-(4-(2-dimethylamino)ethyl)piperazin-1-yl)phenyl)pyrimidin-2-ol: (430 mg, 32%); m.p. 270 °C decomp; IR ν_{max} (cm^{-1}): 3384.10, 2938.02, 2817.55, 1625.28, 1581.61, 1513.15, 1446.39, 1227.64, 1195.28, 1002.23, 823.70; ^{1}H NMR (500 MHz, DMSO-d_6,): δ 2.13 (s, 12H), 2.35-2.37 (t, 4H, J = 5.0 Hz), 2.41-2.44 (t, 4H, J = 5.0 Hz), 2.50-2.55 (t, 8H, J = 5.0 Hz), 3.27-3.31 (t, 8H, J = 5.0 Hz), 7.00-7.02 (d, 4H, J = 10.0 Hz), 7.22 (s, 1H), 8.00-8.02 (d, 4H, J = 10.0 Hz): ^{13}C NMR (125 MHz, DMSO-d_6, TFA): δ 43.94, 47.19, 52.81, 53.56, 54.42, 55.41, 96.46, 114.34, 118.90, 124.65, 129.25, 153.39; HR-ESI (Q-TOF) m/z: calc'd for $C_{32}H_{47}N_8O^+$ $[M+H]^+$: 559.7825, found: 560.0622.

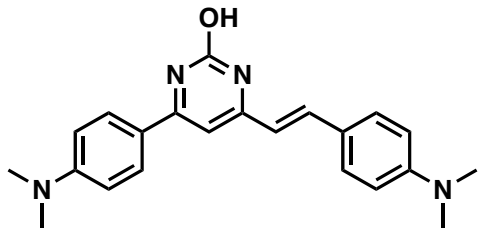

Synthesis of (E)-4-(4-dimethylamino)phenyl)-6-(4dimethylamino)styryl)pyrimidin-2-ol : (195 mg, 35%); m.p. 340-342 °C; IR ν_{max} (cm^{-1}): 2899.74, 1633.21, 1596.87, 1569.37, 1524.03, 1399.35, 1361.30, 1187.44, 1162.09, 945.68, 811.99; ^{1}H NMR (500 MHz, DMSO-d_6,): δ 2.991 (s, 6H), 3.03 (s, 6H), 6.70-6.73 (d, 1H, J = 15.0 Hz), 6.76-6.78 (d,

2H, J = 10.0 Hz), 7.08 (s, 1H), 7.44-7.46 (d, 2H, J = 10.0 Hz), 7.79- 7.82 (d, 2H, J = 15.0 Hz), 5.02 (broad s), 11.34 (s, 1H): ^{13}C NMR (125 MHz, DMSO-d_6, TFA): δ 96.12, 115.16, 112.24, 112.63, 114.38, 115.11, 117.98, 122.11, 131.07, 131.06, 147.28, 149.74, 153.319, 154.51, 159.35, 159.72; HR-ESI (Q-TOF) m/z: calc'd for $C_{22}H_{25}N_4O^+$ $[M+H]^+$: 361.4685, found: 361.2046.

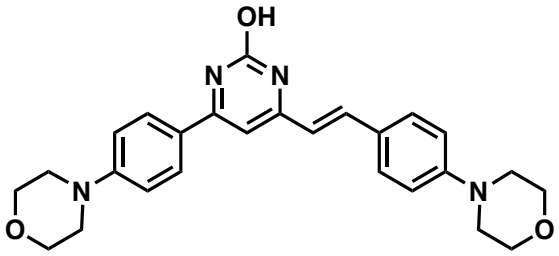

Synthesis of (E)-4-(4-morpholinophenyl)-6-(4-morpholinostyryl)pyrimidin-2-ol: (385 mg, 38%); m.p. 340 °C decomp.; IR ν_{max} (cm^{-1}): 2957.00, 2822.24, 1633.60, 1583.02, 1553.89, 1512.04, 1445.41, 1357.95, 1184.99, 1067.61, 1048.85, 924.86; ^{1}H NMR (500 MHz, DMSO-d_6,): δ 3.18-3.21 (broad d, 8H, J = 15 Hz), 3.74 (broad s, 8H) 6.74-6.77 (d, 1H, J = 15.0 Hz), 6.97-6.99 (d, 2H, J = 10.0 Hz), 7.00 (s, 1H), 7.47-7.49 (d, 2H, J = 10.0 Hz) 7.63-7.66 (d, 1H, J = 15.0 Hz), 7.94-7.96 (d, 2H, J = 10.0 Hz): ^{13}C NMR (125 MHz, DMSO-d_6, TFA): δ 46.72, 47.07, 66.18, 66.22, 96.90, 112.94, 113.68, 114.75, 117.06, 124.44, 131.17, 131.35, 147.23, 149.53, 153.81, 155.03, 160.08, 160.57; HR-ESI (Q-TOF) m/z: calc'd for $C_{26}H_{29}N_4O_3^+$ $[M+H]^+$: 445.5425, found: 445.2243.

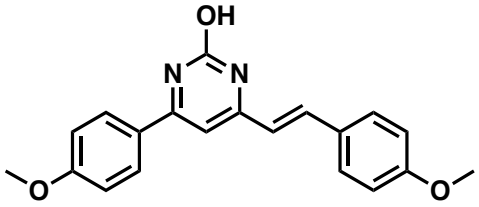

Synthesis of (E)-4-(4-methoxyphenyl)-6-(4-methoxy)styryl)pyrimidin-2-ol: (900 mg, 56%); m.p. 240-242 °C; IR ν_{max} (cm^{-1}): 2728.53, 1730.17, 1627.04, 1565.09, 1269.70, 1190.89, 1167.33, 993.58, 827.73, 804.68; ^{1}H NMR (500 MHz, DMSO-d_6,): δ 3.83 (s, 3H), 3.88 (s, 3H) 7.04-7.07 (d, 1H, J = 15.0 Hz), 7.07-7.09 (d, 2H, J = 10.0 Hz), 7.14-7.16 (d, 2H, J = 10.0 Hz), 7.48 (s, 1H), 7.63- 7.65 (d, 2H, J = 10.0 Hz), 8.13-8.15 (d, 2H, J = 10.0 Hz), 8.22-8.25 (d, 1H, J = 15.0 Hz): ^{13}C NMR (125 MHz, DMSO-d_6, TFA): δ 56.06, 56.37, 98.15, 115.05, 115.54, 117.38, 122.12, 127.44, 131.40, 131.56, 147.38, 150.04, 162.34, 162.45, 162.96, 164.53: HR-ESI (Q-TOF) m/z: calc'd for $C_{20}H_{19}N_2O_3^+$ $[M+H]^+$: 335.3825, found: 335.1400.

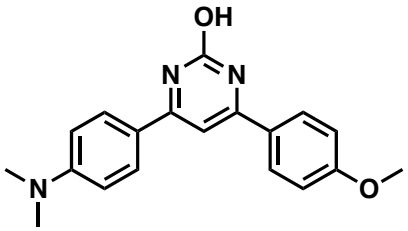

Synthesis of 4-(4-(dimethylamino)phenyl)-6-(4-methoxyphenyl)pyrimidin-2-ol: (714 mg, 72%); m.p. 302-304 °C; IR ν_{max} (cm^{-1}): 3103.45, 1616.48, 1596.57, 1511.27, 1450.21, 1342.56, 1298.97, 1244.57, 1026.71, 989.43, 834.12; ^{1}H NMR (500 MHz, DMSO-d_6,): δ 2.99 (s, 6H), 3.83 (s, 3H) 6.76-6.78 (d, 2H, J = 10.0 Hz), 7.02-7.04 (d, 2H, J = 10.0 Hz), 7.12 (s, 1H), 7.99-8.01 (d, 2H, J = 10.0 Hz) 8.07-8.09 (d, 2H, J = 10.0 Hz);

^{13}C NMR (125 MHz, DMSO-d_6, TFA): δ 56.25, 97.45, 112.26, 114.74, 115.06, 122.83, 131.16, 131.69, 154.77, 158.87, 160.63, 161.88, 163.96: HR-ESI (Q-TOF) m/z: calc'd for $C_{19}H_{20}N_3O_2^+$ $[M+H]^+$: 322.3875, found: 323.1205.

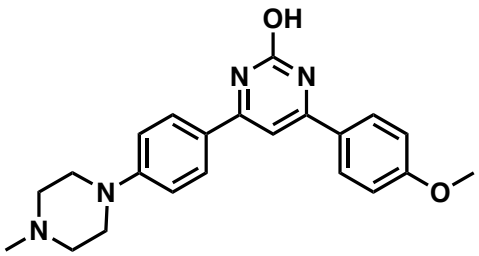

Synthesis of 4-(4-methoxyphenyl)-6-(4-methylpiperazin-1-yl)phenyl)pyrimidin-2-ol: (430 mg, 20%); m.p. 280 °C decomp; IR ν_{max} (cm^{-1}): 29333.96, 2837.93, 1624.10, 1592.64, 1575.52, 1536.18, 1378.22, 1299.43, 1142.29, 829.08; ^{1}H NMR (500 MHz, DMSO-d_6,): δ 2.76 (s, 3H), 3.20 (broad s, 2H) 3.55 (broad s, 2H), 7.07-7.09 (d, 2H, J = 10.0 Hz), 7.10-7.12 (d, 2H, J = 10.0 Hz), 7.37 (s, 1H) 8.08- 8.10 (d, 2H, J = 10.0 Hz): ^{13}C NMR (125 MHz, DMSO-d_6, TFA): δ 42.63, 44.90, 52.47, 55.91, 114.12, 114.60, 115.10, 116.51, 118.89, 124.65, 129.37, 129.80, 152.19, 162.45: HR-ESI (Q-TOF) m/z: calc'd for $C_{22}H_{25}N_4O_2^+$ $[M+H]^+$: 377.4675, found: 378.2005.

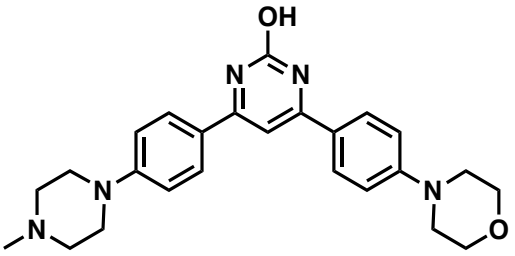

Synthesis of 4-(4-(4-methylpiperazin-1-yl)phenyl)-6-(4-morpholinophenyl)pyrimidin-2-ol: (700 mg, 50%); m.p. 320 °C decomp; IR ν_{max} (cm^{-1}):

2826.00, 1623.43, 1580.12, 1510.64, 1444.70, 1393.57, 1378.51, 1338.75, 1225.89, 1195.54, 1112.78, 923.51; ^{1}H NMR (500 MHz, DMSO-d_6,): δ 2.22 (s, 3H), 2.44 (broad s, 4H) 3.27-3.31 (t, 4H, J = 5.0 Hz), 3.75-3.79 (t, 4H, J = 5.0 Hz), 7.02-7.04 (d, 4H), 7.04-7.06 (d, 2H, J = 10.0 Hz), 7.27 (s, 1H) 8.02-8.04 (d, 2H, J = 10.0 Hz), 8.04-8.06 (d, 2H, J = 10.0 Hz): ^{13}C NMR (125 MHz, DMSO-d_6, TFA): δ 24.58, 42.49, 44.11, 46.76, 52.30, 62.47, 66.23, 97.13, 113.69, 114.56, 131.39, 131.58, 150.35, 153.71, 155.13, 160.74, 161.16: HR-ESI (Q-TOF) m/z: calc'd for $C_{25}H_{30}N_5O_2^+$ $[M+H]^+$: 432.5475, found: 432.2381.

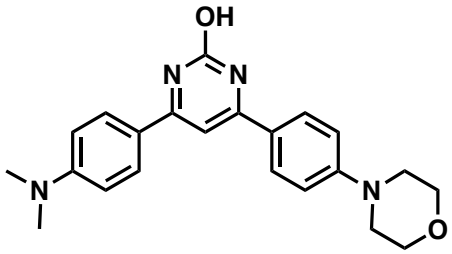

Synthesis of 4-(4-dimethylamino)phenyl)-6-(4-morpholinophenyl)pyrimidin-2-ol: (678 mg, 52%); m.p. 320 °C decomp ; IR ν_{max} (cm^{-1}): 2894.49, 1619.51, 1590.76, 1513.90, 1431.12, 1340.96, 1235.36, 1114.43, 948.39, 930.21; ^{1}H NMR (500 MHz, DMSO-d_6,): δ 3.42 (s, 6H), 3.42 (broad s) 3.74 (broad s), 6.84-6.86 (d, 2H, J = 10.0 Hz), 7.08-7.10 (d, 2H, J = 10.0 Hz), 7.44 (s, 1H), 8.12-8.14 (d, 2H, J = 10.0 Hz), 8.15-8.17 (d, 2H, J = 10.0 Hz): ^{13}C NMR (125 MHz, DMSO-d_6, TFA): δ 25.95, 46.86, 62.25, 96.24, 112.18, 113.77, 113.84, 124.65, 131.04, 131.42, 154.58, 154.381, 160.00, 160.72: HR-ESI (Q-TOF) m/z: calc'd for $C_{21}H_{25}N_4O_2^+$ $[M+H]^+$: 377.4675, found: 377.1954.

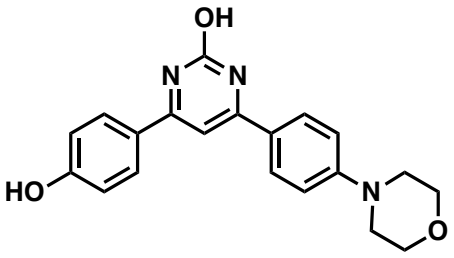

Synthesis of 4-(4-hydroxyphenyl)-6-(4morpholinophenyl)pyrimidin-2-ol: (346 mg, 31%); m.p. 330°C decomp.; IR ν_{max} (cm^{-1}): 3252.12, 2893.92, 1731.51, 1626.81, 1579.09, 1511.92, 1226.18, 1200.78, 1173.91, 1111.36, 821.74; ^{1}H NMR (500 MHz, DMSO-d_6,): δ 3.31-3.33 (t, 4H, J = 5.0 Hz), 3.74-3.76 (t, 4H, J = 5.0 Hz), 6.90-6.92 (d, 2H, J = 10.0 Hz), 7.05-7.07 (d, 2H, J = 10.0 Hz), 7.32 (s, 1H), 8.02-8.04 (d, 2H, J = 10.0 Hz), 8.07-8.09 (d, 2H, J = 10.0 Hz): ^{13}C NMR (125 MHz, DMSO-d_6, TFA): δ 47.22, 66.32, 114.01, 114.13, 116.15, 116.31, 129.76, 130.29, 130.39, 130.78, 153.98, 154.38, 161.77, 162.41: HR-ESI (Q-TOF) m/z: calc'd for $C_{20}H_{20}N_3O_3^+$ $[M+H]^+$: 350.3975, found: 350.1503.

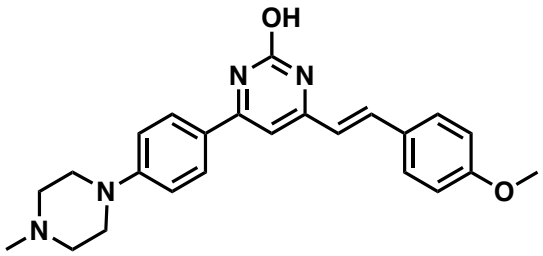

Synthesis of 4-(4-methoxyphenyl)-6-(4-(4-methylpiperazin-1-yl)phenyl)pyrimidin-2-ol: (100 mg, 25%); m.p. 290 °C decomp; IR ν_{max} (cm^{-1}): 2935.03, 2836.11, 1627.23, 1580.86, 1566.25, 1540.09, 1442.75, 1402.41, 1170.86, 922.24, 822.96; ^{1}H NMR (500 MHz, DMSO-d_6,): δ 1.55 (s, 3H), 2.23 (s, 3H), 2.23 (broad s, 4H), 3.81 (broad s, 4H), 6.87-6.90 (d, 1H, J = 15.0 Hz), 7.01-7.03 (d, 2H, J = 10.0 Hz), 7.06 (s, 1H), 7.57-7.59 (d,

2H, J = 10.0 Hz), 7.81-7.84 (d, 1H, J = 15.0 Hz), 7.98- 8.00 (d, 2H, J = 10.0 Hz), 8.56 (s, 1H); ^{13}C NMR (125 MHz, DMSO-d_6,): δ 26.05, 46.31, 47.49, 54.90, 55.75, 97.54, 114.46, 114.91, 126.56, 128.81, 128.94, 129.44, 153.07, 159.48, 160.65, 166.19, 166.87, 174.25; HR-ESI (Q-TOF) m/z: calc'd for $C_{24}H_{27}N_4O_2^{2+}$ $[M+H]^+$: 403.5049, found: 403.2125.

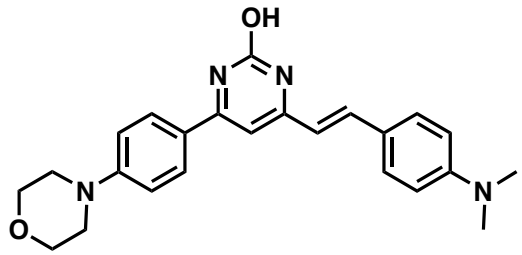

Synthesis of (E)-4-(4-(dimethylamino)styryl)-6-(4-morpholinophenyl)pyrimidin-2-ol: (375mg, 80%); m.p. 310 °C decomp.; IR ν_{max} (cm^{-1}): 2861.73, 1640.31, 1582.77, 1522.44, 1352.40, 1223.70, 1162.14, 1051.40, 982.73, 928.06, 821.40; ^{1}H NMR (500 MHz, DMSO-d_6,): δ 2.99 (s, 6H), 3.28-3.30 (t, 4H, J = 5.0 Hz), 3.74-3.77 (t, 4H, J = 5.0 Hz), 6.74-6.77 (d, 1H, J = 15.0 Hz), 6.77-6.79 (d, 2H, J = 10.0 Hz), 7.03-7.05 (d, 2H, J = 10.0 Hz), 7.09 (s, 1H), 7.45-7.47 (d, 4H, J = 10.0 Hz), 7.81- 7.83 (d, 1H, J = 15.0 Hz), 8.02-8.04 (d, 2H, J = 10.0 Hz): ^{13}C NMR (125 MHz, DMSO-d_6, TFA): δ 46.86, 66.25, 96.24, 112.18, 113.77, 113.84, 120.96, 124.65, 131.04, 131.42, 116.21, 120.96, 124.65, 131.04, 131.42, 154.58, 154.81, 160.00, 160.72; HR-ESI (Q-TOF) m/z: calc'd for $C_{24}H_{27}N_4O_2^+$ $[M+H]^+$: 403.5055, found: 403.2134.

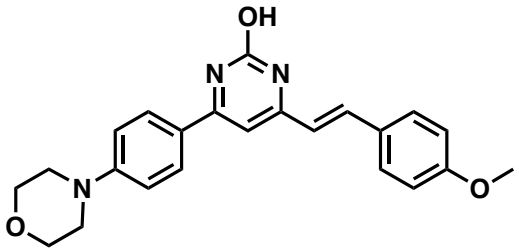

Synthesis of (E)-4-(4-methoxystyryl)-6-(4-morpholinophenyl)pyrimidin-2-ol: (275 mg, 58%); m.p. 280 °C; IR ν_{max} (cm^{-1}): 2827.45, 1638.25, 1603.74, 1551.20, 1510.32, 1486.70, 1444.74, 1232.50, 1172.69, 1119.91, 925.50, 644.74; ^{1}H NMR (500 MHz, DMSO-d_6,): δ 3.20 (broad s, 4H), 3.75 (broad s, 4H), 3.79 (s, 3H), 6.86 (s, 1H), 6.77-6.80 (d, 1H, J = 15.0 Hz), 6.97 (broad s, 2H) 7.54-7.56 (d, 2H, J = 10.0 Hz), 7.60-7.63 (d, 1H, J = 15.0 Hz), 7.92-7.94 (d, 2H, J = 10.0 Hz): ^{13}C NMR (125 MHz, DMSO-d_6, TFA): δ 46.89, 56.00, 66.26, 97.55, 113.88, 115.57, 116.13, 116.41, 118.50, 120.86, 127.69, 130.95, 131.17, 145.17, 155.00, 160.01, 162.53; HR-ESI (Q-TOF) m/z: calc'd for $C_{23}H_{24}N_3O_3^{2+}$ $[M+H]^+$: 390.4619, found: 390.1822.

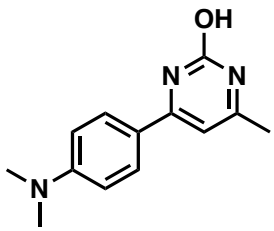

Synthesis of (4-(4-(dimethylaminophenyl)-6-methylpyrimidin-2-ol: (160 mg, 62%); m.p 250 °C; IR ν_{max} (cm^{-1}): 3374.43, 2921.89, 2853.32, 1645.05, 1573.94, 1323.05, 1186.29, 1297.17, 825.85; ^{1}H NMR (500 MHz, DMSO-d_6,): δ 2.20 (s, 3H), 3.00 (s, 3H), 6.73 (s, 1H), 6.74-6.76 (d, 2H, J = 10.0 Hz),

. 7.93- 7.95 (d, 2H, J = 10.0 Hz): ^{13}C NMR (125 MHz, DMSO-d_6, TFA): δ 20.02, 98.85, 111.81, 123.40, 129.23, 152.82, 159.28, 159.45, 168.77; HR-ESI (Q-TOF) m/z: calc'd for $C_{13}H_{16}N_3O^+$ $[M+H]^+$: 230.2899, found: 230.1302.

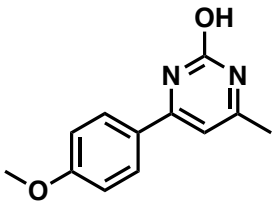

Synthesis of (4-(4-methoxyphenyl)-6-methylpyrimidin-2-ol; (800 mg, 30%); m.p. 230-232 °C; IR ν_{max} (cm^{-1}): 3020.47, 2725.87, 1664.20, 1624.00, 1455.53, 1254.32, 1162.25, 841.84, 820.30; ^{1}H NMR (500 MHz, DMSO-d_6,): δ 2.24 (s, 3H), 3.824 (s, 3H), 6.386 (s, 1H), 7.03-7.05 (d, 2H, J = 10.0 Hz), 8.04-8.06 (d, 2H, J = 10.0 Hz): ^{13}C NMR (125 MHz, DMSO-d_6, TFA): δ 19.91, 55.83, 99.68, 114.49, 129.16, 129.62, 159.17, 160.10, 162.36, 168.89; HR-ESI (Q-TOF) m/z: calc'd for $C_{12}H_{13}BF_2N_2O_2^+$ $[M+H]^+$: 217.2475, found: 217.0984.

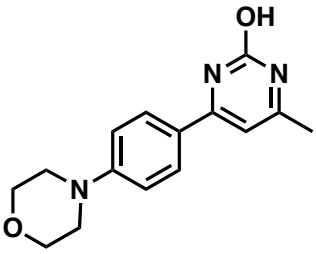

Synthesis of 4-methyl-6-(4-morpholinophenyl)pyrimidin-2-ol: (500 mg, 45%); m.p. 280 °C decomp.; IR ν_{max} (cm^{-1}): 2955.08, 1639.93, 1616.16, 1589.95, 1327.08, 1308.55, 1121.97, 927.06, 790.27; ^{1}H NMR (500 MHz, ACN-d_3,): δ 2.45 (s, 3H), 3.69 (broad s, 4H), 4.06 (broad s, 4H), 6.91 (s, 1H), 7.69-7.71 (d, 2H, J = 10.0 Hz), 8.24-8.26 (d, 2H, J

= 10.0 Hz): ^{13}C NMR (125 MHz, ACN-d_3): δ 24.23, 54.18, 64.30, 98.57, 120.85, 131.18, 147.18, 179.93, 195.21; HR-ESI (Q-TOF) m/z: calc'd for $C_{15}H_{18}N_3O_2^+$ $[M+H]^+$: 272.3269, found: 272.4760

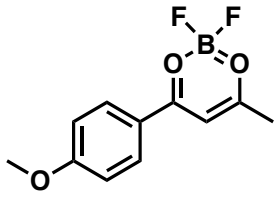

Synthesis of 4-(4-methoxyphenyl)-1,3-propane-dionato-κO, κO')difluoro-borane: (320 mg, 45%); mp 325-329 °C; IR ν_{max} (cm^{-1}): 2923.33, 2852.82, 1605.86, 1539.15, 1424.97, 1373.26, 1265.24, 1016.14, 840.37, 806.38, 750.00; ^{1}H NMR (500 MHz, DMSO-d_6,): δ 2.40 (s, 3H), 3.91 (s, 3H), 7.17 (s, 1H), 7.17-7.19 (d, 2H, J = 10.0 Hz), 8.17- 8.19 (d, 2H, J = 10.0 Hz); ^{13}C NMR (125 MHz, ACN-d_3): δ 23.71, 55.77, 96.89, 114.89, 123.18, 131.69, 166.07, 181.62, 191.61; HR-ESI (Q-TOF) m/z: calc'd for $C_{11}H_{12}BF_2O_3^+$ $[M+H]^+$: 241.0203, found: 241.1694.

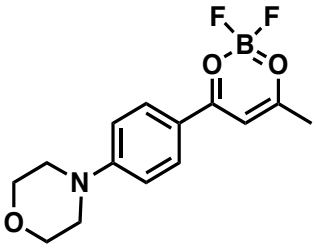

Synthesis of 4-(4-morpholinophenyl)-1,3-propane-dionato-κO, κO')difluoro-borane: (200 mg, 35%); m.p. 163-165 °C; IR ν_{max} (cm^{-1}): 3142.65, 2976.62, 1612.99, 1546.35, 1511.37, 1410.59, 1392.64, 1125.60, 1044.60, 999.48, 886.93; ^{1}H NMR (500 MHz,

DMSO-d_6,): δ 1.97 (s, 3H), 2.31 (broad s, 4H), 3.93 (broad s), 6.78 (s, 1H), 7.11-7.13 (d, 2H, J = 10.0 Hz), 8.11-8.13 (d, 2H, J = 10.0 Hz): ^{13}C NMR (125 MHz, ACN-d_3): δ 23.71, 55.77, 96.89, 114.89, 123.18, 131.69, 166.07, 181.62, 191.61; HR-ESI (Q-TOF) m/z: calc'd for $C_{14}H_{17}BF_2NO_3^+$ $[M+H]^+$: 296.0997, found: 296.3794.

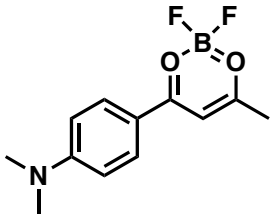

Synthesis of 4-(4-dimethylaminophenyl)-1,3-propane-dionato-κO, κO')difluoro-borane: (1 g, 44%); m.p. 200-203 °C; IR ν_{max} (cm^{-1}): 3123.54, 2782.70, 1608.90, 1567.92, 1536.52, 1512.99, 1477.60, 1360.99, 1055.44, 975.12, 810.78; ^{1}H NMR (500 MHz, ACN-d_3,): δ 2.47 (s, 3H), 3.31 (s, 3H), 6.93 (s, 1H), 7.70- 7.72 (d, 2H, J = 10.0 Hz), 8.25- 8.27 (d, 2H, J = 10.0 Hz): ^{13}C NMR (125 MHz, ACN-d_3): δ 24.28, 46.23, 98.72, 120.98, 131.07, 147.67, 179.89, 195.66: HR-ESI (Q-TOF) m/z: calc'd for $C_{12}H_{15}BF_2NO_2^+$ $[M+H]^+$: 254.0627, found: 254.3424

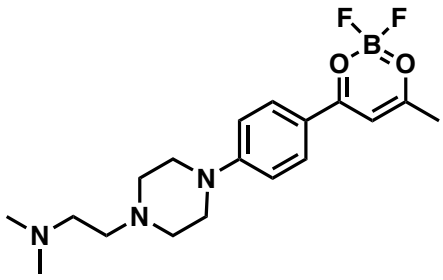

Synthesis of 1-(4-(4-(2-dimethylamino)ethyl)piperazin-1-yl)phenyl)-1,3-propane-dionato-κO, κO')difluoro-borane: (160 mg, 15%); m.p. 180-184 °C; IR ν_{max} (cm^{-1}):

3126.38, 1609.84, 1557.83, 1534.62, 1375.47, 1351.52, 1251.62, 1214.65, 1040.87, 812.59; ^{1}H NMR (500 MHz, DMSO-$d_{6,}$): δ 2.14 (s, 6H), 2.299 (s, 3H), 2.37-2.38 (t, 2H, J = 5.0 Hz), 2.41-2.42 (t, 2H, J = 5.0 Hz), 3.35 (broad s, 4H), 3.51 (broad s, 4H), 6.947 (s, 1H), 7.05-7.07 (d, 2H, J = 10.0 Hz), 7.99-8.01 (d, 2H, J = 10.0 Hz): ^{13}C NMR (125 MHz, DMSO-d_6): δ 24.20, 44.13, 45.13, 50.31, 51.13, 51.71, 96.59, 114.20, 119.07, 129.34, 132.24, 155.04, 180.18, 188.81; HR-ESI (Q-TOF) m/z: calc'd for $C_{18}H_{27}BF_2N3O_2^+$ $[M+H]^+$: 366.2387, found: 366.5184.

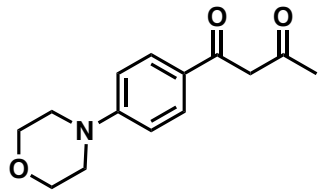

Synthesis of 1-(4-morpholinophenyl)butane-1,3-dione: (1g, 53%); m.p. 110-112 °C; IR ν_{max} (cm^{-1}): 2921.75, 2852.71, 1561.21, 1512.65, 1424.51, 1353.64, 1181.05, 1111.20, 920.56, 786.05; ^{1}H NMR (500 MHz, ACN-$d_{3,}$): δ major tautomer 2.14 (s, 3H), 3.28-3.30 (t, 4H, J = 5.0 Hz), 3.77-3.79 (t, 4H, J = 5.0 Hz), 6.27 (s, 1H), 6.93-6.95 (d, 2H, J = 10.0 Hz), 7.82- 7.84 (d, 2H, J = 10.0 Hz): ^{13}C NMR (125 MHz, ACN-$d_{3,}$): δ major tautomer: 24.01, 29.93, 47.22, 66.17, 95.15, 113.49, 128.83, 154.40, 190.74, 203.73: HR-ESI (Q-TOF) m/z: calc'd for $C_{14}H_{18}NO_3^+$ $[M+H]^+$: 248.3009, found: 248.5806.

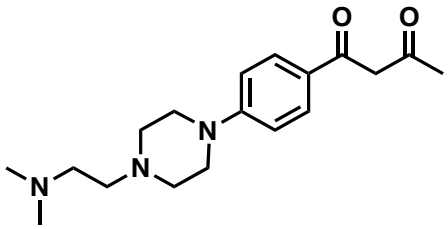

Synthesis of 1-(4-(4-(2-(dimethylamino)ethyl)piperazin-1-yl)phenyl)butane-1,3-dione: (200 mg, 38%); mp 108-110 °C; IR ν_{max} (cm^{-1}): 2949.87, 2821.59, 1570.18, 1442.50, 1286.61, 985.27, 928.82, 848.27, 786.56; ^{1}H NMR (500 MHz, DMSO-d_6,): major tautomer; δ 2.13 (s, 3H), 2.36-2.39 (t, 2H, J = 5.0 Hz), 2.41-2.43 (t, 2H, J = 5.0 Hz), 2.52 (broad s, 4H), 3.32 (broad s, 4H), 6.39 (s, 1H), 6.97-6.99 (d, 2H, J = 10.0 Hz), 7.80- 7.82 (d, 2H, J = 10.0 Hz); ^{13}C NMR (125 MHz, DMSO-d_6): major tautomer δ 24.98, 45.99, 47.02, 53.84, 56.19, 57.09, 95.65, 113.81, 129.35, 154.25, 184.70, 190.46, 204.30; HR-ESI (Q-TOF) m/z: calc'd for $C_{18}H_{28}N_3O_2^+$ $[M+H]^+$: 318.4405, found: 318.7202.

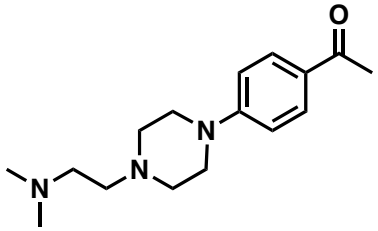

Synthesis of 1-(4-(4-(2-(dimethylamino)ethyl)piperazin-1-yl)phenyl)ethanone: (1g, 65%); mp 88-90 °C; IR ν_{max} (cm^{-1}): 3306.18, 2698.26, 2777.12, 1657.46, 1603.55, 1362.24, 1258.92, 1131.50, 926.01, 812.44; ^{1}H NMR (500 MHz, DMSO-d_6,): δ 2.15 (s, 6H), 2.34-2.36 (t, 2H, J = 5.0 Hz), 2.37-2.40 (t, 2H, J = 5.0 Hz), 2.49-2.51 (t, 4H, J = 5.0 Hz), 3.28-3.30 (t, 4H, J = 5.0 Hz), 6.94-6.96 (d, 2H, J = 15.0 Hz) 7.78- 7.80 (d, 2H, J = 10.0 Hz); ^{13}C NMR (125 MHz, DMSO-d_6): δ 26.54, 46.04, 47.10, 53.25, 56.27, 57.14,

113.48, 127.04, 130.51, 154.32, 195.96; HR-ESI (Q-TOF) m/z: calc'd for $C_{16}H_{26}N_3O^+$ $[M+H]^+$: 276.4035, found: 276.6832.